Unione europea
Fondo sociale europeo

REPUBBLICA ITALIANA

REGIONE AUTÒNOMA DE SARDIGNA
REGIONE AUTONOMA DELLA SARDEGNA

FSE 2007-2013
POR SARDEGNA
obiettivo competitività regionale e occupazione

A.D. MDLXII

UNIVERSITÀ DEGLI STUDI DI SASSARI

SCUOLA DI DOTTORATO DI RICERCA IN SCIENZE BIOMEDICHE

Direttore della Scuola: Prof.ssa Franca Deriu

INDIRIZZO IN NEUROSCIENZE

Responsabile di Indirizzo: Prof.ssa Maria Speranza Desole

XXVI CICLO

Development, characterization and optimization of an implantable biosensor for real-time monitoring of ethanol in the brain of freely moving rats

Direttore:

Prof.ssa Franca Deriu

Tutor:

Dott.ssa Gaia Rocchitta

Co-tutor:

Prof. Robert D. O'Neill

Tesi di dottorato di:

Dott. Ottavio Secchi

Anno Accademico 2012 - 2013

La presente tesi è stata prodotta nell'ambito della scuola di dottorato in Scienze Biomediche dell'Università degli Studi di Sassari, a.a. 2012-13 – XXVI ciclo, con il supporto di una borsa di studio finanziata con le risorse del P.O.R. SARDEGNA F.S.E. 2007-2013 - Obiettivo competitività regionale e occupazione, Asse IV Capitale umano, Linea di Attività l.3.1

Gaia Rocchitta is Lecturer at the Department of Clinical and Experimental Medicine, Medical School, *University of Sassari*, Viale S. Pietro 43/b, 07100 Sassari, Italy.

Robert D. O'Neill is Professor of Electrochemistry at the UCD School of Chemistry and Chemical Biology, *University College Dublin*, Belfield, Dublin 4, Ireland.

Ottavio Secchi is PhD student at the Doctoral School in Biomedical Sciences, Neuroscience Section, XXVI cycle, in the Department of Clinical and Experimental Medicine, Medical School, *University of Sassari*, Viale S. Pietro 43/b, 07100 Sassari, Italy.

My PhD was carried out during three years at the Department of Clinical and Experimental Medicine of the Medical School of the University of Sassari, and for a period of nine months at the UCD School of Chemistry and Chemical Biology. The collaboration between these two research groups contributed to the publication of the following papers:

Development and characterization of an implantable biosensor for telemetric monitoring of ethanol in the brain of freely moving rats.
Rocchitta G, **Secchi O**, Alvau MD, Migheli R, Calia G, Bazzu G, Farina D, Desole MS, O'Neill RD, Serra PA.
Anal Chem. 2012 Aug 21;84(16):7072-9. doi: 10.1021/ac301253h. Epub 2012 Aug 1.

Further in-vitro characterization of an implantable biosensor for ethanol monitoring in the brain.
Secchi O, Zinellu M, Spissu Y, Pirisinu M, Bazzu G, Migheli R, Desole MS, O'Neill RD, Serra PA, Rocchitta G.
Sensors (Basel). 2013 Jul 23;13(7):9522-35. doi: 10.3390/s130709522.

Simultaneous telemetric monitoring of brain glucose and lactate and motion in freely moving rats.
Rocchitta G, **Secchi O**, Alvau MD, Farina D, Bazzu G, Calia G, Migheli R, Desole MS, O'Neill RD, Serra PA.
Anal Chem. 2013 Nov 5;85(21):10282-8. doi: 10.1021/ac402071w. Epub 2013 Oct 21.

Some sections and figures of the above-cited papers appear in this dissertation.

Table of contents

List of abbreviations

5-HT	Serotonin
AA	Ascorbic acid
AAO	Aromatic alcohol oxidase
ADH	Alcohol dehydrogenase
ALDH	Aldehyde dehydrogenase
AMPA	α-Amino-3-hydroxy-5-methyl-4-isoxazole propionic acid
AOx	Alcohol oxidase
AUX	Auxiliary electrode
BALs	Blood alcohol levels
BSA	Bovine serum albumin
cAMP	Cyclic adenosine monophosphate
CNS	Central nervous system
CoA	Coenzyme A
CPA	Constant potential amperometry
CV	Cyclic voltammetry
DA	Dopamine
DAT	Dopamine transporter
EC(number)	Enzyme Commission number
EtOH	Ethanol
FAD	Flavin adenine dinucleotide
FAS	Fetal alcohol syndrome
FMN	Flavin mononucleotide

GA	Glutaraldehyde
GABA	γ-Aminobutyric acid
H_2O_2	Hydrogen peroxide
HPLC	High performance liquid chromatography
LCAO	Long-chain alcohol oxidase
LOD	Limit of detection
LOQ	Limit of quantification
LRS	Linear region slope
MAPK	Mitogen-activated protein kinase
MCU	Microcontroller unit
MEOS	Microsomial ethanol oxidizing system
MRI	Magnetic resonance imaging
MRS	Magnetic resonance spectroscopy
NAChRs	Nicotinic acetylcholine receptors
NAD^+	Nicotinamide adenine dinucleotide
NADH	Nicotinamide adenine dinucleotide hydrogen
NADP	Nicotinamide adenine dinucleotide phosphate
NADPH	Nicotinamide adenine dinucleotide phosphate hydrogen
NMDA	N-Methyl-D-aspartate
NMR	Nuclear magnetic resonance
OPA	Operational amplifier
oPD	*ortho*-Phenylenediamine
PBS	Phosphate buffered saline
PEI	Polyethyleinimine
PET	Positron emission tomography
PPD	Poly-*ortho*-phenylenediamine

ppm	Parts per million
Pt	Platinum
PU	Polyurethane
RE	Reference electrode
SAO	Secondary alcohol oxidase
SCAO	Short-chain alcohol oxidase
THF	Tetrahydrofuran
VTA	Ventral tegmental area
WE	Working electrode

1 - Introduction

1.1 Ethanol

Ethanol (EtOH) is the main non-aqueous component of alcoholic drinks: wine, beer, liquor spirits, *etc*. all contain this molecule, and are therefore referred to generically as "alcohol". Thus, ethanol and alcohol will be used with the same meaning in this dissertation. Alcoholic beverages have been strongly associated with human society since the early stages of civilization. Nowadays, the consumption of EtOH is a legal, commonly-accepted and widespread practice in nearly all societies, particularly in western cultures. As a consequence, ethanol is the most widely-used psychoactive drug.

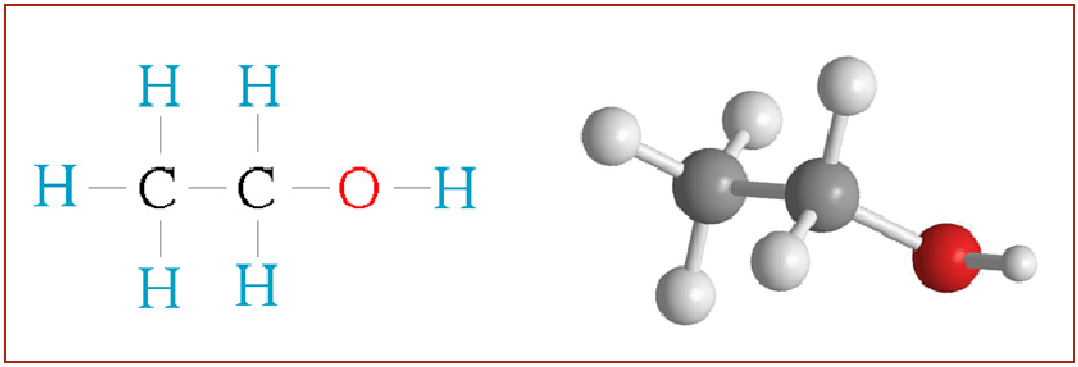

Figure 1: The ethanol molecule: planar and 3D representations

The chemical nomenclature of ethanol, appearing as a transparent liquid, is ethyl alcohol, a small organic amphiphilic molecule with formula CH_3CH_2OH and molecular weight of 46.07 g/mol (Figure 1). It is composed of a short two-carbon aliphatic chain and an hydroxyl group, which confer on the molecule both hydrophilic and lipophilic properties. This amphiphilic characteristic is critical for its biological activity, allowing alcohol to pass through biological membranes as well as to dissolve in blood and extracellular fluids.

When orally ingested, alcohol is absorbed by the digestive system and delivered by the cardiovascular system to all the organs.

Ethanol soon interacts with human body in various ways, producing a magnitude of effects depending on the intake level. It has been demonstrated that a low regular moderate consumption of alcohol may have positive effects; in particular, red wine contains some antioxidant molecules (mainly resveratrol) helpful to the heart, and may facilitate the early outcome after acute infarct and diminish the risk of cardiac death (Carrizzo et al., 2013; Tung et al., 2013).

Moreover, an unregulated use of alcohol is truly unsafe, due to its toxic action on organs (chiefly the liver), the teratogenic properties and its psychoactive effects. A clear example of the consequences of excessive alcohol consumption is represented by the elevated number of victims from road accidents: high levels of ethanol found in drivers' blood is the major cause of death from car crashes, especially among young drivers. In order to discourage the driving of vehicles under the influence of alcohol and reduce the cases of death, several laws have been adopted in recent years in many countries (Voas et al., 2013; Voas and Fell, 2013).

When high doses of ethanol are chronically assumed, psychophysical damage happens. An individual who loses control over alcohol use, becoming unable to drink responsibly, could develop a severe disorder called alcoholism, a progressive disease causing peripheral organ and brain damage, and contributing to the deterioration of cognitive functions. Alcoholism is considered the main cause of dementia (Oslin et al., 1998) and affects the ability to decide correctly and to feel emotions (Pfefferbaum et al., 1998). This underestimated disease represents a plague for the society, because of the medical and social impacts and the health-care costs (Mokdad et al., 2004; Hasin et al., 2007). Ethanol abuse compromises the physiological function of several organs and systems: the liver is particularly involved, alcohol being able to induce cirrhosis and steatosis (Fickert and Zatloukal, 2000); pancreas and the entire digestive system are also affected (Seitz et al., 1994), as well as skeletal muscle (Panzak et al., 1998), hematopoiesis (Wartenberg, 1998), the cardiovascular system, body temperature (Hardman and Limbird, 2005), the endocrine system (Noth and Walter, 1984), and the nervous system (Charness et al., 1989). Moreover, alcohol passes through the placental barrier and inhibits fetal growth or weight, creating typical facial stigmata and a series of mental and physical

damage, producing the so-called fetal alcohol syndrome or FAS (Lemoine et al., 2003).

So, although alcohol drinking has been common in human culture since the beginning of recorded history for hygienic, dietary, medicinal, and religious reasons, as well for recreational purposes, the above discussed negative aspects related to its uncontrolled assumption make it a dangerous drug for human health.

Compared with other kinds of abuse substances, larger amounts of alcohol are required to elicit the toxicological effects, resulting in its intake more as a food than a drug in non-heavy drinkers. Anyhow, alcohol is the most consumed psychoactive drug due to its abilities to change human consciousness and to its easy availability. It acts mainly as a depressant substance while its effects depend on the intake (the term depressant means that EtOH weakens brain function, and not that is able to induce depression as a disease).

Ethanol pharmacokinetic profiles of absorption, distribution and elimination determine the level of systemic exposure to ethanol. In fact, ethanol blood levels are linked with the amount assumed, which can be expressed as alcoholic units. An alcohol unit is equal to 12 grams (0.26 mol), corresponding to standard volumes of beer (330 mL, 4.5°), wine (125 mL, 12°) and hard alcoholic drinks (40 mL, 40°). Not surprisingly, the more alcohol is assumed, the higher will be its blood concentration. The intake is then distributed to all body fluids, so ethanol blood levels are also the result of its dilution.

When small amounts of ethanol (2–20 mM) arrive to the central nervous system (CNS), a lack of inhibition and euphoric behaviors appear. Higher concentrations lead to psychoactive effects, such as anxiety reduction. Gradual increases (21–86 mM) lead to several and progressive changes in its effects: behavior can turn from being expansive and vivacious to uncontrolled mood swings and emotional reactions, that could even possess a violent component. During acute intoxication, an increase in reaction time clearly appears, coupled with a decrease of motor control and impaired judgment, as well as a reduction in pain perception (Hardman and Limbird, 2005).

Moreover, symptoms of severe intoxication (about 65 mM) are vomiting, a condition of general anesthesia and brain-impaired functionality. Coma and lethal effects following an acute very high intoxication (86–100 mM) are mainly related to respiratory depression (Schuckit, 1995).

Even if alcohol is commonly consumed among people of most populations, not everybody who experiences alcohol develops an addiction. Recent studies have revealed how genetic differences are critical for individual and racial variations of EtOH effects. Indeed, for acute or chronic exposure, susceptibility to alcohol-related diseases are linked to heterogeneity in alcohol metabolism and of its first metabolite, acetaldehyde (Meier-Tackmann et al., 1990; Eckey et al., 1990).

The reasons of the transition from regular alcohol consumption to alcohol addiction development could be the consequence of several factors, still not fully understood. However, as argued below (Sections 1.3.7 and 1.4), impairment of the mesocorticolimbic dopaminergic system and the resulting increase of alcohol consumption seem to fit a possible explanation (Munson et al., 1995).

1.2 Ethanol pharmacokinetics

A brief summary of ethanol pharmacokinetics is discussed to describe how this molecule is absorbed, distributed, metabolized and eliminated in humans, and how these processes could be affected by the co-assumption of other drugs.

The pharmacokinetics of ethanol orally ingested starts when it reaches the gastrointestinal system. In this site it is absorbed into the bloodstream and then distributes to all the tissues and fluids. The relative water content of a tissue determines the equilibrium concentration of ethanol. Three important factors influence the rate of equilibration of ethanol within a tissue: its water content, its mass and the rate of local blood flow (Hardman and Limbird, 2005).
Ethanol absorption starts in the stomach (20%), where, exploiting its amphiphilicity, it diffuses across cells that line the gastric wall. The main site of its absorption occurs when it passes into the small intestine (80%) as the characteristics of the duodenum and jejunum walls make absorption much more rapid than from the stomach.
The rate of alcohol passage into the circulatory system is affected by several aspects, such as the rate of ingestion or the presence of food in the stomach. Food, particularly fatty foods, slows the absorption process, while carbonated drinks accelerate the passage of ethanol trough the gastric wall. When the stomach is empty, the ethanol hematic peak is reached about 30 minutes after its intake.
Through the enterohepatic circulation, ethanol reaches the liver where several enzymatic systems transform it into its metabolites. The first-pass effect, which reduces blood alcohol levels (BALs), is chiefly exerted by the hepatic organ but starts in the stomach, where the enzyme alcohol dehydrogenase (ADH) converts ethanol into acetaldehyde. Gastric ADH is not homogeneously expressed in men and women; females have less enzyme present in the stomach wall; so, ethanol bioavailability is higher, leading to generally higher BALs in women (Hardman and Limbird, 2005).

Additional, but tiny, amounts of ethanol are transformed by mean of non-oxidative reactions in the kidneys and lungs, or excreted unmodified in urine, sweat, and breath (Hardman and Limbird, 2005).
Alcohol eliminated by the lungs is readily detectable in expired air. The common ratio between blood:expired air ethanol is about 2100:1. Thus, by quantifying its concentration in the breath, it is possible to calculate alcohol blood levels (Holford, 1987). Common breathalyzer tests work by estimating ethanol breath concentrations.

The largest part of ethanol intake, corresponding to about 80-90%, is metabolized in the liver by means of hepatic oxidation. In the hepatocytes, different systems contribute to exert the first-passage effect and to convert alcohol into its metabolites.
The major pathway present in liver parenchymal cells (Figure 2, panel A) uses two sequential oxidative reactions, involving the cytosolic enzyme ADH and aldehyde dehydrogenase (ALDH), both located in hepatocytes cytosol and mitochondria (Crow, 1985; Hardman and Limbird, 2005). The first reaction converts ethanol into acetaldehyde, which is then further oxidized to acetic acid by ALDH. Both reactions require the presence of NAD^+ as cofactor (Nicotinamide adenine dinucleotide), which is converted to its reduced form NADH. The ethanol-derived acetate is linked by coenzyme A, forming acetyl CoA that reaches the pathway of the Kreb cycle or is used to form fatty acids or ketone bodies.
The rate of ethanol metabolism performed by this pathway is limited by the maximum capacity of ADH (Blomstrand and Theorell, 1970; Salaspuro et al., 1977). The rate of the reaction is also affected by NAD^+ availability. Drinking high amount of ethanol causes an increase in the hepatic NADH:NAD^+ ratio. As a consequence, NADH is accumulated into cytosolic and mitochondrial compartments, so other enzymes requiring NAD^+ are inhibited. When this happens, lactate accumulates, NADH and acetyl CoA levels increase, leading to acidosis and fatty acid synthesis. Also, oxidation of fatty acids is compromised by the excess of H^+ derived from the conversion of NAD^+ into NADH, which is used by mitochondria instead of H^+ normally product from fatty acid metabolism.

In this way, fatty acid accumulates in the hepatocytes, leading to steatosis and others alcohol-related hepatic diseases (Blomstrand and Theorell, 1970).

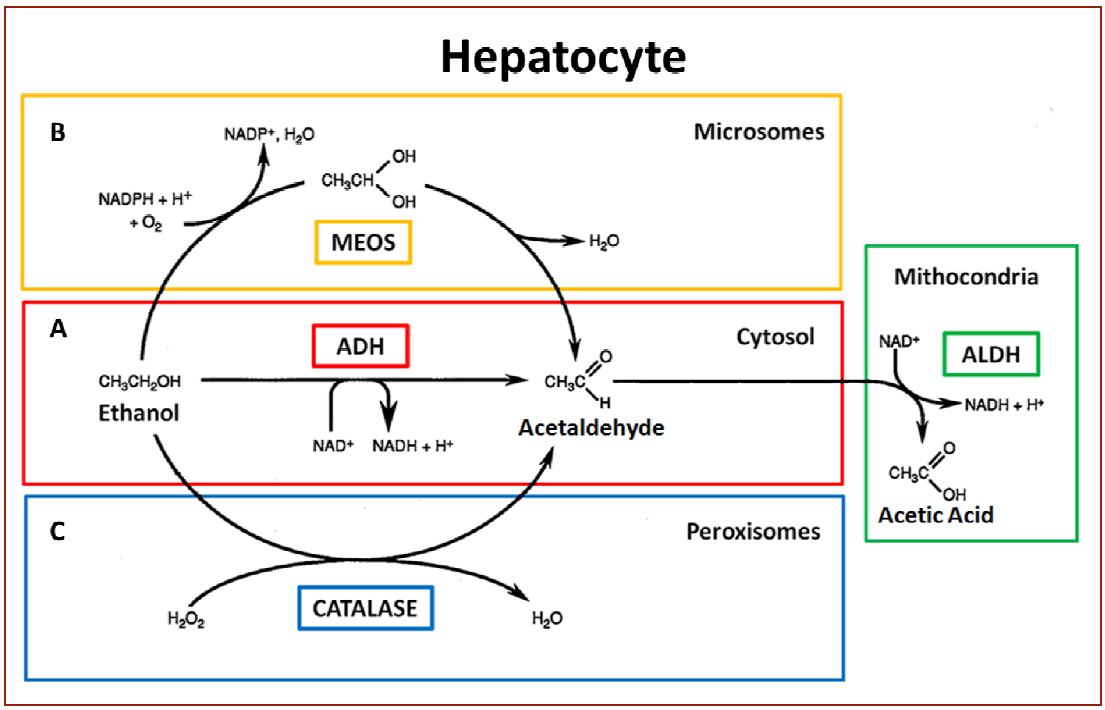

Figure 2: Scheme of Ethanol metabolism

A second pathway (Figure 2, panel B) responsible for hepatic alcohol oxidation is represented by the microsomal ethanol oxidizing system (MEOS). It involves NADPH (Nicotinamide adenine dinucleotide phosphate hydrogen) as cofactor, and, using molecular oxygen, transforms ethanol into acetaldehyde and water as byproduct. Acetaldehyde is then oxidized by ALDH. MEOS is an inducible system, the whole activity, and particularly that of the cytochrome P450, is increased by continual exposure to ethanol, regulating its activity in regard to the need. Heavy drinkers have 2–3 higher levels of microsomal enzymes (Grunnet et al., 1973).

When MEOS is over stimulated, in conjunctions with an absence of adequate antioxidant concentration, free radicals are generated and accumulate in the hepatocytes. The production of hydrogen peroxide (H_2O_2) and oxygen radicals enhances oxidative stress, damaging the hepatic cells by affecting biological membranes, protein synthesis and intracellular signals.

A small part of ethanol is converted into acetaldehyde by a minor pathway which plays a marginal role. It involves peroxisomes, specialized small cell organelles, using the oxidizing enzyme catalase to metabolize alcohol with H_2O_2 (Figure 2, panel C). H_2O_2 availability is usually low in the liver, so this pathway does not significantly support ethanol metabolism (Crow, 1985).

Only for very low concentrations of EtOH does the rate of alcohol elimination follow first-order kinetics, and linearity is observed since ADH is no longer saturated with ethanol. For higher concentrations, EtOH elimination follows Michaelis–Menten kinetics. For very high concentrations, alcohol elimination is defined as zero-order kinetics because the rate becomes independent of the alcohol blood concentration. (Holford, 1987; Adams, 1988).

BALs reached in individuals are generally strictly connected with body weight and with total body water amount. Because generally women are smaller than men, body water per unit weight is less and EtOH is distributed in a smaller volume. Together with difference in gastric ADH expression, this is the other main reason of higher BALs found in women with respect to men (Niaura et al., 1987).

Individuals show a great variation in the proportion of fat and water in their bodies. Due also to the low lipid:water partition coefficient of ethanol (Niaura et al., 1987) the same intake of alcohol per unit body weight can lead to very different BALs. The ratio between total body mass and total body water changes when people age. In particular, lean body mass diminishes and adipose tissue increases, so the volume of total body water decreases. This trend also displays a gender difference: aging from 25 to 60 years leads men to double the fat portion of the total body mass, while in women is increased by only 50%. Given that, because alcohol concentrates more into the body fluids, it is prudent to limit ethanol assumption to only one alcoholic unit for older men, to avoid or diminish ethanol-related risks (Dufour et al., 1995).

Nevertheless, there are many other differences affecting alcohol metabolism depending on gender, ethnicity, age, genetics, enzymatic variations, liver efficiency, the presence of relevant co-morbidities, as well as the co-administration of drugs that interact with alcohol (Vestal et al., 1977). For example, it appears that some individual and inter-ethnic variability is due to allelic variants in genes coding for the enzymes involved in the major metabolic pathway: ADH and ALDH (Inoue et al., 1984). Alcohol dehydrogenase is an oxidoreductase enzyme. It is a dimeric zinc-containing protein, tasked to oxidize the small part of endogenous ethanol produced by microorganisms in the intestine, and mainly to oxidize alcohols introduced with the diet. It is an aspecific enzyme, able to metabolize primary and secondary short chain alcohols such as methanol, ethanol or other exogenous alcohols, using NAD^+ as cofactor. Five ADH classes have been recognized based on the structure of the two subunits and kinetic characteristics, and further subdivided into subclasses according to their alleles composition.

The class I ADH isoforms play the chiefly role in ethanol oxidation. The variability in efficiency for metabolizing ethanol showed by human populations seems to be related with ability to form many isoforms, with varying kinetic properties (Edenberg et al., 1999). Populations expressing genotypes ADH2*1 and ADH3*1 are subjected to an increased risk of developing alcoholism, due to the higher efficiency in alcohol metabolism of those enzymes (Lee et al., 2004)

Aldehyde dehydrogenase also has been well studied. Nine different families of ALDH has been identified, but seems that only isoform 1 and 2 are involved in acetaldehyde metabolism (Agarwal, 2001). Several studies has shown how ALDH2 is genetically involved in alcoholism. This isoform is present in humans with four different allelic variants (Crabb et al., 1993). Variant 2 has a low catalytic activity, and seems to have a protective role against alcoholism because it leads to the accumulation of acetaldehyde, resulting in rapid appearance of severe adverse effects, such as facial flushing, and discouraging a further intake of alcohol.

ALDH2, variant 2, has been found in 50% of Asian people, and discourages those from becoming hard drinkers (McCarver et al., 1997; Li, 2000).

Moreover, genetic variations explain a direct correlation between genes and alcoholism in human. Studies conducted on twins and adopted children has revealed how alcohol addiction is related to genetic variations, as well as to environmental variations, for between 40 and 60% of cases (Begleiter and Kissin, 1995).

1.2.1 Ethanol and drugs interaction

Drinking alcoholic beverages while consuming drugs could affect the pharmacodynamic and pharmacokinetic effects of both. Alteration of ethanol bioavailability, as well as of the drugs, is a potential hazard of intoxication and adverse effects. A very high percentage of adults use prescription medications. Many of these, as well as herbal medicines and illegal drugs are known to interact with alcohol, increasing the risk of illness, injury, or death.

It is difficult to predict what could happen when an individual consumes both alcohol and medication, and the more drugs taken, the harder to estimate the effects on the user. Patients who assume a large number of drugs deserve special attention because of the increased risk and severity of potential drug–alcohol interactions (Nolan et al., 1988).

Ethanol and drugs could interact in several ways (Saunders, 1986). When certain medications and alcohol compete in the body for absorption, the potency of the medication and/or alcohol is often increased. An acute dose of alcohol may inhibit a drug's metabolism by competing for the same or similar metabolizing enzymes. This could increase the risk of adverse side effects, because the prolonged interaction could enhance the drug's availability.

Furthermore, as mentioned above (Section 1.2), a chronic intake of alcohol may activate hepatic drug-metabolizing enzymes, such as the inductive systems of MEOS, chiefly cytochrome P450. If the drug is metabolized by that system, an increase in number of enzyme molecules reduces the drug's availability leading to diminished drug efficacy. In addition, enzymes activated by long-term alcohol consumption may transform some drugs into toxic chemicals able to damage the liver or other organs.

A range of drugs are known to interact with alcoholic beverages. Aspirin, for example, enhances ethanol bioavailability by inhibiting gastric ADH. Simultaneous assumption of aspirin and alcohol can increase gastrointestinal blood loss and damage the mucosal lining of the stomach (Risto Roine et al., 1990). ADH is also inhibited by 4-methylpyrazole (Blomstrand and Theorell, 1970; Salaspuro et al., 1977), isobutyramide, and by drugs acting as histamine H_2 receptor blockers such as cimetidine or ranitidine (Di Padova et al., 1992).

As discussed later (Sections 4.7 and 5.6), ranitidine, a competitive histamine H_2 receptor antagonist widely used in peptic ulcer disease treatment (El-Bakary et al., 2010) was found to affect ethanol metabolism by inhibiting the cytochrome P450 (CYP2E1), alcohol dehydrogenase and aldehyde dehydrogenase enzymes, increasing ethanol bioavailability (Arora et al., 2000).

Moreover, interaction between ethanol and drugs such as antibiotics, cardiovascular medications, and antidiabetic medications can reduce drug effectiveness, and provoke nausea, headache and other more severe adverse effects.

Alcohol can also enhance the inhibitory effects of sedative and narcotic drugs at their site of action in the brain. Alcohol increases the rate of absorption of benzodiazepines and can intensify its depressant effects on the CNS (Sellers and Busto, 1982). Even more dangerous is the mix of ethanol and opiates (morphine, heroin, codeine or methadone), as well as with barbiturates (Stead and Moffat, 1983; Harris and Schroeder, 1982). Acting of the same neurotransmitter system, mainly GABA, can lead to a reduction in the level of consciousness and to a severe CNS depression, followed by suppression of vital functions such as respiration. The risk of overdose is very high. Other lethal effects can arise following depression of cardiac functions (Saunders, 1986).

Cannabis, used in combination with alcohol can decrease wakefulness, motor and intellectual abilities, and cause hallucinogenic effects (Ashton, 2001). This practice is currently very widespread in western societies, mostly among younger people (Julien, 1993).

Ethanol can also counteract the effect of stimulant drugs, such as amphetamine and cocaine. Thus, the number of alcoholic drinks required to feel euphoric effects is greatly increased, leading to a false sense of sobriety.
Then, in contrast, a negative effect called 'coming down', characterized by anxiety and depression, prevails (Burrows et al., 1993). Alcohol also increases the sedative effect of tricyclic antidepressants, impairing driving ability (Watson et al., 1980).

1.3 Ethanol pharmacodynamics

Ethanol crosses the blood–brain barrier and acts as a psychoactive drug primarily affecting brain functions altering perception, mood, consciousness, cognition, and behavior. Ethanol exerts a biphasic effect on the CNS, inducing prevalently euphoric effects at low doses, while depressing its function when BALs increase.

Alcohol affects the physiological action of a range of brain neurotransmitters and signaling molecules, such as GABA (γ-aminobutyric acid), glutamate, serotonin, acetylcholine, dopamine, norepinephrine, endorphin, encephalin and neuropeptide Y. Proteins, as molecular receptors, represent the primary sites of action for ethanol (Hardman and Limbird, 2005). Alcohol is able to reversibly reduce sodium transport in neurotransmission (Israel and Kalant, 1963), interacts with protein kinase C (Harris et al., 1995) and the intracellular signal-transduction cascades of MAPK protein (mitogen-activated protein kinase), tyrosine kinases, and also neurotrophic-factor receptors (Valenzuela and Harris, 1997). Several ion channel types in the brain are sensitive to ethanol, such as voltage-gated ion channels, as well as G protein-coupled and the ligand-gated receptor families. The effects of alcohol on the various neurotransmitter systems differ with acute or chronic consumption. A summary of the acute interactions between alcohol and the main signaling pathways is discussed now.

1.3.1 Ethanol and GABA

GABA is the principal mediator of inhibitory neurotransmission in the brain. Located both on pre- and postsynaptic neurons, GABA receptors are divided into two classes based on their structure. GABA-B receptors are G protein-coupled metabotropic receptors that regulate ion channel activation, using G proteins as the signal mechanism.

GABA-A receptors (Figure 3) are ionotropic receptors. Physiologically, GABA interacting with the ligand-gated GABA-A receptors triggers the opening of chloride ion channels allowing the chloride ions to flow across the membrane of the cell from the extracellular fluid (high Cl^- levels) into the cytoplasm (low Cl^- levels). The negative charge thus transferred into the cell causes hyperpolarization of the transmembrane potential (Siegel et al., 1999).

Consistent data have emerged from biochemical, electrophysiological, and behavioral studies indicating that the GABA-A receptor mediates some of *in-vivo* actions of ethanol by means of binding with a specific site (Figure 3).

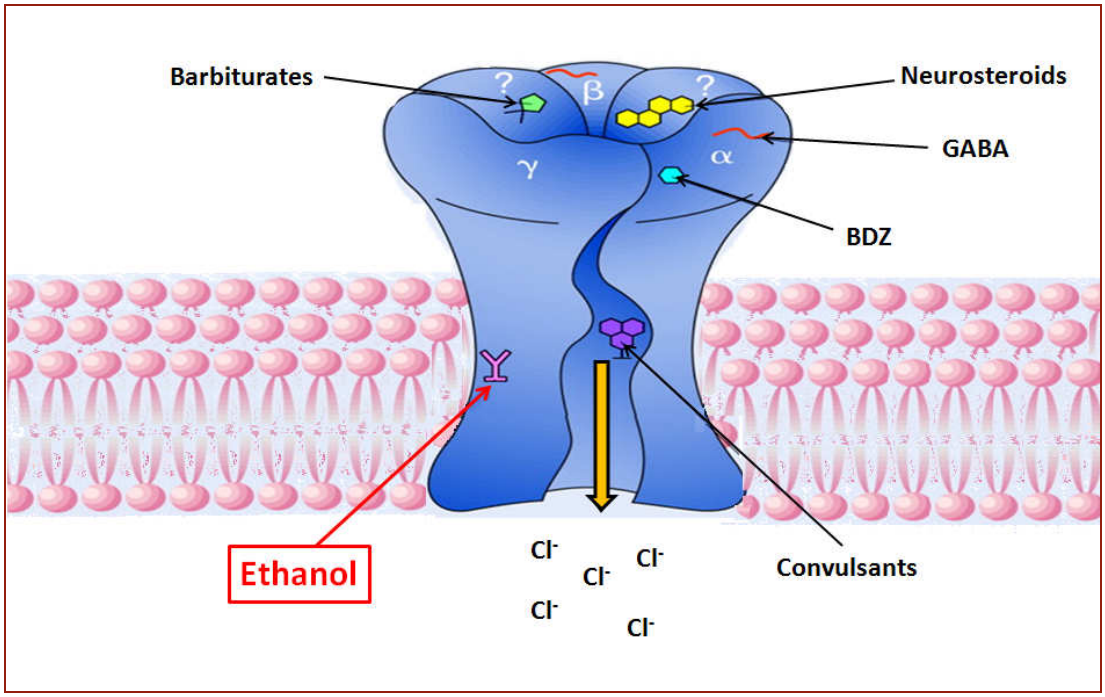

Figure 3: The GABA-A receptor

Through a positive allosteric modulation of its receptor, acute ethanol enhances the effects of this inhibitory neurotransmitter (Santhakumar et al., 2007). The interaction between ethanol and GABAergic systems, combined with its effect on catecholaminergic pathways, is thought to be responsible for the motor impairment associated with alcohol intake (Kiianmaa, 1990).

GABAergic neurotransmission is also facilitated by several others exogenous molecules known as GABA analogues or GABAergic drugs. GABA-A receptors are the target of a number of classes of sedatives, hypnotics, barbiturates, benzodiazepines, and volatile anesthetics. The protein in fact contains different allosteric binding sites for these molecules, which indirectly modulate the activity of the receptor. If more than one drug bind simultaneously to their respective sites, the opening of the ion channel can be significantly facilitated because of the summation of stimulations. The risk of respiratory depression is therefore increased in the presence of co-administration or co-abuse of these drugs (Siegel et al., 1999).

1.3.2 Ethanol and Glutamate

Ethanol is also known to interact with receptors that mediate the excitatory transmission systems in the CNS. Glutamate is a non-essential amino acid precursor for GABA and represents the main brain excitatory neurotransmitter (De Witte, 2004). Moreover, it plays a pivotal physiological role in memory formation, learning and regulation, and in pathological processes such as epileptiform seizures and neurotoxicity. It interacts with its receptors in the glutamatergic synapses, being responsible for the glutamate-mediated postsynaptic excitation of neurons (Gonzales and Jaworski, 1997).
Glutamate receptors in the CN- are divided two groups, ionotropic (NMDA, kainate, and AMPA) and metabotropic receptors. The nomenclature of the different ionotropic glutamate receptors derives from the names of several compounds found to interact with these in the first characterization studies.

- NMDA receptor, at which N-methyl-D-aspartate acts as a specific agonist.
- AMPA receptor, able to bind α-amino-3-hydroxy-5-methyl-4-isoxazole propionic acid, an artificial glutamate analog.
- Kainate receptor, at which kainic acid mimics the effect of glutamate.

NMDA receptors have a voltage dependent activity and an ion channel blockable by extracellular Mg^{2+}. When the receptor is activated by binding with glutamate, the block is removed and Ca^{2+} ions flow across the pore, generating an excitatory postsynaptic current.

It has been demonstrated that acute ethanol is able to interact with glutamatergic neurotransmission (De Witte, 2004). Alcohol has not a specific binding site in glutamatergic receptors, as is the case for GABA-A, but its interaction with NMDA- and kainate-receptor function leads to their inhibition, while AMPA receptors seem to be for the most part resistant to alcohol (Hoffman et al., 1989; Carta et al., 2003).

The acute ethanol-derived increase of GABAergic transmission, together with the disruption of the glutamatergic tone in the CNS are responsible for the euphoric, sedative, tranquilizing and anesthetic properties of beverage alcohol at low–medium concentrations (Lovinger et al., 1989). The dual effect of alcohol manifests when BALs increase further. The alteration of the glutamate system is responsible for staggering, slurred speech, and memory blackouts, while the further contribution of GABA effects, related to high ethanol doses, leads to a severe depressant effect on brain functionality, which in extreme cases can lead to loss of consciousness, coma and even death as a result of respiratory depression (De Witte, 2004).

1.3.3 Ethanol and Norepinephrine

The euphoric and stimulant effects of low ethanol doses in the brain are also related to a marked increase in noradrenalin (norepinephrine) release. Several studies indicate that, during a drinking session, norepinephrine metabolism in the human CNS is stimulated, maybe by increasing the firing of central noradrenergic neurons (Borg et al., 1981) and that acute ethanol exposure increases norepinephrine turnover both centrally and peripherally by increasing spontaneous norepinephrine release (Degani et al., 1979). Prefrontal norepinephrine transmission seems to be a critical factor in the rewarding and reinforcing effects of ethanol as discussed in Section 1.3.4 (Ventura et al., 2006).

1.3.4 Ethanol and Acetylcholine

Acetylcholine is a neurotransmitter that displays a variety of actions in both the peripheral and central nervous systems. Muscarinic and nicotinic are the two principal types of cholinergic receptors. Nicotinic acetylcholine receptors (nAChRs) are transmembrane receptors particularly responsive to nicotine and whose main physiological ligand is the neurotransmitter acetylcholine. It has emerged that nicotinic acetylcholine receptors sited in the CNS are target sites for ethanol, increasing the function of some nAChR subtypes and inhibiting the activity of others (Narahashi et al., 1999). Both human and animal models suggest that nicotinic receptors may be involved in the acute response to ethanol and in mediation of brain alcohol effects (Kamens and Phillips. 2008). Nicotinic acetylcholine receptors are involved in the acute locomotor responses that appear during a drinking session (Blomqvist et al.,1992; Larsson et al., 2002). Because nAChR are activated by nicotine, alcoholism and tobacco addiction often co-occur, although the biological factors that regulate the contemporary and addictive consumption of nicotine and alcohol in smokers and drinkers still remain unclear (DiFranza and Guerrera, 1990).

1.3.5 Ethanol and Serotonin

Serotonin (5-hydroxytryptamine, 5-HT) actions have been related to acute alcohol effects on the brain as well as to alcohol addiction. This monoamine is produced and released in the brain by specific neuronal population, especially in a cerebral areas called the raphe nuclei (Berger et al., 2009). 5-HT-releasing terminals from the raphe nuclei innervate a wide variety of forebrain regions, including the *amygdala* and *nucleus accumbens* that play an important role in the control of emotions and specific behaviors, such as the consumption of drugs of abuse. 5-HT elicits signal transmission between neurons by activating 5-HT receptors, subdivided into seven subtypes mediating both excitatory and inhibitory outcomes. All serotonin receptors are seven-transmembrane domain receptors coupled with G protein, except the 5-HT3 subtype which is a ligand-gated ion channel (Berger et al., 2009).

Ethanol particularly interferes with 5-HT3 ionotropic receptors. Alcohol exposure increases the electrical signal generated by 5-HT3 receptors in the brain, leading to a massive stimulation of neuronal synapses linked with serotonergic terminals (Pivac et al., 2004). As a consequence, the firing of adjacent non-serotonergic neurons increases the release several neurotransmitters strongly involved in ethanol addiction, such as dopamine (as discussed later in Section 1.3.7). Higher levels of serotonin metabolites are found in blood and urine after a drinking session, suggesting that alcohol augments the release of this neurotransmitter (Lovinger, 1999). Serotonergic transmission could represent a pharmacological target for drugs aimed at reducing alcohol consumption.

1.3.6 Ethanol and Opioids

Opioid systems represented by the endogenous opioids, endorphins, encephalins and dynorphins appear to influence alcohol drinking behavior by interacting with the mesolimbic dopamine system (Section 1.3.7) (Janecka et al., 2004). Furthermore, increases in extracellular endorphin levels in the nucleus accumbens were found following acute alcohol intake, acting independently from the mesolimbic dopamine system and demonstrating a dual mechanism exerted by opioids (Olive et al., 2001). As a consequence, positive alcohol reinforcement could be partly due to the release of endogenous opioids in the brain with their G-protein coupled μ, δ, and κ subtypes of receptors (Janecka et al., 2004).

1.3.7 Ethanol and Dopamine: mesocorticolimbic dopaminergic pathways

Dopamine (DA), a catecholaminergic neurotransmitter released by neurons as a signaling molecule, plays a pivotal role in several distinct pathways in the CNS, controlling hormonal release as well as being involved in the control of motor functions and mood tone (Schultz, 2007). DA is also implicated in psychoses and neurodegenerative diseases; for example, a drastic reduction of striatal dopamine content, due to the loss of dopaminergic neurons in the midbrain area (*i.e.* the *substantia nigra*), is a hallmark of Parkinson's disease (Bazzu et al., 2010; Serra et al., 2002; Serra et al., 2000)

When released into the synaptic cleft, DA interacts with its receptors, classified into D1- and D2-like families. Both families are G-protein coupled receptors, but their activation exerts different neuronal effects. The D1-like receptor family includes D1 and D5 subtypes, postsynaptic receptors whose stimulation leads to activation of the enzyme adenylate cyclase, increasing the intracellular concentration of the second messenger cAMP (cyclic adenosine monophosphate). In contrast, the D2-like family of receptors (D2, D3 and D4 subtypes) located on both pre- and postsynaptic membranes, inhibit the production of cAMP by directly acting on adenylate cyclase (Sesack, 2002).

The DA transporter (DAT) is responsible for determining the duration of dopamine's interaction with its receptors, removing this neurotransmitter from the synaptic cleft. Usually, the dopaminergic neurons are just tonically active and DAT uptake activity is quiescent (Nirenberg et al., 1997). When they are excited, however, the synapse floods with DA, leading to briefly increased tone (phasic activation) of mesocorticolimbic dopaminergic pathways. The increased dopaminergic activity which occurs in the *nucleus accumbens* increases both D1- and D2-type receptor signaling.

DA has been demonstrated to play a key role in modulating fundamental survival mechanism of species, such as how to obtain food, water or mating. These action are defined as reward-motivated behaviors (Hyman et al., 2006), because they are

associated with the activation of a specific brain neuronal reward system, which uses DA as neurotransmitter: the mesocorticolimbic dopaminergic system.

This pathway has been widely accepted to be the epicenter of reward in the brain, and has been proposed to be involved in movement, motivation, learning, arousal and orgasm, emotion and attention (Gonzales et al., 2004). Each kind of reward that has been characterized (for example, food, sex, drug of abuse, gambling, *etc*.) augments the level of released DA in the associated brain areas (see below), whereby both responses to natural rewards and various drugs of abuse show several similarities and shared pathways (Avena and Hoebel, 2003).

The mesocorticolimbic dopaminergic pathway begins in a region of the midbrain called ventral tegmental area (VTA) and reaches the limbic system through connections with the *nucleus accumbens*, *amygdala*, *hippocampus* and medial prefrontal cortex (Figure 4).

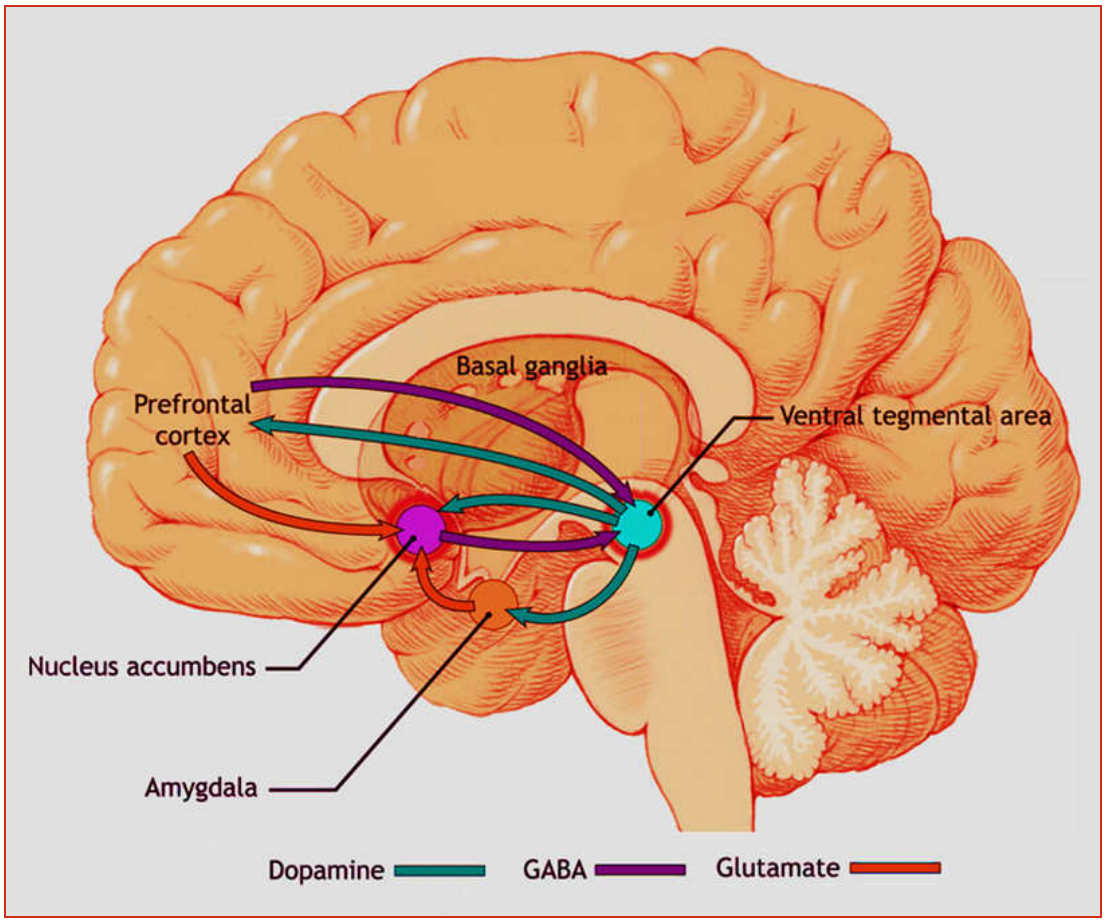

Figure 4: Scheme of the mesocorticolimbic dopaminergic system

The VTA consists of dopaminergic, GABAergic interneurons, and glutamatergic neurons located in the midbrain. The dopaminergic cell-body group (A10) is the origin of the mesocorticolimbic dopamine system. Even though quite small in absolute terms, it represents the main cluster of DA cells in the human brain. The bodies of these neurons project to prominent terminal areas such as the *nucleus accumbens* and the prefrontal cortex (Haber, 2002).

Whilst drugs of abuse are markedly heterogeneous in chemical structure, as well as in molecular targets and the related physiological effects, it has been widely ascertained that they all share a common effect of enhancement on the mesolimbic DA pathway, leading to increased release of DA in the nucleus accumbens (Mogenson and Huang, 1973). Hence, the reinforcing properties of drugs such as cocaine, amphetamine, opiates or nicotine are related to their ability to increase, at least acutely, the levels of this neurotransmitter in specific areas and activate the multisynaptic dopaminergic reward circuitry (Wise and Rompre, 1989).

Ethanol too has been found to have the same profile of interaction with the dopaminergic system as many drugs of abuse. As a matter of fact, acute ethanol assumption promotes an increase of activity in the mesolimbic DA system, causing higher levels of dopamine release, predominantly in the *nucleus accumbens* (Di Chiara and Imperato, 1986; Koob and Bloom, 1988). It has been observed that alcohol causes a dose-dependent enhancement in the spontaneous firing rate of dopaminergic neurons *in vivo* in the VTA; indeed, dopaminergic neurons located in the VTA are preferentially activated by lower doses of ethanol compared to adjacent DAergic neurons of the *substantia nigra* (Gessa et al., 1985). Furthermore, ethanol directly excites dopaminergic VTA reward neurons when synaptic transmission is blocked (Brodie et al., 1999). Although subjected to diverse studies, the molecular mechanisms through which ethanol alters the function of the mesolimbic DA system have still not been entirely elucidated (Karahanian et al., 2011; Mostofa et al., 2003; Munson et al., 1995).

1.4 Ethanol and Alcoholism

The continual consumption of ethanol can cause alcoholism, a pathological chronic relapsing disorder characterized by the high and compulsive consumption of alcohol, and loss of control over intake.

The long-term abuse of alcohol produces physiological changes in the brain. The neurotransmitter systems disrupted by acute ethanol are even more deeply altered during a chronic exposure, generating adaptive processes resulting in a compensatory balance. The changes in the activity of GABA, glutamate, serotonin, opioids and other neuronal systems concur to develop neuroadaptive phenomena, such as sensitization, tolerance and psychophysical dependence.

Sensitization seems to be the first step leading a subject from alcohol use to abuse, due to an increment in the reinforcement value of ethanol after repeated exposure, when an individual associates the liking of alcohol with the positive stimulus of wanting (Robinson and Berridge, 1993). After repeated consumption of alcohol, the wanting is amplified into a pathological status characterized by craving for the drug. The mesocortical DA pathway is involved in this sensitization phenomenon (Gilpin and Koob, 2008).

Tolerance is observed when a drinker shows a reduced physiological or behavioral response after consuming the same dose of alcohol. So, as a consequence of the decrease in the reinforcing efficacy of the drug, the individual requires progressively higher doses of ethanol to reproduce the effect experienced before (Leblanc et al., 1975). Tolerance is mediated by changes in metabolism of neurotransmitters and the activity of their receptors. GABA-A receptor function is decreased by long-term alcohol consumption, as the result of a reduction in the number of receptors, or by changes in their protein structure, resulting in a decrease in GABAergic neurotransmission tone. On the other hand, the activity of NMDA receptors is up-regulated by the chronic intake of ethanol, augmenting glutamatergic excitatory transmission.

This dysregulation also involves neural circuits implicated in the control of motivational processes (arousal, reward, stress, *etc*.), such as serotonin, opioids and norepinephrine. The impairment of those systems deeply contributes to the allostatic state that characterize the development of alcohol dependence (Hardman and Limbird, 2005; Volkow et al., 2007). Furthermore, it has been indicated that corticotrophin-releasing factor may be involved, and that the neuropeptide-Y brain antistress system may be compromised (Roy and Pandey, 2002).

As described above, the CNS of an alcoholic becomes unbalanced in the delicate physiological equilibrium between excitatory and inhibitory transmission. In chronic ethanol exposure, the brain tries to compensate the disequilibrium by antagonizing the depressant effect of alcohol, both by decreasing the activity of inhibitory transmission, as well as by increasing the glutamatergic excitatory circuits (Valenzuela and Harris, 1997).

But when alcohol consumption is reduced or suddenly interrupted, the disequilibrium manifests as a withdrawal syndrome, characterized by a state of hyperexcitation, anxiety and *delirium tremens* (Sullivan et al., 1989). Withdrawal states result from the lack of ethanol effects on the compensatory changes induced by tolerance. In attempting to restore the "pathological neurotransmitter equilibrium" and avoid the negative psychophysical effects, the individual needs a continuous consumption of ethanol (Valenzuela and Harris, 1997). Appearance of the withdrawal syndrome represents the irrefutable signal of physical dependence (O'Brien, 2005).

The physical dependence is always accompanied by a psychological component characterized by the increase of the motivation to compulsively seek and ingest alcohol. Rewarding effects of alcohol have an extremely important role (Littleton and Little,1994). Alcohol removal produces a negative-affective state, that merges with physical withdrawal effects to increase the propensity for relapse in recovering alcohol-dependent subjects (Koob, 2003). Alterations in the stress system, as well as decreases in the dopaminergic reward pathway function, seem to be implicated in psychological withdrawal symptoms and in the susceptibility to alcohol-seeking behavior (Thorsell et al., 2007; Gilpin and Koob, 2008; Melis et al., 2005; Volkow et al., 2007).

In the critical phase of transition from a controlled use of alcohol to dependence, positive reinforcement is essential, being linked with the activation of the mesocorticolimbic system and the increase in dopaminergic neuronal activity in the VTA (Theile et al., 2011; Karahanian et al., 2011). Reinforcement can be defined as a process in which a response or behavior is strengthened, based on previous experiences (Gilpin and Koob, 2008), and is characterized by positive or negative side effects.

Alcohol-drinking behavior is determined and maintained by both positive and negative reinforcement, and their specific contribution varies during the transition from ethanol-controlled use to addiction.

Positive reinforcement in alcoholism seems to be linked to rewarding stimulus, such as the euphoric effects, which increase the probability that the individual exhibits alcohol-seeking behavior in the future. Dopamine, serotonin and opioid peptide neurons, as well as GABAergic interneurons, acting on the VTA and *nucleus accumbens*, fire during acute ethanol assumption, such as in the early stages of dependence, as well as in the binge stage, and are deeply involved in the positive reinforcement (Rassnick et al., 1993; Gonzales et al., 2004). The positive reinforcement due to the opioidergic system is reduced by antagonists of opioid receptors (*e.g.,* naltrexone) which, acting on the VTA, nucleus accumbens, and central nucleus of the *amygdala*, decrease the rewarding effects of ethanol, justifying their use in alcoholism pharmacological therapies (Williams and Broadbridge, 2009; Koob, 2003). Acamprosate is a GABA analogue capable of reducing the relapse in a dose-dependent way, having a similar action and efficacy as naltrexone (Paille et al., 1995.)

Negative reinforcement occurs in alcohol dependence whenever motivational and affective symptoms such as anxiety, dysphoria, irritability, and emotional pain appear. These effects manifest during withdrawal or in the absence of alcohol, subsequent to previous discontinuation of ethanol intake. As a consequence, individuals, who already experienced alcohol withdrawal, could be pushed to drink again to prevent or alleviate the anxiety, or more generally to avoid and escape from the aversive stimulus they previously experienced (Gilpin and Koob, 2008).

Due to its features, the role of negative reinforcement increases following the transition to dependence, although it seems to appear even in earlier stages (Boileau et al., 2003). Key elements sustaining negative reinforcement and the stress circuit are corticotrophin-releasing factor and norepinephrine-releasing neurons. Their interaction with GABA interneurons in the central nucleus of the amygdala increases during the development of the allostatic state (Rassnick et al., 1993).

1.5 Techniques used in vivo to study ethanol in the brain

By outlining above the significant neurobiological implications of ethanol ingestion and addiction, it clearly emerges how critical and essential it is to further deepen our knowledge of alcohol toxicokinetics in humans. The varied and complicated set of interactions with several neuronal pathways makes the investigation of ethanol pharmacodynamics quite difficult. Several researchers focused their efforts to better understand the causes and the mechanisms involved in this very complex disorder; however, it is arduous to reproduce all the features of alcoholism. Different reliable animal models, recreating the specific symptoms of alcohol dependence, have demonstrated their usefulness in investigating alcohol-related neuronal changes. Alcohol addiction is easily reproducible in mice and rats (*e.g.*, self-administration), and shows similar characteristics of the different stages of dependence in humans, including binge-intoxication, relapse, withdrawal-negative effects, and preoccupation-anticipation stages (Loos et al., 2013). Even if much progress has been made, many other unsolved questions and issues remain for further investigation.

Ethanol detection in the brain kindles a particular interest, especially the monitoring of its concentration dynamics. New technologies are being combined with traditional approaches to study the transition from alcohol use and abuse to dependence, using the most appropriate techniques. Techniques used to measure ethanol concentration in the brain range from invasive to non-invasive approaches.

Non-invasive methods employ spectroscopic techniques such as magnetic resonance spectroscopy (MRS), magnetic resonance imaging (MRI) or positron emission tomography (PET) to monitor directly alcohol and its metabolites, both in animals and humans.

Invasive techniques include microdialysis, the most widely used in the last decades, and biosensors, new emerging and promising tools.

Both techniques are very reliable, but due to the necessity to implant probes in the tissue they can only be used in animal models and, except with some exceptions, suitable for preclinical studies only (Rocchitta and Serra, 2013).

In particular, we will focus on biosensors by generally describing the principles of their function. Because an accurate disquisition of the large and growing field of biosensors fall outside the remit of this dissertation, we will limit the discussion to just electrochemical biosensors, specifically amperometric biosensors that use enzymes as the biological element (Section 1.5.3). These have a number of advantageous features that make them particularly applicable in neurochemical biosensing (O'Neill et al., 2008), and were the technique of choice in the present studies.

1.5.1 Spectroscopic techniques

Clinical and preclinical studies of ethanol kinetics have been carried out by means of spectroscopic techniques, exploiting their main advantage, *i.e.*, the absolute non-invasiveness of the procedures to monitor changes in ethanol tissues concentrations in animal models as well as in humans.

Despite the fact that the ethanol monitoring range is of the order of millimolar, spectroscopic techniques show a limitation in its temporal range of detection, allowing monitoring sessions of only a few minutes. Additionally, even when no tethering is required, the experimental procedure requires that both animals as well as humans have to stay motionless during sessions (Rocchitta and Serra, 2013).

1.5.1.1 MRS

Magnetic resonance spectroscopy (MRS), also known as nuclear magnetic resonance (NMR) spectroscopy, is a noninvasive analytical technique used to study metabolic changes in numerous pathologies and in chemistry applications. MRS allows the identification and quantification of a number of molecules in samples of different origin (McRobbie et al., 2007).

In-vivo MRS records peaks of different radio frequencies and intensities given by molecules that possess fundamental molecular properties, *viz.* nuclear spins, typical resonance frequencies, spin couplings, and unique relaxation properties. Usually, the most studied nuclei are proton [^{1}H], carbon [^{13}C], phosphorus [^{31}P], lithium [^{7}Li], fluorine [^{19}F], and sodium [^{23}Na]. Among these, hydrogen is the main nucleus investigated nucleus due to the high sensitivity to the hydrogen (^{1}H) nucleus and its abundance in molecules. Clinical imaging of the brain is commonly coupled to clinical MRS equipment during the analysis.

MRS has been widely used *in vivo* to assess brain alcohol levels, especially because it allows monitoring of ethanol-induced changes in the spectroscopically visible brain metabolites (Adalsteinsson et al., 2006; Ross and Bluml, 2001; Sammi et al., 2000; Hetherington et al., 1999). Ethanol is detectable by MRS *via* the methyl protons that can be identified by a distinctive triplet at the 1.3 ppm (parts per million) region of the spectrum.

As a matter of fact, because the two carbon atoms of the aliphatic chain are in different structural environments, each of them produces a distinct signal in the ^{13}C NMR spectrum of ethanol. The carbon linked to the more electronegative oxygen shifts its signal toward the left of the spectrum, while the carbon of the methyl group appears at the right of the spectrum.

Because ^{1}H MRS signals are considerably affected by their intramolecular environment, ethanol metabolite signals do not interfere with the signal of ethanol itself in the brain, which yields the most intense signals in such spectra (Xiang and Shen, 2011; Rooney et al., 2000; Fein and Meyerhoff, 2000; Hanstock et al., 1990).

1.5.1.2 Isotopic techniques

Isotopic techniques are widely used to detect a wide variety of chemicals, such as the metabolites of energy substrates in the brain. Combined with a radioactivity test and PET, ^{14}C- and ^{11}C-labeled ethanol molecules were used in a study with the aim to monitor ethanol metabolites in humans (Mushahwar and Koeppe,1972). However, the use of these isotopes had some disadvantages, in which a large dose of ^{14}C-labeled chemicals are known to produce dangerous radiation effects, while ^{11}C-labeled ethanol shows a short half-life of about 20 minutes (Rocchitta and Serra, 2013).

However, *in-vivo* ^{13}C MRS, combined with the infusion of ^{13}C-labeled ethanol, is commonly used to directly detect both ethanol and its metabolites in the CNS; ^{13}C-acetate, produced by aldehyde dehydrogenase, is extremely useful to study cerebral metabolism, neurotransmission, and neuronal–glial interactions in both humans and animals (Yun Xiang and Jun Shen, 2011; Dimitrakopoulou-Strauss et al., 1999).

1.5.2 Microdialysis

Microdialysis has been one of the most common techniques used in neuroscience since the 1970s to obtain information about the interstitial fluid composition, by inserting a dialysis probe into brain tissues (Ungerstedt and Hallström, 1987; Tossman and Ungerstedt, 1986; Delgado et al., 1972). The principles of microdialysis are the same as classical dialysis: the probe has a semipermeable membrane which separates two fluid compartments and allows passage and exchange of only low molecular weight compounds (Nurmi et al, 1994). An appropriate fluid (Ringer) is perfused through the probe and neurochemical molecules diffuse in both directions depending on their concentration gradients to move in and out of the probe (Figure 5).

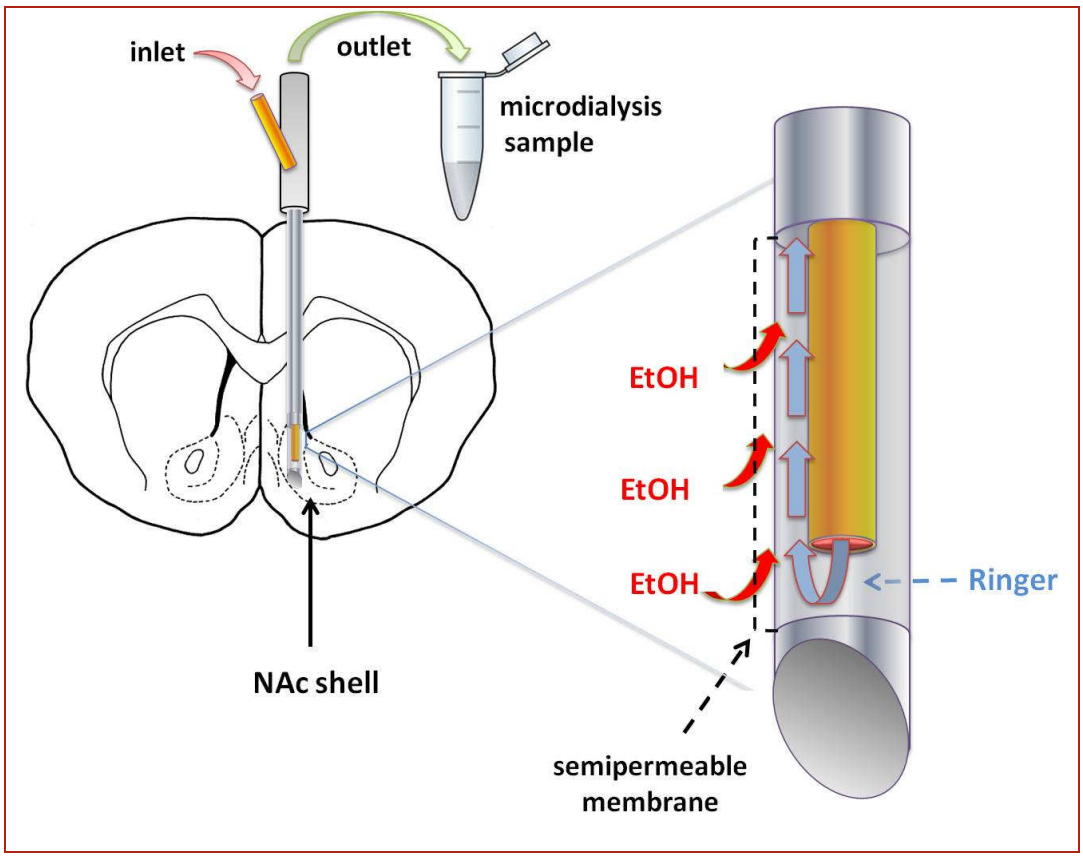

Figure 5: Scheme of ethanol sampling by means of a microdialysis probe

In this way, microdialysis allows the simultaneous sampling and unambiguous assignment of a wide range of chemical species in the tissue extracellular space (Bazzu et al., 2012; Bazzu et al., 2011).

However, this useful approach possesses some limitations such as invasiveness, poor temporal resolution, and the sensitivity of the chosen analytical technique, which is always needed to analyze the dialysate. The temporal resolution represents the main limiting factor, because several minutes are usually required to collect an adequate volume to allow the analysis of the sample by means of a suitable analytical technique, for example HPLC (High Performance Liquid Chromatography). Moreover, microdialysis is generally performed under non-equilibrium conditions. Thus, analyte concentrations are generally underestimated, because dialysate concentrations represent only a small fraction (which depends on the flow rate) of the real concentrations of the medium surrounding the microdialysis probe (Brunner and Langer, 2006). Despite these technical limitations, microdialysis has been demonstrated to be appropriate to detect ethanol levels in the CNS.

After sampling, ethanol concentration in the interstitial fluid is usually measured by means of gas chromatography technique (generally supplied with a headspace autosampler and flame ionization detector) or *via* an enzymatic assay, down to very low micromolar concentrations (Peris et al., 2006; Quertemont et al., 2003).

In vivo microdialysis has been applied in preclinical studies to investigate the relationship between ethanol-related behaviors and neurochemical variations (Gonzales et al., 1998). Furthermore, local perfusion of ethanol in specific brain region has been used to investigate the potential involvement of local mechanisms, and also to assess the effects of some therapies for alcoholism (Nurmi et al., 1994).

1.5.3 A new possible approach: Biosensors

The major limitations emerging from the description of the techniques described above are related to many factors. For spectroscopic techniques, despite their non-invasive approach that make them reliable for *in vivo* experiments in humans, ethanol cannot be detected for concentrations lower than millimolar levels, and only for a short time. Moreover, labeled chemicals could be toxic for long-term exposure, and the technique is applicable for only non-dynamic experiments.
For microdialysis, invasiveness limits its use in clinical trials, as do the need to use connecting tubes to carry out the experiments, and the low temporal resolution, especially to achieve an excellent recovery fraction by varying some microfluidic parameters (Bazzu et al., 2012; Bazzu et al., 2011).

Because ethanol concentration in the brain can vary dynamically, as well as those of the neurotransmitters it affects, its study would require a real-time approach. Biosensors are emerging tools which have already been demonstrated to be useful and reliable in the dynamic detection of a number of neurobiological molecules on a very short time-scale (Rocchitta et al., 2013; Secchi et al., 2013; Rocchitta et al., 2012; Mohd Zain et al., 2012; Calia et al., 2009; McMahon and O'Neill, 2006; Lowry et al., 1988). As a consequence, the monitoring of fast ethanol concentration changes represents an ideal field of application.

The biosensing technique is relatively recent, having been developed in the last decades thanks to its advantageous versatility, variety of applications, and in particular for its high temporal and spatial resolutions. Biosensors allow the detection of very low concentrations of several analytes *in vivo*. Because of their invasiveness, these tools have not proven to be suitable for clinical studies in humans, but they are still extremely reliable for preclinical studies of neurochemical modifications in the brain (see Table 10 in Section 5.7, and Rocchitta and Serra, 2013).

According to the IUPAC definition, a biosensor is a self-contained integrated device which is capable of providing specific quantitative or semi-quantitative analytical information using a biological recognition element (biochemical receptor) which is in direct spatial contact with a transducer element. A biosensor should be clearly distinguished from a bioanalytical system, which requires additional processing steps, such as reagent addition. Furthermore, a biosensor should be distinguished from a bioprobe which is either disposable after one measurement, *i.e.* single use, or unable to continuously monitor the analyte concentration (Thévenot et al., 2001).

A biosensor basically consists of two elements:

- the sensitive biological element, such as enzymes, antibodies, nucleic acids, cells or tissues which selectively recognize and reacts with the analyte (*e.g.,* enzyme substrate, antigen, complementary DNA, *etc*.) and generates a chemical or physicochemical signal. Enzymes are the most common type of biological element used in biosensors.

- a transducer which converts the signal resulting from the biological reaction into an electronic one. The intensity of the electronic signal generated on the transducer surface is directly or inversely proportional to the analyte concentration. An amperometric electrode is the most common transducer used in biosensors, and enzyme-based amperometric biosensors were designed and used in this thesis.

Owing to electrical interference generated by the electronic components and the transducer itself, the signal deriving from the transducer is usually low and overlaid on a noisy baseline. The subtraction of a reference baseline signal, the amplification of the resultant signal difference and the use of electronic filters allows minimization of the unwanted signal noise, thus generating an analyte-derived current. The analogue signal produced is then converted into a digital signal.

Finally a microprocessor converts the current into concentration units, easily monitorable on a computer display.

So, biosensors basically differ from chemical sensors by the presence of an immobilized biological element that permits the quantification of analytes by means of the biological reactions. Biosensors are normally grouped in three generations, based on the mechanism of how the response is generated:

- In first generation tools, the product or by-product of the biological reaction diffuses to the transducer surface, giving the electrical response.
- Second generation biosensors use specific mediators as intermediate between the biological reaction and the transducer, with the aim to improve the response.
- Finally, the third generation includes biosensors in which the response is caused by the biological reaction itself. In this case, no product or mediator is directly involved.

Biosensors can use very different transducers. For example, electrochemical (*i.e.*, amperometric, potentiometric or conductometric) and fiber optical transducers are commonly used in biosensors (Gronow, 1999). Each kind can be functionalized with a different biological elements. For the aim of this dissertation only a brief description of operation principles of the main electrochemical transducers is given.

1.5.3.1 How amperometric electrochemical transducers work

Electrochemical biosensors allow the specific analysis of several species with high selectivity and sensitivity in very rapid time. These tools are utilized in many fields for biochemical, forensic, industrial and environmental analysis. Potentiometric, conductometric and amperometric sensors are the main kind of electrochemical transducers (Gronow, 1999; Thévenot et al., 2001).

Potentiometric detection is based on the measurement of the potential generated by charge accumulation. Potentiometric biosensors exploit a reaction between a sensitive organic membrane or surface towards the analyte to generate a potential proportional to the logarithm of the concentration of the electrochemically molecule, compared to the reference electrode potential.

Conductometric biosensors exploit conductivity change of a medium as detection method. They are commonly used to quantify the change of the electrical conductivity of cell solution, in which the majority of reactions lead to a modification of solution ionic composition.

However, a very large number of biosensors have been developed based on amperometric transducers. In the majority of designs, immobilized enzymes represent the biological element, since they guarantee reproducible results as the same catalytic activity is preserved for a series of analyses. Amperometric transducers are therefore to be considered as reliable components when developing a biosensor based on an enzyme.
Amperometric biosensors function by the production of a current when a potential is applied between two electrodes. The measurable current is generated by a biological reaction, usually enzyme catalyzed. Amperometric biosensors indirectly detect non-electroactive analytes by means of the biological reactions generating an electroactive product or by-product, while a constant potential is being applied.

This approach is required because many biological compounds are non-electroactive. Then, the electroactive compound reacts with the transducer and leads to a change of current intensity proportional to the initial concentration of analyte (Kowalska et al, 2011; Vasylieva et al, 2011; Njagi et al, 2010; Ahmet Koyun, et al., 2012). Amperometric devices are able to quantify the electric signal produced both with voltammetric or amperometric techniques:

- Amperometry: a constant potential is applied between electrodes to drive the current

- Voltammetry: measures the current under controlled potential variations

CPA (Constant Potential Amperometry) is an amperometric technique which allows the measurement of the signal by using a hardware unit (potentiostat) to apply a constant potential. Commonly, *in vitro* amperometric experiments are performed in an electrochemical cell, using a three-electrodes system:

1-Working electrode (WE)
2-Reference electrode (RE)
3-Auxiliary (counter) electrode (AUX)

The measured current (faradaic current) is generated by the reduction (cathodic) or oxidation (anodic) of the target molecule at the working electrode surface.
Biosensors are forms of working electrodes. Their potential is maintained constant relative to a reference electrode by the potentiostat, which is able to adjust the 'balancing' current generated at the auxiliary electrode. In this way, biosensors work under constant voltage conditions, and the measured current resulting is related to the analyte concentration.
The reference electrode establishes the electrical potential against which the applied potentials is measured. One of the most common reference electrodes is the Ag/AgCl electrode, consisting of a silver wire coated with AgCl immersed in a NaCl solution.

The saturated calomel electrode (SCE: $Hg/Hg_2Cl_2/KCl(sat.)$) is also widely used.
The auxiliary or counter electrode consists of electrochemically inert materials (such as gold, platinum, stainless steel, or carbon), and generally has a bigger surface area than of the working electrodes. The counter electrode has a double operational mode: if the working electrode is operating as an anode, the counter electrode works as a cathode and *vice versa*. The half-reaction which occurs at the auxiliary electrode surface has to be fast enough not to limit the reaction at the working electrode. The potential of the auxiliary electrode is always adjusted (by the potentiostat) to balance the reaction occurring at the working electrode, allowing the potential of the working electrode to be measured versus the reference electrode (Kissinger and Heineman, 1996; Bard and Faulkner, 2000; Zoski, 2007).
Finally, among voltammetric techniques, cyclic voltammetry (CV) is generally used to determine diffusion coefficients and half-cell reduction potentials (Ahmet Koyun, et al., 2012).

1.5.3.2 Enzymes suitable for developing an ethanol biosensors: AOx *vs* ADH

Although other biological systems may be utilized in biosensor design (antibodies, nucleid acids, whole cells, tissues, *etc*.) we will focus on enzymes, the more commonly-used biologically responsive material, and particularly on suitable enzymes to develop an ethanol biosensor: oxidoreductase Alcohol Oxidase (AOx) and Alcohol dehydrogenase (ADH).

Enzymology refers to an oxidoreductase as an enzyme catalyzing the transfer of electrons from one molecule (electron donor) to another one (electron acceptor). The enzymatic reaction requires the presence of O_2, involves a reductant specie, an oxidant one, and a specific cofactors such as NAD^+, NADP (nicotinamide adenine dinucleotide phosphate), FAD (flavin adenine dinucleotide) or FMN (flavin mononucleotide). The big family of oxidoreductases enzymes includes the subclasses of dehydrogenase and oxidases enzymes.

Alcohol dehydrogenase belongs to the big subclass EC 1.1.1 of dehydrogenases, oxidizing enzymes which convert the substrate by a reduction reaction that transfers one or more H^- to a cofactor, which represents the electron acceptor. The subclass includes enzymes with NAD or NADP as acceptor such as malate dehydrogenase, glucose 1-dehydrogenase, L-lactate dehydrogenase and many others have been used in biosensing (http://www.chem.qmul.ac.uk/iubmb/enzyme/EC1/intro.html). Aldehyde dehydrogenase catalyzes the reaction (eq 1, see also Figure 2, Panel A):

$$\text{Ethanol} + NAD^+ \rightarrow \text{Acetaldehyde} + NADH + H^+ \qquad (1)$$

The subclass of oxidases, EC 1.1.3, consists of enzymes that catalyze an oxidation-reduction reaction involving molecular oxygen as the electron acceptor, being reduced to hydrogen peroxide (H_2O_2) or water. Even oxidase enzymes are usually linked to a cofactor. Malate oxidase, glucose oxidase, choline oxidase, cholesterol oxidase, catechol oxidase and alcohol oxidase all belong to the oxidase subclass.

The flavoprotein alcohol oxidases (Alcohol: O_2 Oxidoreductase) are enzymes that

catalyze the oxidation of alcohols to the corresponding carbonyl compounds by forming hydrogen peroxide. Based on substrate specificity, they are divided in four groups:

- SCAO short-chain alcohol oxidase
- LCAO long-chain alcohol oxidase
- AAO aromatic alcohol oxidase
- SAO secondary alcohol oxidase

In particular, Alcohol Oxidases EC 1.1.3.13 are SCAO flavoenzymes employing FAD as cofactor. These oligomeric enzymes consist of eight identical sub-units, each strongly bound to a FAD molecule (Azevedo et al., 2005).

AOx are chiefly present in bacteria, yeast, fungi, plant, insect, and mollusks. In particular, alcohol oxidases extracted from the yeast *Hansenula polymorpha* are contained in peroxisomes, where are involved in the first reaction of methanol utilization pathway. Because AOx has a low affinity for oxygen, a great number of this enzymes are synthesized to supply the poor catalytic activity and satisfy the cell's metabolic need (Cregg et al., 1989). These aspecific oxidoreductases are able to oxidize short-chain, saturated primary alcohols (*i.e*. methanol, ethanol, propanol or butanol) specifically acting on the CH-OH group of the electron donor. Unsaturated or branched-chain alcohols, as well as secondary alcohols, are not substrates of Alcohol Oxidase. AOx catalyzes the biochemical reaction (eq 2):

primary alcohol + O_2 → aldehyde + H_2O_2 *(2)*

Structural and kinetics characteristics of Alcohol Dehydrogenase have been already discussed in the ethanol pharmacokinetics Section 1.2 above. ADH is involved in the major pathway of ethanol metabolism, and its efficiency is closely related with the amount of NAD^+ co-factor available in the cytoplasmatic environment.

Several ADH-based ethanol biosensors have been developed and used in agri-food, chemical, forensic, clinical and industrial fields, generally demonstrating a very good stability and specificity (Gao et al., 2013; Zhen et al., 2011; Alpat and Telefoncu, 2010; Luo et al., 2008; Luo et al., 2008b; Liaw et al., 2006; Walters et al., 1998). Nevertheless, ADH-based biosensors require the external addition of NAD^+ as co-factor which needs to stay in intimate contact with the enzyme. In contrast, AOx-based tools do not require the adding of supplement cofactor in the medium to perform its catalytic reaction, because the FAD cofactor is already tightly bound to the redox center.

This important issue could result in limiting some uses of ADH-based biosensors, and drives the choice of using the more practical AOx as the biologically responsive material.

Moreover, in AOx-based biosensors it is simple to follow the changes of ethanol concentration by monitoring the decreasing of oxygen tension or alternatively by monitoring the concentration of the by-product hydrogen peroxide, which is easily oxidizable or reducible at the transducer surface. Because of these advantages, flavin-based redox enzymes are now widely used in several industrial processes (Smyth et al., 1999; Patel et al., 2001; Hämmerle et al., 2011), and make them extremely reliable for the development of miniaturized biosensors (Secchi et al., 2013; Goswami et al., 2013; Rocchitta et al., 2012).

2 - AIM

The detection of ethanol concentration dynamics in the brain kindles a particular interest because alcohol is the most widely-used psychoactive drug with global socio-economic and health consequences. Unregulated consumption can lead to toxic actions on peripheral organs and the CNS, as well as the development of a severe progressive disease called alcoholism, characterized by the disruption and alteration of the main CNS neurotransmitter systems.

Despite a wide range of studies, using different approaches, in attempts to investigate the complicated range of ethanol mechanisms of action and interactions in the brain, an insufficiency of detailed knowledge remains. This paucity is also related to limiting factors, such as time resolution, that affect the reliability of the detection methods used to date, mainly microdialysis and spectroscopic techniques.

Because ethanol concentration in the brain can vary dynamically, as do those of the neurotransmitters it affects, its optimal study would require a real-time approach, in which the temporal gap between ethanol arrival in the CNS and its interaction would be as short as possible. In this regard, the emerging 'biosensing' technique has been demonstrated to be a successful approach that allows the quantification of specific neurobiological molecules with high selectivity and sensitivity on a near real-time time scale.

Thus, the aim of this study was to develop, characterize and optimize an implantable amperometric biosensor, capable of real-time monitoring of the fast ethanol concentration changes in brain ECF of animals, to better clarify the cause-and-effect relationships existing between alcohol and the neurotransmitter systems it affects, as well as to provide a technique for the future testing of new drugs for the treatment of alcohol addiction.

3 - Experimental procedures

3.1 Chemicals, reagents and solutions

All chemicals were purchased from Sigma–Aldrich (Milano, Italy). Phosphate buffered saline (pH 7.4) was obtained by dissolving NaCl (8.9 g), NaOH (1.76 g), and NaH_2PO_4 (6.89 g) powders in 1 L of bidistilled water.

Alcohol oxidase stock solutions range from 100 to 800 U/mL were prepared in PBS from *Hansenula polymorpha* (AOx, EC 1.1.3.13). Hydrogen peroxide (H_2O_2) stock solution (100 mM) was prepared in bidistilled water by proper dilution of the original 30 % (w/w) solution. Ethanol solutions (1 M and 10 mM) were obtained from absolute ethanol by dilution in bidistilled water. Ascorbic acid solution (AA, 100 mM) was prepared by dissolving L-ascorbic acid in 0.01 M HCl. Polyethyleneimine (PEI) and glycerol (Glyc) solutions were obtained by diluting the stock solutions (50% w/v and 87% w/v, respectively) in bidistilled water.

ortho-Phenylenediamine monomer solutions (50, 100 and 300 mM oPD) were obtained by dissolution of the powder in different media. We tested several background electrolyte solutions, dissolving oPD in water (MilliQ, distilled or bidistilled), deoxygenated PBS, HCl (10 and 100 mM in water). Special caution is needed when using phenylenediamines.

Glutaraldehyde (GA, 1% w/v) and bovine serum albumin (BSA, 10% w/v) solutions were prepared in bidistilled water, while polyurethane solution (PU, 1% w/v) was obtained by dissolving PU beads in tetrahydrofuran (THF).

Teflon®-coated platinum (90% Pt, 10% Ir; Ø = 175 μm) and silver wires (Ø = 250 μm) were purchased from Advent Research Materials (Eynsham, England). Epoxy resin, Araldite-M and graphite were also purchased from Sigma–Aldrich (Milano, Italy). Ultrapure (>99.9%) oxygen and nitrogen were purchased from Sapio s.r.l. Special Gases Division (Caponago, Italy).

Ranitidine hydrochloride solution was prepared in saline (0.9 % w/v) immediately before *in vivo* administration.

3.2 Biosensor fabrication and characterization

All alcohol biosensor designs developed in this work were based on the same cylindrical geometry (see Figure 7, Section 3.4). Using a new sharp scalpel blade, the bare metal surface was exposed to a length of 1 mm (± 5%) and 125 μm diameter by cutting away the Teflon insulation (50 μm) from the tip of the wire (175 μm diameter). For a more accurate result, the cut was made under an optical microscope.Polymer deposition strategies

In this study we used different strategies in order to differentiate biosensors designs, modifying components and manufacture procedures. Nevertheless, all designs had in common the same approach for blocking interference species present in the target system, chiefly ascorbic acid (AA). Interference is a particularly marked problem when the biosensors are implanted in biological tissues for real-time monitoring.
The electro-deposition of a poly-*ortho*-phenylenediamine (PPD) nanometer-thick membrane has proven to be a reliable procedure to drastically limit the passage of AA trough the biosensor component layers, allowing simultaneously a good hydrogen peroxide permselectivity (Kirwan et al., 2007).
The PPD electrosynthesis was commonly performed starting from stock solutions of 300 mM oPD monomer dissolved in pH 7.4 nitrogen-saturated PBS. All the solutions were freshly prepared immediately before electropolymerization, carried out amperometrically at +0.7 V versus Ag/AgCl reference electrode, for a standard time of 30 minutes. In order to maximize the selectivity of the device, PPD deposition occurred at different stages of manufacture for the various biosensor designs. At first, the PPD layer was deposited over the enzyme layer already loaded onto the platinum wire surface(Figure 8, Section 3.6). Another approach was to electro-deposit the PPD directly on the bare metal, before the enzyme loading (Figures 9-11, Section 3.6).

3.3 Further characterization of PPD deposition strategies

In a different experimental environment, carried out in the *Biosensors & Electrochemistry Laboratory* of the *School of Chemistry & Chemical Biology* at University College Dublin, a further investigation of polymer deposition strategies was conducted.

The main purpose was to examine the behavior and the efficiency of the PPD polymer when dissolving the *ortho*-phenylenediamine monomer in media other than PBS, which had been used up to this point in our laboratory in Sassari. Furthermore, different oPD concentrations (50, 100 and 300 mM) were investigated in this study.

For each solution, pH and conductivity parameters were checked immediately after the electropolymerization was terminated (Figure 6). Electropolymerization conditions are shown in Table 7, Section 4.8

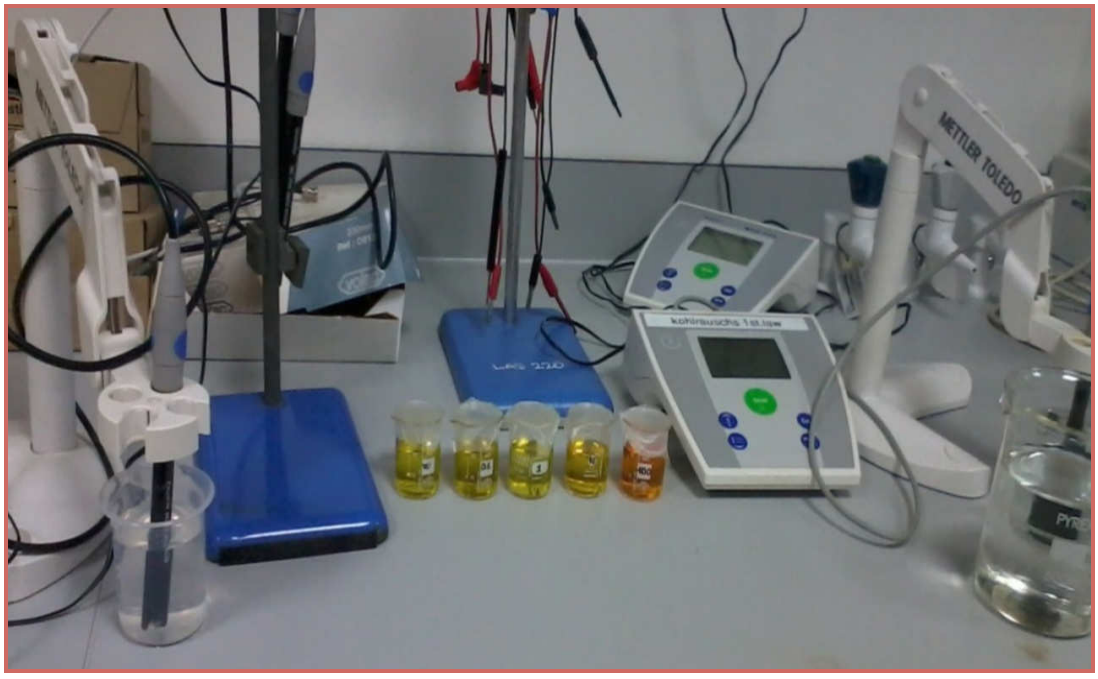

Figure 6 Different monomer solutions for pH and conductivity determinations

The effectiveness of novel polymer layers was assessed by comparing electropolymerization and AA-calibration parameter values such as *Q*(poly), $t^{1}/_{2}$(poly), I_{max}(AA), t_{max}(AA), as well as by calculating the biosensor apparent permeability parameters: P(HP)%, P(AA)%, and S% (see eqs 3–5, and Tables 8-9, Section 4.8).

Q(poly) is the integral of the electrodeposition current, measured from the baseline recorded before the sensors' immersion into the oPD solution and the limiting current reached at the end of the polymerization. *Q*(poly), expressed in mC. This is a measure of the number of electrons passed during the electropolymerization process, but not necessarily deposited on the surface, during the formation of the non-conductive polymer.

The time required by the sensors to complete the self-sealing electrodeposition (exponential decay; see Killoran and O'Neill, 2008) was evaluated and expressed in seconds as $t^{1}/_{2}$(poly) for each different monomer solution. It represents the half-life required to reach the polymerization limiting current, which indicates that no more electrons are transferred and the reaction is completed.

I_{max}(AA) reflects the polymer properties to reject the AA during AA calibrations, and indicates the maximum current reached by the biosensors when 0.5 mM AA was injected in the electrochemical cell, calculated as the difference between the baseline current and the AA peak, expressed in nA.

The value of t_{max}(AA) expressed in minutes indicates how fast the peak of 0.5 mM AA current (I_{max}(AA)) was reached, and is a measure of time response of the PPD to this interference compound (slow responses desirable).

The sensitivity of the bare platinum electrodes to H_2O_2 and AA, as well as for after the PPD coating, was calculated by using the slopes of the linear calibration plots. Apparent analyte permeabilities parameters P(HP)% and P(AA)% (Rothwell et al., 2009; O'Neill et al., 2008) have been used to quantify and compare the capacity of the various non-conducting polymers to allow H_2O_2 through while inhibiting the flux of the interference electroactive molecule AA to the electrode surface (Lowry and O'Neill, 1994; Centonze et al., 1994).

These parameters were determined for individual electrodes and then averaged over populations of sensors for each design. In this way, the small differences in sensors' dimension due to the Teflon removal (described in Section 3.4, see Figure 7), as well as intrinsic properties of PPD are normalized (Rothwell et al., 2009; O'Neill et al., 2008).

The H_2O_2 slopes (nA mM^{-1}) were obtained from linear regression analysis of the respective calibration plots for H_2O_2 at the same Pt electrodes, before and after polymer deposition (eq 3). Three injections of H_2O_2 (40, 80 and 120 μM) were made.

$$P(HP)\% = \frac{\text{Slope (HP) at Pt/PPD}}{\text{Slope (HP) at bare Pt}} \times 100\% \qquad (3)$$

Two injections of 0.5 and 1 mM AA were performed into the electrochemical cell. These concentrations were chosen because baseline brain AA levels are about 0.5 mM (Miele and Fillenz, 1996) and could reach millimolar levels during a period of behavioral stimulation (Boutelle et al., 1989; O'Neill and Fillenz, 1985). The apparent AA permeability for Pt/PPD was defined for 1 mM AA, calculated by plotting the AA slopes (nA mM^{-1}) obtained from linear regression analysis of the calibration plots for AA at the bare metal surface, versus the limiting currents obtained at 1 mM AA for PPD-modified electrodes (eq 4)

$$P(AA)\% = \frac{\text{IAA (1 mM) at Pt/PPD}}{\text{IAA (1 mM) at bare Pt}} \times 100\% \qquad (4)$$

where IAA(1 mM) at the bare electrode was determined as the numerical value of the slope (nA mM^{-1}) of the linear calibration plots for AA, and IAA(1 mM) at Pt/PPD was the effective plateau response (nA) for 1 mM AA at the same Pt surface following its modification by the PPD polymer. Thus, both numerator and denominator in eq 4 correspond to AA responses at the same concentration, imparting a dimensionless quality to P(AA)% (Rothwell et al., 2009; O'Nei et al., 2008).

Polymer selectivity (S%) was defined by eq 5 (O'Neill et al., 2008; Kirwan et al., 2007) and represents the percentage interference by AA in H_2O_2 detection (Rothwell et al., 2009).

For biosensor applications, the ideal value of S% defined in this way is zero. The use of equimolar concentrations in this definition allows S% to be interpreted as a permselectivity for two analytes with the same *z*-value, which indicates the number of electrons transferred per molecule. In the case of AA and H_2O_2 the *z*-value is 2.

$$S\% = \frac{IAA\ (1\ mM)at\ Pt/PPD}{IHP\ (1\ mM)at\ Pt/PPD} \times 100\% \qquad (5)$$

where IAA(1 mM) at Pt/PPD was the same as for eq 4, while IHP(1 mM) was determined as the numerical value of the slope (nA mM^{-1}) of the linear calibration plots for H_2O_2 at Pt/PPD. Values of parameters are presented as mean ± standard error (SEM), with *n* the number of electrodes (Rothwell et al., 2009; O'Neill et al., 2008).

3.4 Alcohol Oxidase immobilization and kinetics

The enzyme Alcohol Oxidase extracted from the yeast *Hansenula polymorpha* (EC 1.1.3.13), was immobilized as the biological element in all biosensor designs, using different concentrations of solution enzyme (Figure 7).

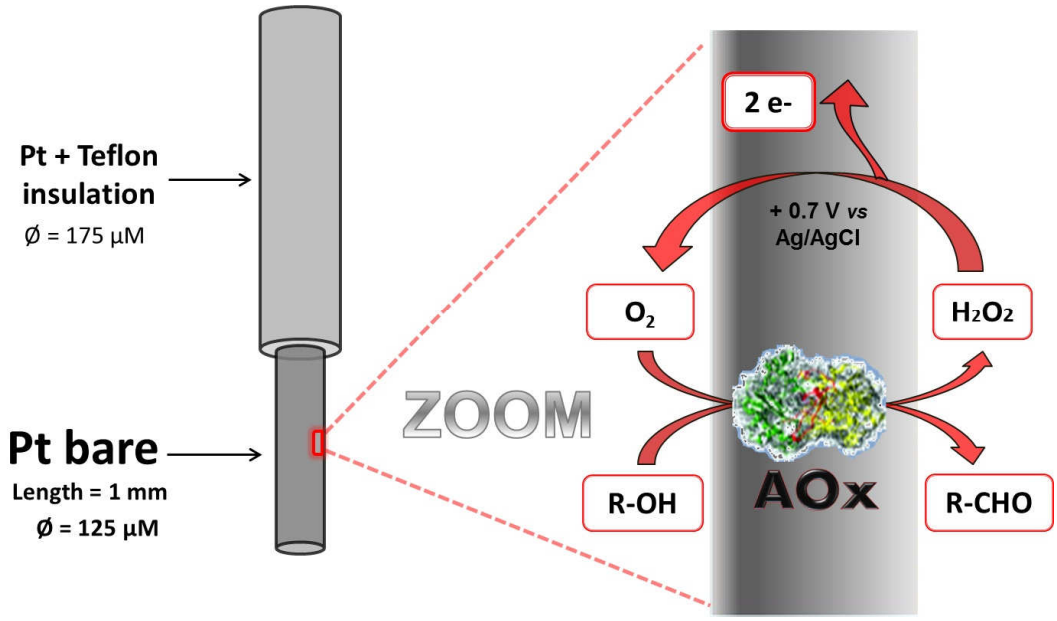

Figure 7 Schematic representation of ethanol biosensor

Five different enzyme solutions were prepared by dissolving the enzyme powder in 1 mL of PBS buffer (phosphate buffered saline), and the concentration expressed as units of protein dissolved per mL, specifically 100, 200, 400, 600 and 800 U/mL.
One unit of AOx catalyzes the oxidation of 1 micromole of alcohol to aldehyde and hydrogen peroxide per minute in an air-saturated solution at pH 7.5 and 25 ºC.

The technique of dip-evaporation, described here, was used to immobilize the enzymes at the biosensor surface. The biosensors were quick-dipped into the enzymatic solution, and then let dry at room temperature for 5–7 minutes in order to allow the evaporation of the solvent (water). This procedure was repeated 5, 10 or 15 times, depending on the number of dips required to make each biosensor design.

As already discussed (Section 1.5.3.2), AOx is an eight-subunit flavoprotein, each containing a flavin adenine dinucleotide (FAD) cofactor molecule, fundamental for the enzymatic activity. This aspecific enzyme catalyzes the oxidation of primary short-chain aliphatic alcohols (such as ethanol or methanol) into their respective aldehydes.

When AOx is immobilized in the biosensor, it reacts with its substrate to produce hydrogen peroxide (H_2O_2). With the use of the CPA technique (see Section 1.5.3.1), the hydrogen peroxide is amperometrically detected by oxidation at the Pt transducer surface, by applying a constant anodic potential of +0.7 V vs Ag/AgCl (eqs 6–8). The generated current is directly proportional to ethanol concentration (first generation biosensor, see Section 1.5.3.1) over the effective linear region of the Michaelis–Menten response plot.

$$RCH_2OH + AOx/FAD \rightarrow RCHO + AOx/FADH_2 \quad (6)$$

$$AOx/FADH_2 + O_2 \rightarrow AOx/FAD + H_2O_2 \quad (7)$$

$$H_2O_2 \rightarrow O_2 + 2H^+ + 2e^- \quad (8)$$

Immobilization procedures can affect the stability of the enzyme, and so the kinetic behavior of an enzyme deposited in a biosensor could change appreciably with respect to its activity in free solution.

Conformational alterations of the protein, due to internal structural changes or limited access to the active site, as well as the characteristic of the supporting material, and the co-deposition of other biosensor components could represent the reasons for these changes (Chaplin and Bucke, 1990).

As a consequence, Michaelis–Menten parameters for an immobilized enzyme are normally expressed in terms of apparent kinetics parameters, by expressing V_{max} as I_{max}, indicating a current response.

The form of the Michaelis–Menten enzyme kinetics equation (O'Neill et al, 2008), even for a two-substrate system (reactions 6 and 7), can be expressed for the alcohol EtOH as eq 9:

v= *??*I_{max}*??1+* *????K??*M *??(*EtOH*)??*

$$I = \frac{I_{MAX}}{1 + \frac{K_M(EtOH)}{[EtOH]}} \qquad (9)$$

Eq 9 expresses the rate of product conversion, and therefore of hydrogen peroxide flux, a fraction of which is detected at the electrode surface. Thus eq 9 is usually expressed in terms of current, for enzymes immobilized on amperometric biosensors, and I_{MAX} is the maximum biosensor signal recorded when the enzyme is saturated with substrate (O'Neill et al, 2008). Therefore, different values of I_{MAX} determined under the same conditions can reflect differences in enzyme activity (loading) on the biosensor surface.

The apparent Michaelis constant K_M is equal to concentration of substrate corresponding to half of the I_{MAX} response and is mainly determined by how avidly the enzyme binds its substrate. The K_M value is also important for determining the linear region slope (LRS), that can be approximated by I_{MAX}/K_M (O'Neill et al., 2008).

3.5 Enzyme stabilizers: PEI and glycerol

The use of enzyme stabilizers could be useful when immobilizing enzymes at a biosensor surface (Chaplin and Bucke, 1990). Generally enzyme stabilizers are positively charged molecules that interact with the negative charges of the proteins and help attain or recover the native conformation of the enzyme, limiting the internal structural changes and improving access to the active site. In this study we used two compounds, *i.e.*, polyethyleneimine (PEI) and glycerol (Glyc) with the aim to improve the enzymatic activity of AOx when immobilized on the biosensor surface.

PEI is a polycationic polymer formed by repeating units composed of an amine group (primary, secondary and tertiary) and a 2-carbon aliphatic spacer: $–CH_2CH_2–$. A 1% PEI solution was prepared by appropriate dilution of a 50% w/v commercial stock solution with bidistilled water.

Glycerol is a viscous polyol compound with an hygroscopic nature widely used in pharmaceutical formulations, and soluble in water due to the presence of three hydroxyl groups. A 1% solution was prepared by diluting in bidistilled water the 87% w/v stock solution. In addition, a mixed PEI-Glyc aqueous solution (both at 1%) was accurately prepared.

Enzyme stabilizers were immobilized with the dip-evaporation technique (Section 3.4), by alternating a dip in the stabilizer solution, letting the solvent (water) dry, and then dipping in the AOx solution. This protocol was repeated in relation to the number of dips needed.

3.6 Biosensors designs

The different strategies used to differentiate biosensor designs involved the variation of the sequence of PPD electro-deposition and of enzyme immobilization, as well as changes in the amount of enzyme loaded, the addition or co-addition of enzyme stabilizers, as well as their arrangement in the multi-layered pattern.

During the first stages of ethanol biosensors development, a constant enzymatic solution concentration of 200 U/mL was chosen, while varying the other components. Once the best configuration was found, AOx concentration was then varied, as discussed before. The main features of the developed designs can be schemed in four general groups (Secchi et al., 2013; Rocchitta et al., 2012; see Figures 8–11).

The first group is represented by the design in which AOx was deposited onto the platinum surface by dip-evaporation(Figure 8). Afterwards, the PPD layer was deposited upon the enzyme layer by electropolymerization (see Section 3.2).

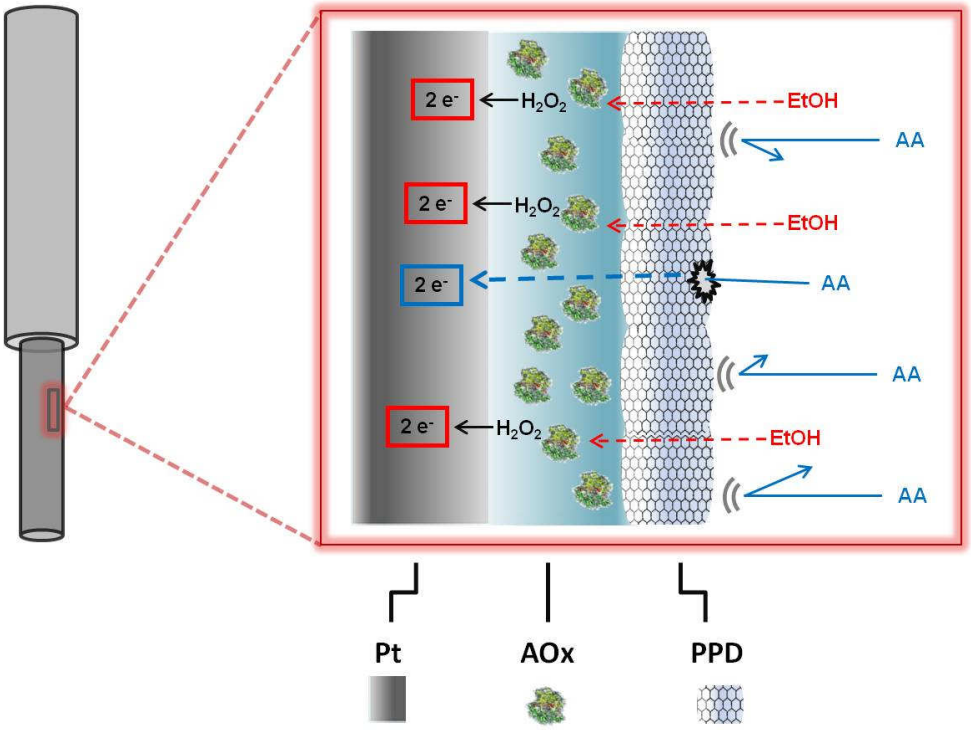

Figure 8: Schematic representation of the first design group

In the second group PPD layer was directly deposited on bare metal; the enzyme was then loaded over the polymer by dip-evaporation. After that, in order to immobilize the previously added layers, the biosensor was quickly dipped in a 1% PU solution (Figure 9). This precaution was also necessary because protease enzymes present in the brain can attack, damage and inactivate the core of the biosensor, *i.e.*, the AOx.

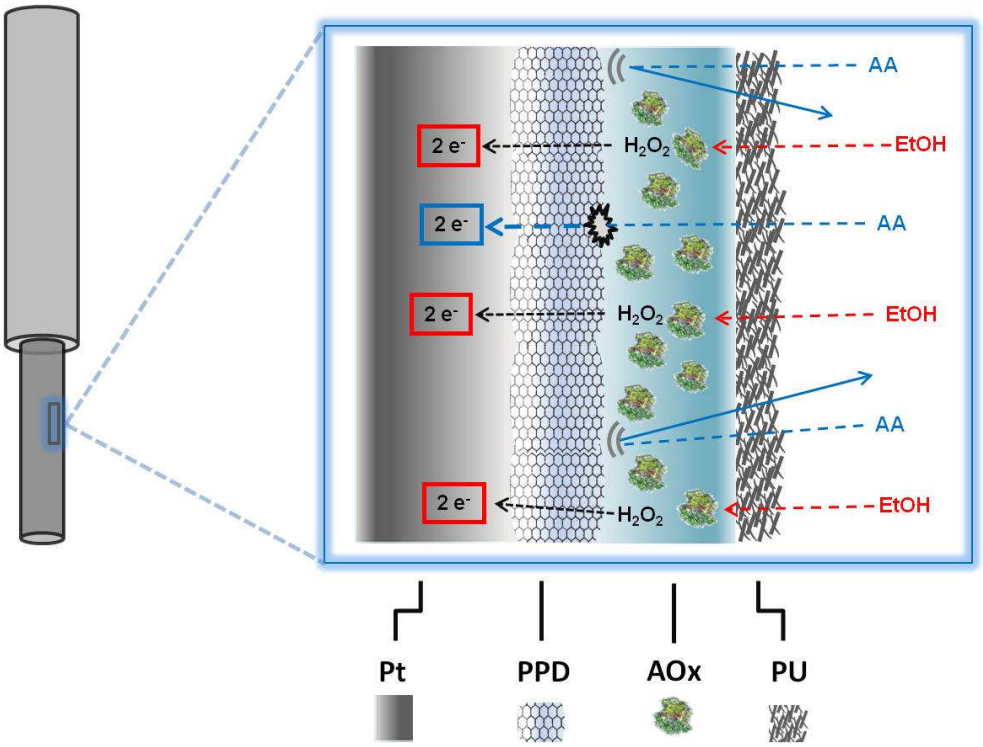

Figure 9: Schematic representation of the second design group

The third protocol involved PPD electrosynthesis on bare platinum, followed by the addition of AOx loaded by dip-evaporation. At this stage, however, an additional element was loaded: PEI, glycerol or their mixed solution were added by dip-evaporation (indicated as Enzyme Stabilizers (E.S.) in Figure 10). Finally, the biosensor was dipped in a 1% PU solution.

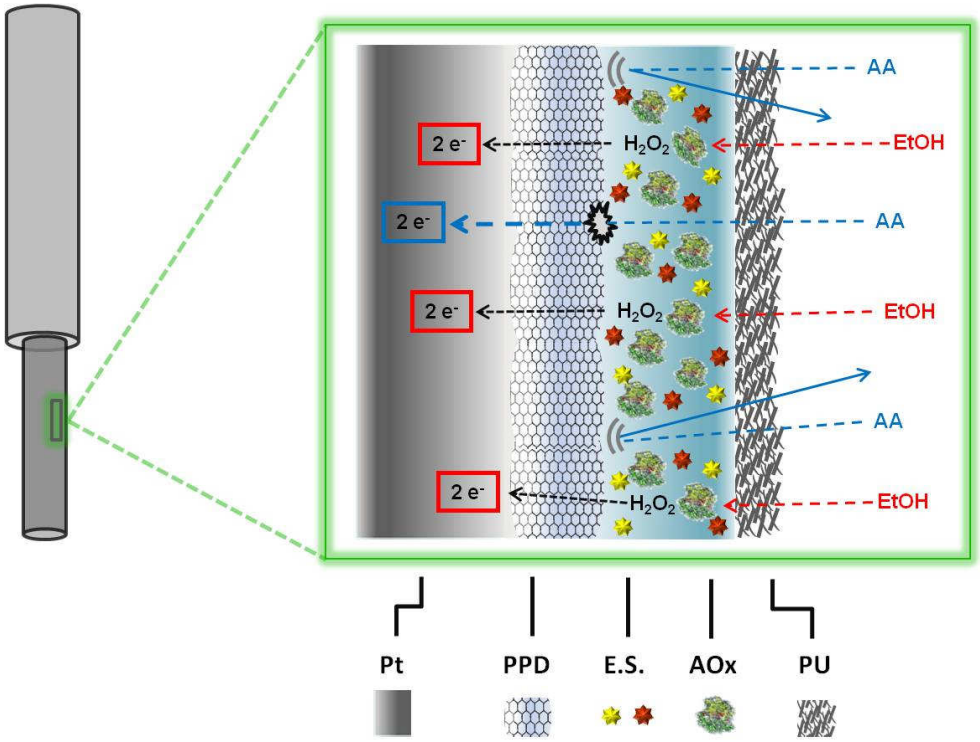

Figure 10: Schematic representation of the third design group

The fourth group followed the same scheme as the third one, but with a different "trapping net" used instead of the final PU layer. In fact, at this stage the biosensors were dipped in a BSA (10%) and GA (1%) solution. The cross-linking occurred between the three components (AOx, BSA and GA), trapping the biosensor elements (Figure 11).

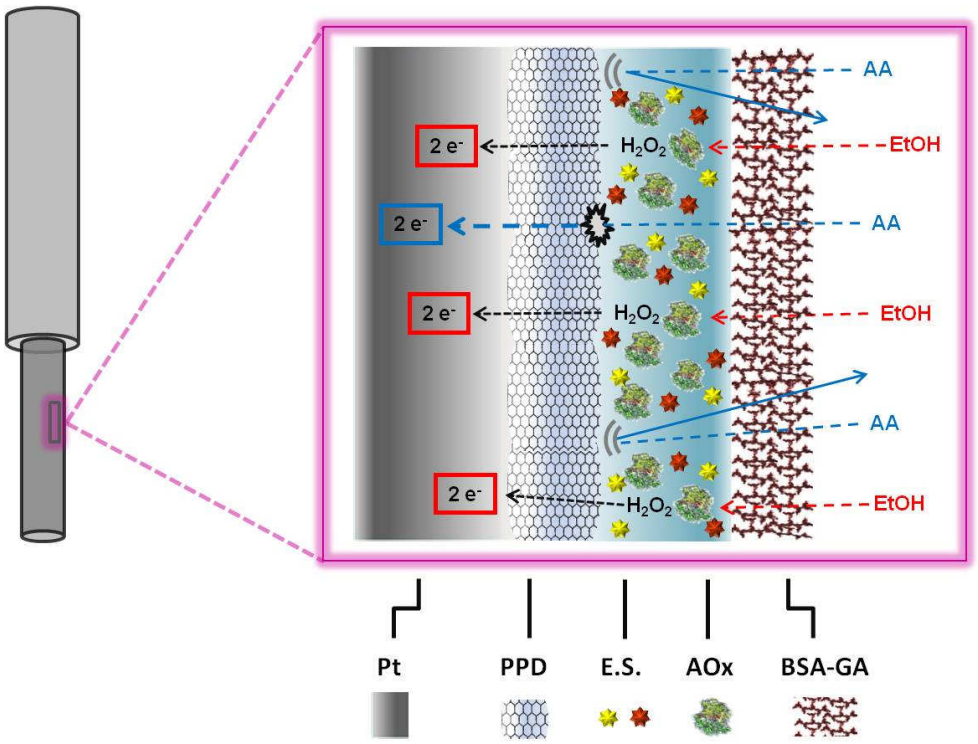

Figure 11: Schematic representation of the fourth design group

3.7 *In vitro* biosensor calibration

After their manufacture, all the biosensors were characterized *in vitro*. These studies were performed in an electrochemical cell containing 20 mL of fresh PBS at room temperature (23 ± 2 ^{o}C). The apparatus consisted of working electrodes (WE, ethanol biosensor, n=4), an Ag/AgCl (NaCl, 3 M) electrode as reference electrode (RE) and a large surface-area Pt wire as auxiliary electrode (AE).

Ethanol and AA calibrations were performed with CPA (see Section 1.5.3.1) by applying a constant potential of +0.7 V versus Ag/AgCl, using the four-channel equipment (eDAQ QuadStat, e-Corder 410, eDAQ, Australia) to respectively test ethanol response and AA interference blocking, respectively. AA was chosen as the representative interference specie of biosensor function because of its relatively high levels in brain extracellular fluids, compared with other electroactive molecules (Ryan et al., 1997). *In vitro* response to ethanol was assessed by following a protocol of 16 successive injections (0–120 mM) of known volumes of ethanol stock solutions (10 mM and 1 M) and fitted to eq 9, using nonlinear regression.

Figure 12 A-C shows an example of ethanol calibration time course (A) and calibration plots (B-C). The concentrations used correspond to: a):0.1 mM b):0.4 mM c):0.6 mM d):1 mM e):2 mM f):4 mM g):6 mM h):10 mM i):20 mM j):30 mM k): 40 mM. Injections made to reach the smaller concentrations (0.01, 0.02 and 0.05 mM) as well as those to reach the plateau of biosensor response (80 and 100 mM) were not included in Figure 12A

Injections of 0.5 mM and 1 mM of AA were made in fresh PBS (Figure 35, Section 4.8), in order to assess the blocking ability of the biosensor against the main interference species present in rat brain (Calia et al., 2009). All biosensors were calibrated immediately after their construction (day 0) as well as after 24 h (day 1). Among all studied designs, the four most promising biosensors were selected for a study of their stability over time (Sections 4.1.2 and 4.2.2). The criterion was based on their better ethanol sensitivity and AA shielding capability at day 1 relative to the other designs developed, as discussed is Sections 4.1.1 and 4.2.1.

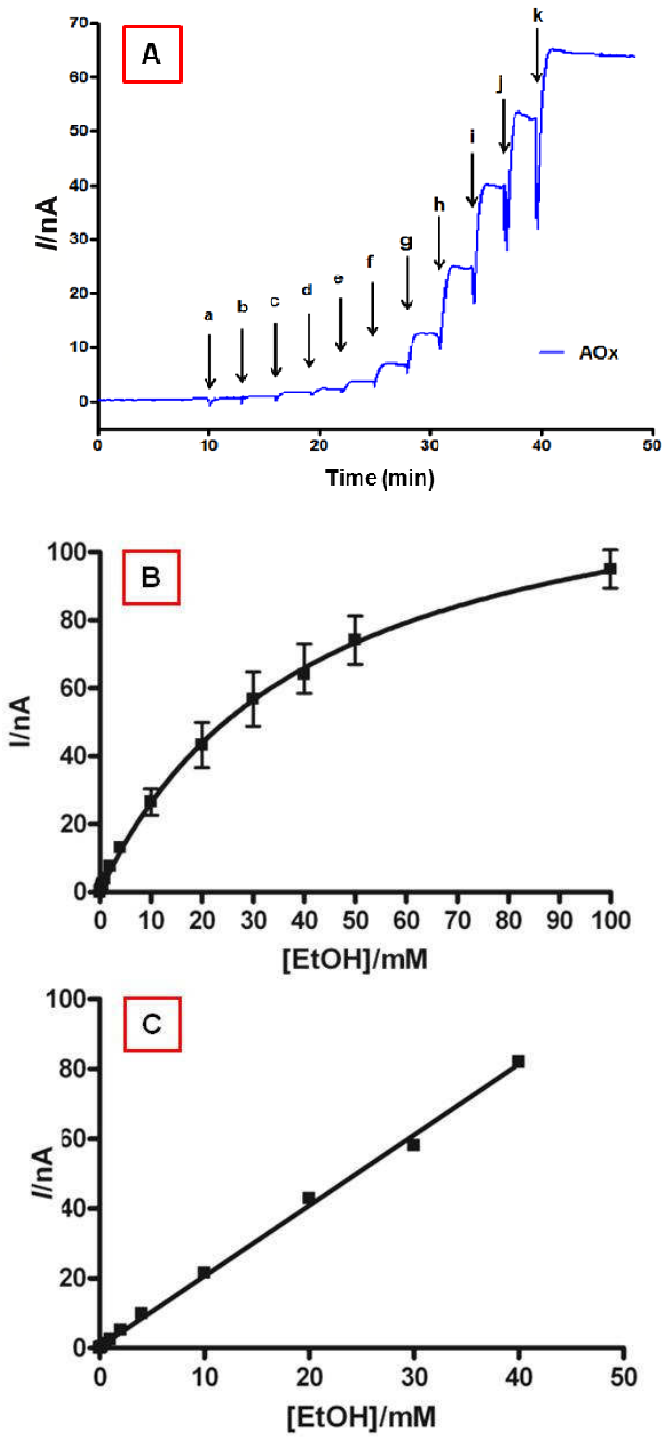

Figure 12: Typical ethanol biosensor response time course (A) and calibration plots (B-C).

The study over time was carried out by means of full calibrations of ethanol and AA from day 2 up to day 28 after the manufacture, by evaluating the trend values of parameters such as K_M, I_{MAX}, linear region slope, AA blocking, LOD and LOQ. After the calibrations the biosensors were rinsed with deionized water and stored dry in a fridge at 4 °C.

3.8 Preparation and calibration of oxygen microsensors.

The O_2 microsensors (Bazzu et al, 2009) were made using Teflon-insulated silver wires (30 mm in length; i.d. 125 μm) by modifying a previously described procedure developed in our laboratory (Migheli et al, 2008). Approximately 1 mm of the wire was exposed and inserted into a silica capillary tube (10 mm in length; i.d.) 180 μm, Polymicro Technologies, Phoenix, AZ) partly filled with graphite-loaded (55% w/w) epoxy resin (Araldite-M, Sigma-Aldrich, Milan, Italy). A preliminary 180 μm diameter carbon-composite disk electrode (area, 2.5×10^{-4} cm^2) was fabricated by mixing 850 mg of graphite powder with 500 mg of Araldite-M and 200 mg of hardener, and filling the silica capillary tubing with the mixture. The silver wire guaranteed a good electrical contact. After 24 h at 40 °C, the shape of the working electrode (WE) was transformed from circular to conical (Figure 13A) using a high speed drill (Dremel 300) equipped with an aluminum oxide grinding wheel.

The final O_2 microsensors had a length of about 250 μm, a surface approximately of 1.5×10^{-3} cm^2, and a tip <25 μm, dimensions well below those associated with significant tissue trauma caused by the implantation of larger probes (Duff and O'Neill, 1994; Fumero et al., 1994). Cellulose nitrate treatment was performed by immersing the WE in the colloidal solution three times and drying it for 60 min after each coat at 40 °C.

O_2 reduction was experimentally demonstrated on the microsensor surface (Figure 13B) starting from –350 mV vs Ag/AgCl, using cyclic voltammetry (CV37 voltammograph, BAS, Bioanalytical Systems Inc., West Lafayette) with a scan rate of 25 mV/s. Constant potential amperometry (CPA) was used for *in vitro* and *in vivo* calibrations and experiments, fixing the O_2 reduction potential at –400 mV vs Ag/AgCl reference electrode (Bazzu et al., 2009).

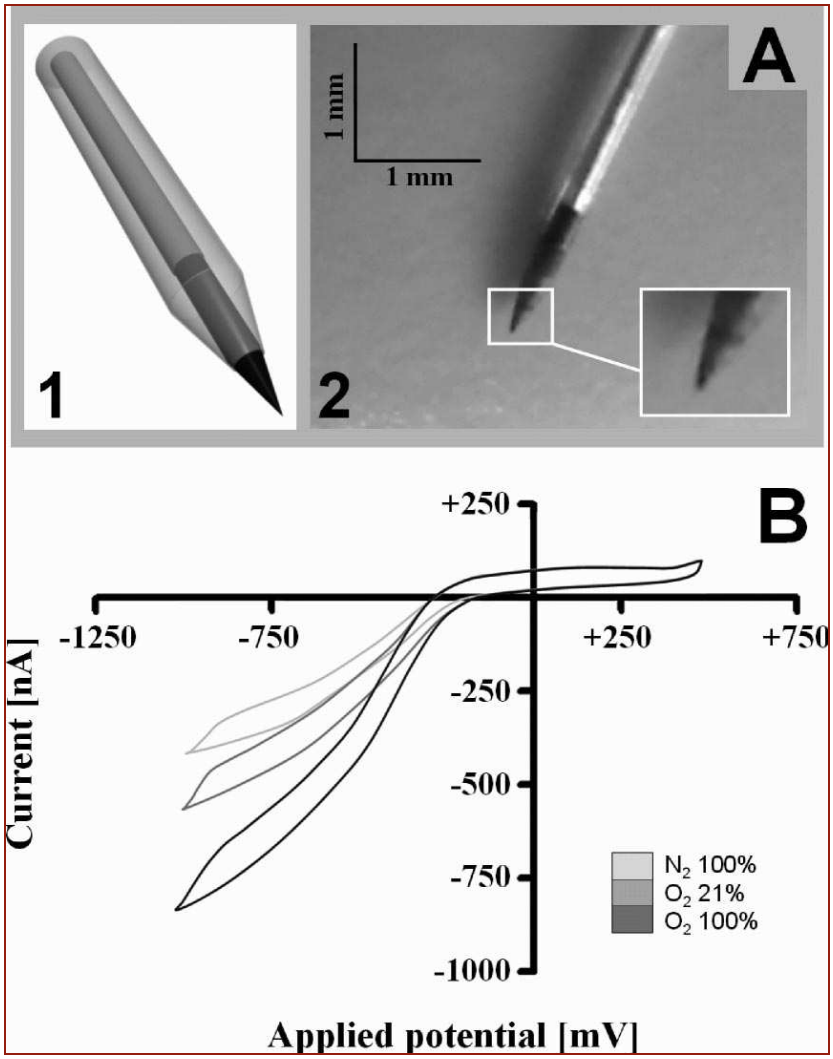

Figure 13 : Schematic (A1) and microphotograph (A2) of the conical oxygen microsensor developed and used in this study and its electrochemical characterization (B) (Bazzu et al., 2009).

No significant interference signals were observed on exposing the sensors to other electroactive molecules: ascorbic acid (AA); uric acid (UA); dopamine (DA); 3,4-dihydroxyphenylacetic acid (DOPAC) and homovanillic acid (HVA) present in the striatal extracellular fluid (Migheli et al., 2008), even at pharmacologically relevant concentrations (0.5 mM for AA, and up to 5 μM for the other neurochemicals).

Oxygen microsensors were calibrated by adding known volumes of a standard O_2 solution (100%) to nitrogen-saturated PBS in an air-tight electrochemical cell (Figure 14), in order to obtain an oxygen concentration ranging from 0 to 260 µM. A more accurate calibration was performed at low oxygen concentrations.

Figure 14 Picture of the apparatus used for calibrating O_2 microsensors and to test the oxygen dependence of ethanol biosensors.

3.8.1 Oxygen dependence study setup

The conical-shaped oxygen microsensor described above was used to monitor the dissolved oxygen in the electrochemical cell for the study of ethanol biosensors oxygen dependence. All the experiments were performed in a three-electrode air-tight electrochemical cell.

Due to the co-presence of three ethanol biosensors and one oxygen microsensor in the same cell, the application of two different potentials was required to allow oxygen reduction and H_2O_2 oxidation. Thus, the three ethanol biosensors were polarized at +0.7 V, while the oxygen microsensor was polarized at –0.4 V using a Ag/AgCl as RE.

The protocol used in the biosensors oxygen-dependence study is shown on Table 1, while an example of calibration time course is shown in Figure 16.

mL of O_2 -saturated buffer injected	Volume in the cell (mL)	O_2 in the cell [%]	O_2 in the cell [µM]
0	10	0	0
0.5	10.5	1	12.4
0.5	11	1.9	23.6
0.5	11.5	2.7	34
0.5	12	3.5	43.3
0.5	12.5	4.2	52
0.5	13	4.8	60
7	20	10.5	130
air bubbling (21%)	20	21	260

Table 1: Protocol used for the oxygen dependence study

Initially, the sensors were immersed in the cell containing 15 mM ethanol in a volume of 10 mL of PBS.

When a stable baseline for both oxygen microsensor and ethanol biosensor was reached (about 1 hour), the cell was saturated with pure nitrogen (arrow a, Figure 16), bubbled in directly from a cylinder (100% N_2), using an appropriate apparatus of tubes and syringes (Figure 15, left).

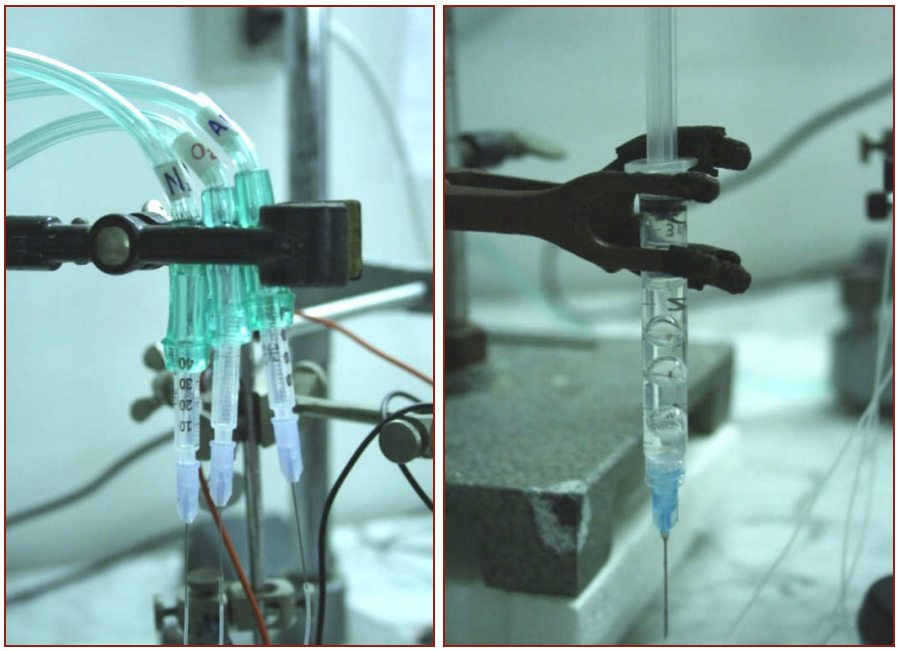

Figure 15 Syringes and tubes used to inject the different gas into the cell (left) and the pure O_2 saturated PBS syringe (right).

When the sensors were polarized and had reached a stable baseline current, known aliquots of a 100% oxygen-saturated PBS solution containing 15 mM of ethanol were added (Figure 15, right), ranging from 0 (100% N_2) to 260 µM O_2 (Table 1). In this way, the PBS volume in the cell passed from 10 mL up to 20 mL, but the ethanol concentration remained the same for the entire experiment course.

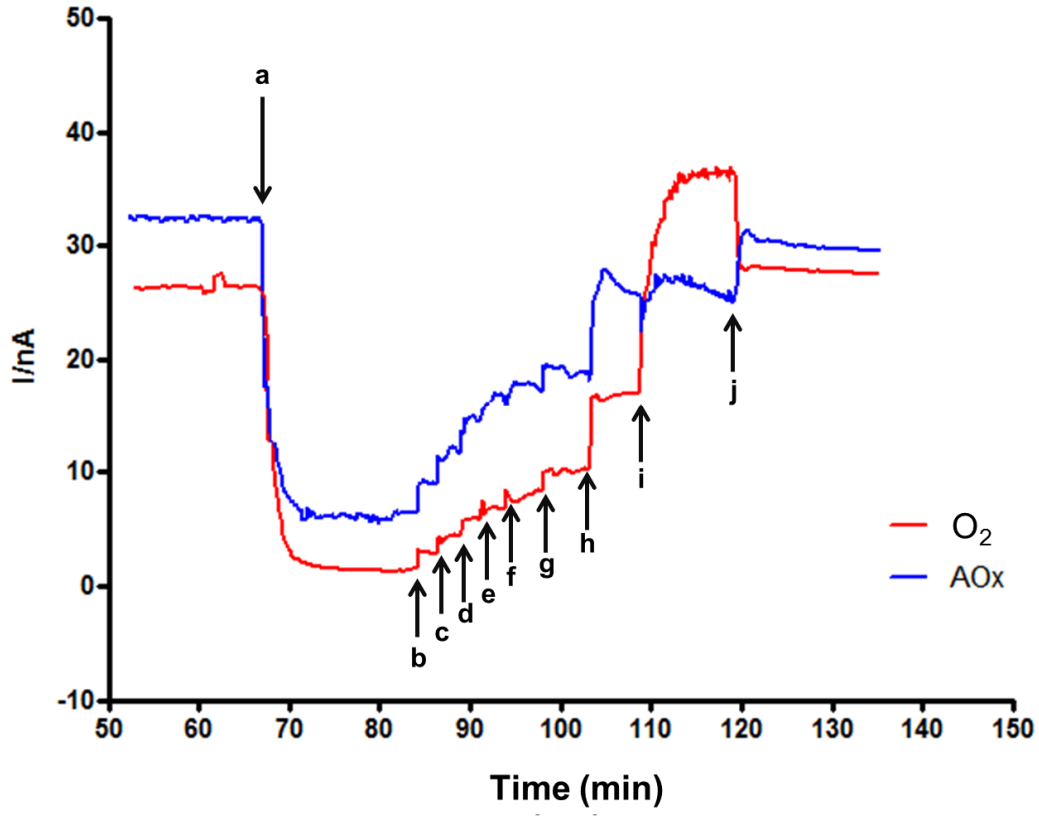

Figure 16: Biosensors oxygen dependence experiment. O_2 current values are inverted. Arrows correspond to: a) 100% N_2 bubbled into the cell b): 12.4 µM O_2 c): 23.6 µM O_2 d): 33.9 µM O_2 e): 43.3 µM O_2 f): 52 µM O_2 g): 60 µM O_2 h): 130 µM O_2 and i): bubbling O_2 (21%) j) stop bubbling 260 µM O_2.

The presence of the oxygen microsensor assessed the variation of the oxygen concentration in the electrochemical cell, as shown on Figure 16. Oxygen current values (red) were inverted for an easier graphical interpretation. When nitrogen was bubbled (arrow a, Figure 16), a decrease in sensor currents was observed, due to the decrease in oxygen tension and the absence AOx electron acceptor substrate. Then oxygen was added in the N_2 saturated cell, and biosensor activity gradually increased (blue) as [O_2] became higher. Tested oxygen concentrations were: b): 12.4 µM c): 23.6 µM d): 33.9 µM e): 43.3 µM f): 52 µM g): 60 µM h): 130 µM and i): 260 µM. The last concentration was reached by bubbling air into the tight electrochemical cell (arrow i, Figure 16).

The limiting currents for both types of sensors were reached immediately after the bubbling was stopped (arrow j, Figure 16,), and reached approximately the same baseline values for the corresponding oxygen concentration.

3.9 pH and temperature dependence study setup

Variation in pH values in the brain could affect ethanol biosensor performance. The optimum pH for the enzyme Alcohol Oxidase used in our study, extracted from *Hansenula*, ranges from 5.5 to 8.5, as previously described (Barsan and Brett, 2008). The influence of pH on biosensor activity was studied at room temperature, by preparing different PBS solutions ranging the pH from 6.0 up to 9.8. The tests were conducted on the more suitable biosensor design for *in-vivo* implantation, selected on the basis of the oxygen dependence results (see discussion on Sections 4.3 and 5.4). The study was carried out by injecting a fixed ethanol concentration (15 mM) in each pH sample (Rocchitta et al., 2012). The relative currents obtained from each experiment were then plotted, as shown in Figure 30 of Section 4.5.

The temperature dependence was also determined for 15 mM EtOH at physiological pH (7.4) in a range between 20 and 40 ^{o}C (Figure 31, Section 4.6).

3.10 Biotelemetric device hardware

The electronic circuit of the implantable biotelemetric device was built using surface mount components and comprised two different parts: the amperometric module and the microcontroller/transceiver module (Figure 17).

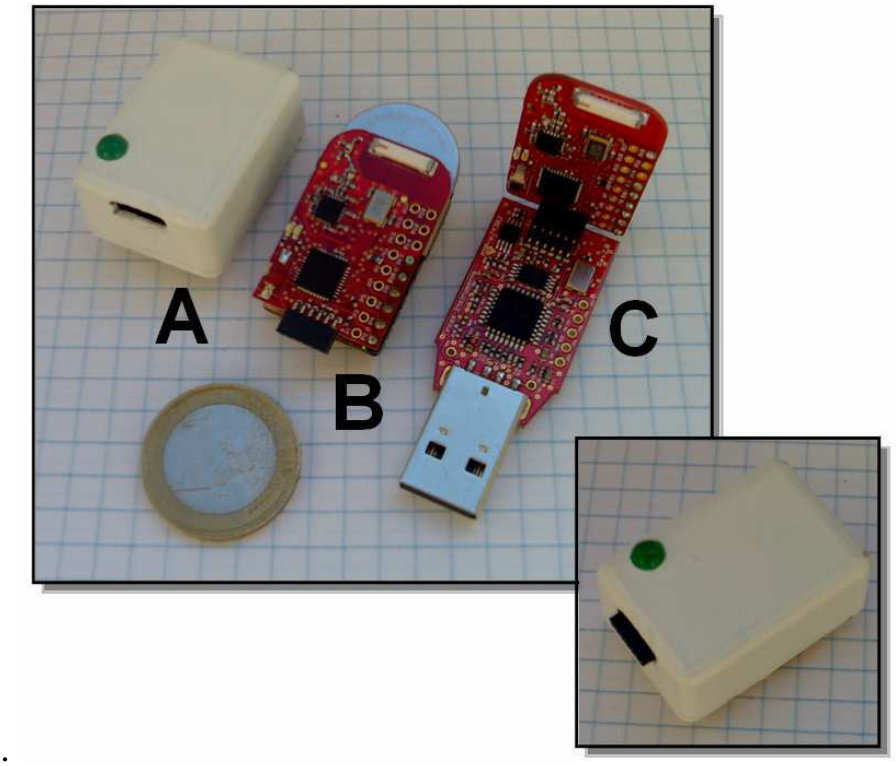

Figure 17 The biotelemetry system used in this study ((Rocchitta et al., 2012; Bazzu et al., 2009).

The amperometric module (Figure 17) was made soldering a quad operational amplifier (OPA, MCP6044), a Zener diode (ZXRE4001), four resistors, and one capacitor on a 30 mm × 18 mm PCB.

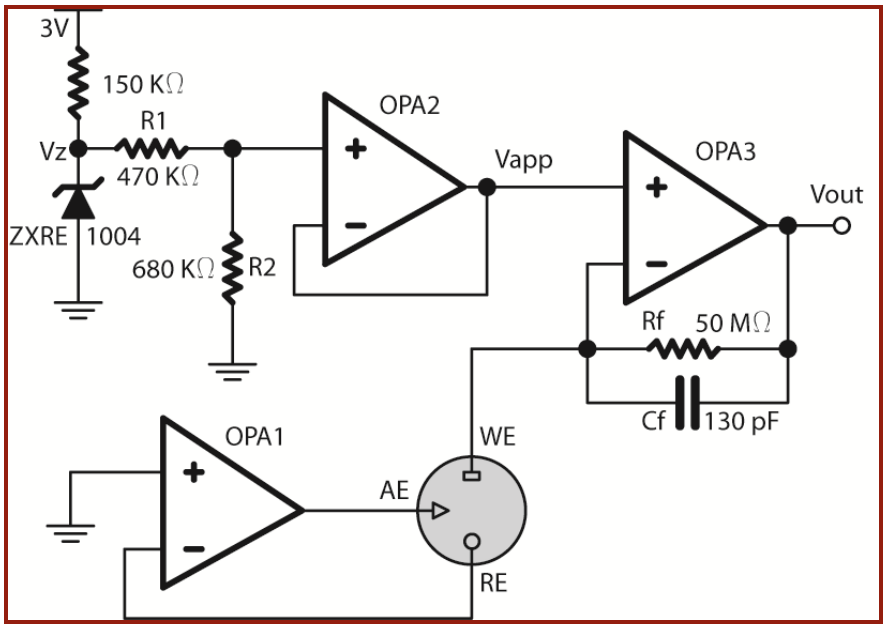

Figure 18 Circuit diagram of the amperometric module made by soldering a quad-OPA integrated circuit, a zener diode, four resistors and one capacitor on a 30 mm × 18 mm PCB incorporated in a small plastic enclosure. A microcontroller-driven digital module, an AM radio transmitter and a lithium battery completed the miniaturized device weighing only 12.4 grams. A detailed explanation of how thecircuit works is provided in the text (Rocchitta et al., 2012; Bazzu et al., 2009).

The MCP6044 can operate from a single-supply voltage with "rail-to-rail" inputs and outputs; it has been designed for micropower applications consuming only 600 nA per OPA with low input bias current (1 pA) and high input resistance (>1013D). The zener diode plays a pivotal role in the amperometric circuitry: as bandgap voltage reference, it generates a fixed voltage (1.22 V) consuming around 10 EA in virtue of a limiting resistance (150 k_). The non-inverting input of the potentiostat (OPA1) was grounded, resulting in a positive potential applied to the working electrode (WE) ranging from 0 V (GND) to 1.22 V. The inverting input of the potentiostat was directly connected to the reference electrode (RE) and its output wired to the auxiliary electrode (AE). This allows the implementation of a feedback circuit in which RE and AE potentials are maintained at the 2 same value as the non-inverting input (potentiostatic circuit). The buffered voltage divider, composed of two resistors (R1 and R2 in Figure 18) and the voltage follower (OPA2), generated the fixed potential (+700 mV vs GND) necessary to polarize the WE (ethanol biosensor).

The current-to-voltage (I/V) converter is a single-supply adaptation of a classic transimpedance amplifier (OPA3, Figure 18) and derived from previously published designs.[1-5] The transfer function of the I/V converter is:

$V_{out} = -(IOx \cdot R) + V_{app}$ *(10)*

in which IOx is the current flowing through the WE, R is the feedback resistor and Vapp is the potential applied to the WE (vs GND). A maximum anodic current of about 40 nA can be read without saturation (Vapp = 0.7 V; R = 50 MD). A feedback resistor (Rf, Figure 18) with a capacitor in parallel (Cf) completes a low-pass filter with a cut-off frequency (Fcut-off) of 25 Hz. The value of Cf was calculated in Farads according to the equation:

$Cf = 1 / (Fcut\text{-}off \bullet 2\pi \bullet R)$ *(11)*

A dummy cell was made based on a previously published design for testing the amperometric module of the biotelemetric device before sensor calibration (Serra et al., 2007). The aim of the design was to devise a Thevenin current source which would reproduce the constant amperometric response of a true electrochemical cell. The voltage applied to the dummy cell was generated between the WE and RE/AE and is equal to the voltage difference between the above electrodes. The resulting currents were converted in an output voltage (Vout) as illustrated in Figure 18. Data obtained from electronics calibration were similar to those obtained in previous studies (Rocchitta et al., 2007; Calia et al., 2009; Bazzu et al., 2009). The PIC12F683 (Arizona Microchip) is the heart of the digital module. This is a 8-bit CMOS IC with low power features equipped with internal 10 bit ADCs. The microcontroller unit (MCU) performed the A/D conversion of Vout and Vapp voltages. After the digital signal processing (DSP) of acquired raw data, a serial data packet was generated and sent to the 433.92 MHz Amplitude Modulation (AM) transmitter (RT4-433.92, Telecontrolli. IT). In conjunction with the MCU, this component allows the realization of a serial data transmitter working at a speed of 2400 baud. A short range, miniaturized “loop” antenna was designed and integrated into the PCB board (Myron Loewen. 2003).

The in-circuit-serial-programming 3 (ICSP) bus provides the possibility of programming the MCU "on-board" in a few seconds. A 210 mA h, 3 V lithium coin battery (Maxell CR2032) provided the power to the biotelemetric device for up to three weeks of continuous transmission (0.067 Hz). A small plastic enclosure (32 × 21 × 14 mm) completed the mountable device, weighing 12.4 g including battery. A RR3-433.92 module (Telecontrolli. IT) was selected as AM receiver and connected to a personal computer (PC) by means of a serial-to-universal serial bus (USB) converter (FTDI-FT232R-based module).

3.10.1 Firmware and software

The firmware to drive the PIC12F683 MCU was realized in Microchip assembly language (MPLAB) freely available from www.microchip.com. The program consisted of a timer-interrupt routine for digitizing analogue values (Vapp and Vout) at fixed time intervals. When the analogue signals were digitized, the hardware ADC resolution (10 bit) was improved following an oversampling and averaging method,1 increasing the ADC resolution to 12 bits. The software, running on the PC under Windows XP Professional™ or Windows 7™, communicates through the USB. The graphic user interface was developed using Profilab ExpertR (version 4.0 from Abacom), whereas the dynamic link library (DLL) serial-data-parser was programmed in C (Dev-C++ ver. 4.9.9.2) (Rocchitta et al., 2012; Bazzu et al., 2009).

3.11 Animals

Male Sprague-Dawley rats (Charles Rivers, Milan, Italy), weighing 280–330 g, were used for *in vivo* experiments. The rats were maintained under standard animal care conditions (12 h / 12 h light/dark cycle, light on at 07.00 h; room temperature 21 °C), with food and water provided *ad libitum*. Prior to the start of any experimental procedure, the health of the animals was assessed according to published guidelines (Wolfensohn and Lloyd, 2003). All procedures were specifically licensed under the European Community directive 86/609 included in Decreto No. 116/1992 of the Italian Ministry of Public Health.

3.11.1 Stereotaxic surgery and in vivo experimental procedures

The alcohol biosensors, as well as the silver reference electrode (RE) and auxiliary electrode (AE) were implanted under chloral hydrate (400 mg kg^{-1} i.p.) anesthesia. For accurately implant the biosensors in the right *nucleus accumbens* (shell) of the rats, coordinates from the atlas of Paxinos and Watson were used:

+1.7 A/P from the bregma

–0.9 M/L from the dura

–7.6 D /V from the dura.

The reference and auxiliary electrodes were implanted in the left parietal cortex (Figure 19), and two screws were inserted in the skull for reinforcing the biotelemetric device adhesion. The “basement” portion of the device (without battery) was fixed to the skull using dental cement (Paladur, Heraeus Kulzer, GmbH), and the electrodes were connected and the skin was sutured (Figure 20A).

A “dummy cover” was coupled to the “basement” to prevent its fouling. Body temperature during anesthesia was maintained at 37 °C by means of an isothermal heating pad.

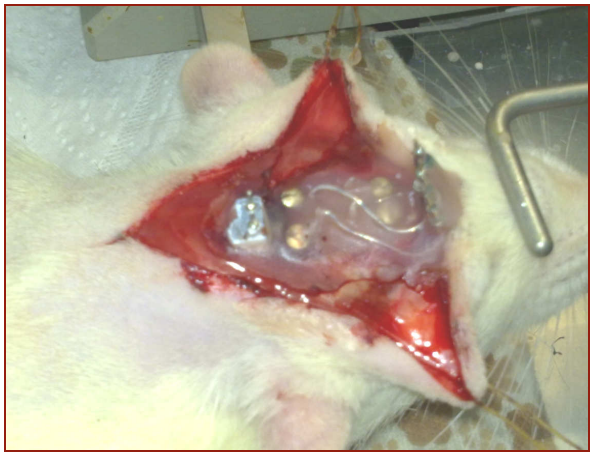

Figure 19 Photograph of the neurotaxic surgery for biosensors implantation

Figure 20: How the animals appear immediately after the implant still anesthetized (A) and before the *in vivo* experiment in its bowl at day 1, coupled with the telemetric device (B).

After the surgery the animals were housed in large plastic bowls (45 cm diameter) and maintained in a temperature- and light-controlled environment, with food and water *ad libitum*. The *in vivo* experiments started 24 h after surgery (day 1), coupling the rats with the telemetric device (see Section 3.10 and Figure 17) and were performed maintaining the animals in their own bowl (Figure 20B). In this way, rat free movement is guaranteed, and handling and other forms of stress are significantly reduced (Bazzu et al., 2009; Calia et al., 2009). The alcohol biosensor was polarized at + 0.7 V and the telemetric signal recorded (see Section 4.7, Figure 34) until a stable baseline was obtained. In a control group of animals (n = 3) intra gastric (i.g.) ethanol (1 g kg^{-1}) was administered 20 min after the intra peritoneal (i.p.) injection of saline (1.5 mL). Using a similar protocol, a selective inhibitor of alcohol dehydrogenase (as discussed in Section 1.2.1), ranitidine (30 mg kg^{-1} dissolved in 1.5 mL of saline), was administered i.p. (El-Bakary et al., 2010) in a second group of rats (n = 3). The biosensor current was monitored for 2 hours after ethanol administration (see Section 4.7, Figure 34).

3.11.2 Histology

Following the experiments, an overdose of chloral hydrate (800 mg kg^{-1} i.p.) was used to sacrifice the rats. The location of biosensors was confirmed by post-mortem histology. Brains were fixed in formal saline, and 50 mm coronal sections made with a cryostat. The slices were stained with cresyl violet and examined under a microscope (data not shown).

3.12 Statistical Analysis

Currents were expressed in nanoampere (nA) and given as baseline-subtracted values ± standard error of the mean (nA or ΔnA ± SEM). The AA Δ*I* value represents the difference between the current resulting from the injection of 1 mM and 0.5 mM AA in the electrochemical cell (Ryan et al., 1997). The limit of detection (LOD, eq 12) and limit of quantification (LOQ, eq 13) were determined using a statistical method based on the standard deviation (σ) of the response and the linear region slope (LRS) of the calibration curve (www.ich.org , 2005).

$$LOD = 3.3\ \sigma / LRS \qquad (12)$$

$$LOQ = 10\ \sigma / LRS \qquad (13)$$

Variations in hydrogen peroxide sensitivity were calculated as percentage changes compared to enzyme-free sensors responses (100%). Statistical significance (*p* values) between groups was evaluated using unpaired *t*-tests. Concentrations of dissolved O_2 were expressed in micromoles per liter while the oxygen reduction current was expressed in nA ± SEM. The sign of the oxygen currents (cathodic) was inverted to improve the readability of these data.

In vivo statistical significance between groups was evaluated by averaging signals at different times and calculating unpaired *t*-tests, as illustrated in Figure 34 of Section (Secchi et al., 2013; Rocchitta et al., 2012).

4 - Results

4.1 Biosensors response to ethanol and ascorbic acid

4.1.1 Comparison at day 1

For each different amperometric biosensor design (n = 4 for each group) the sensitivity to ethanol and ascorbic acid at day 1 was compared *in vitro*, because day 1 would be the critical time of the *in vivo* monitoring for the implanted biosensors.
Ten different biosensor designs were characterizated in terms of the apparent Michaelis–Menten kinetic parameters (I_{MAX} and K_M, eq 9) and AA interference parameters (Tables 2). Ascorbic acid interference values are expressed as 1 mM AA limiting current and AA ΔI, resulting from the difference in the measured current in the transition from 0.5 to 1 mM AA). Moreover, ethanol sensitivity of the ten different biosensor designs was analyzed in terms of linear region slope (LRS), LOD and LOQ (Tables 3, eqs 12 and 13).
The basic design is named design 1:

1 - Ptc/AOx_{10}/PPD

As schematically represented in Figure 8, the enzyme AOx (200U/mL) was loaded onto the bare metal by means of 10 dips into the enzymatic solution, being let dry between each dip (see dip-evaporation technique description, Section 3.4). Afterward it was coated with the PPD layer. Design 1 resulted in a very low response in terms of both I_{MAX} (2.95 ± 0.75 nA, R^2= 0.962), and LRS (0.05 ± 0.05 nA mM^{-1}, R^2= 0.979), coupled with a high K_M value (82 ± 10 mM); the response to 1 mM AA was 1.90 ± 0.21 nA.

In design 2, component disposition was inverted, and coated with PU:

2 - Ptc/PPD/$[AOx]_{10}$/PU (1%)

PPD was electropolymerized on bare metal (see Section 3.2) and Alcohol Oxidase immobilized over the polymer by means of a 10 dip-evaporation sequence. Then, the sensors were dipped once in a 1% PU solution as a "containment net" (Figures 9-10). As shown on Tables 2 and 3, this change did not significantly increase the I_{MAX} (3.84 ± 0.30 nA, R^2= 0.993) and the LRS (0.032 ± 0.035 nA mM^{-1}, R^2= 0.994), as well as the K_M (73 ± 12 mM). This design, however, showed one of the best shielding power against 1 mM AA (0.99 ± 0.02 nA, with a ΔI of 0.19 ± 0.01 nA).

Next designs (3-5) were obtained by adding the enzyme stabilizer PEI to design 2. The sensors were alternatively dipped first in a 1% PEI solution, then into the AOx solution (Figure 10). Different number of dips in both enzyme stabilizer and Alcohol Oxidase solutions were tested.

3 - Ptc/PPD/$[PEI(1\%)/AOx]_5$/PU(1%)
4 - Ptc/PPD/$[PEI(1\%)/AOx]_{10}$/PU(1%)
5 - Ptc/PPD/$[PEI(1\%)/AOx]_{15}$/PU(1%)

This led to a quite large increase in I_{MAX}, K_M and slope relative to design 1 (Tables 2 and 3). Increasing the number of PEI/AOx dips from 5 (design 3) to 10 (design 4) and 15 (design 5) resulted in a proportional increase in I_{MAX}, K_M and slope. As consequence of this, the most efficient loading of enzyme in these designs was considered the 15 dips one, and for which the response to 1 mM AA (and ΔI) was similar to design 2.

In design 6, the main change on biosensor configuration was represented by the deposition of a mixed AOx+1% PEI solution (10 dips):

6 - Ptc/PPD/$[PEI(1\%) + AOx]_{10}$/PU(1%)

A partial precipitation of the enzyme in the solution was observed. No benefit in terms of biosensor performance was observed (Tables 2 and 3) relative to design 5 where PEI and AOx were separately deposited (10 dips).

Biosensor design	*In vitro* electrochemical characterization at day 1				
	Michaelis–Menten Kinetics			AA interference	
	I_{MAX} (nA)	K_M (mM)	R^2	AA 1 mM (nA)	AA ΔI (nA)
1 - $Pt_c/AOx_{10}/PPD$	3.0 ± 0.8	82 ± 10	0.86	1.90 ± 0.21	0.57 ± 0.18
2 - $Pt_c/PPD/[AOx]_{10}/PU$ (1%)	3.8 ± 0.3	73 ± 12	0.98	0.99 ± 0.02	0.19 ± 0.01
3 - $Pt_c/PPD/[PEI(1\%)/AOx]_5/PU(1\%)$	13.0 ± 0.9	23 ± 4	0.97	1.21 ± 0.11	0.23 ± 0.13
4 - $Pt_c/PPD/[PEI(1\%)/AOx]_{10}/PU(1\%)$	35.7 ± 0.7	27 ± 1	0.99	2.01 ± 0.25	0.49 ± 0.21
5 - $Pt_c/PPD/[PEI(1\%)/AOx]_{15}/PU(1\%)$	42.9 ± 3.4	36 ± 6	0.94	2.55 ± 0.15	0.84 ± 0.15
6 - $Pt_c/PPD/[PEI(1\%) + AOx]_{10}/PU(1\%)$	6.6 ± 0.2	58 ± 13	0.93	1.37 ± 0.11	0.72 ± 0.13
7 - $Pt_c/PPD/[Glyc(1\%)/AOx]_{10}/PU(1\%)$	2.7 ± 0.3	76 ± 12	0.97	1.70 ± 0.10	0.63 ± 0.08
8 - $Pt_c/PPD/[\{PEI(1\%)+Glyc(1\%)\}/AOx]_{10}/PU(1\%)$	116 ± 6	41 ± 5	0.98	1.72 ± 0.36	0.55 ± 0.12
9 - $Pt_c/PPD/[PEI(1\%)/AOx]_{10}/BSA(10\%)/GA(1\%)$	56 ± 2	36 ± 2	0.99	0.80 ± 0.08	0.17 ± 0.03
10 - $Pt_c/PPD/[\{PEI(1\%)+Glyc(1\%)\}/AOx]_{10}/BSA(10\%)/GA(1\%)$	52 ± 2	28 ± 3	0.98	0.93 ± 0.06	0.19 ± 0.04

Table 2: *In vitro* characterization of ten different biosensor designs at day 1 in terms of the apparent Michaelis–Menten kinetic parameters (eq 9) and AA interference parameters. The R^2 value (coefficient of determination) is a measure of the goodness-of-fit of the EtOH calibration data with eq 9.

Due to the failure of this attempt, a new approach was investigated to obtain a better design. In particular the substitution of PEI with glycerol, also used as enzyme stabilizer in 1% solution (design 7, Figure 10). Again, we alternately dipped 10 times the sensors into the 1% glycerol solution and then in the Alcohol Oxidase solution.

7 - $Ptc/PPD/[Glyc(1\%)/AOx]_{10}/PU(1\%)$

This change caused a decrease in terms of I_{MAX} (2.65 ± 0.25 nA, R^2= 0.969) and LRS (0.023 ± 0.002 nA mM^{-1}, R^2= 0.907) while causing an increase in K_M (76 ± 12 mM). AA blocking properties were basically unaffected (Tables 2 and 3).

Biosensor design	*In vitro* electrochemical characterization at day 1				
	Michaelis–Menten Kinetics			AA interference	
	Concentration limit for LRS (mM)	LRS (nA mM^{-1})	R^2	LOD ± SEM (mmol L^{-1})	LOQ ± SEM (mmol L^{-1})
1 - $Pt_c/AOx_{10}/PPD$	20	0.05 ± 0.05	0.88	2.72 ± 1.10	8.1 ± 3.3
2 - $Pt_c/PPD/[AOx]_{10}/PU$ (1%)	40	0.03 ± 0.01	0.99	3.03 ± 1.40	9.0 ± 4.1
3 - $Pt_c/PPD/[PEI(1\%)/AOx]_5/PU(1\%)$	10	0.37 ± 0.01	0.99	0.60 ± 0.04	1.7 ± 0.1
4 - $Pt_c/PPD/[PEI(1\%)/AOx]_{10}/PU(1\%)$	40	0.63 ± 0.03	0.96	0.32 ± 0.10	1.0 ± 0.3
5 - $Pt_c/PPD/[PEI(1\%)/AOx]_{15}/PU(1\%)$	40	0.81 ± 0.02	0.98	0.18 ± 0.06	0.6 ± 0.2
6 - $Pt_c/PPD/[PEI(1\%) + AOx]_{10}/PU(1\%)$	40	0.11 ± 0.01	0.99	1.10 ± 0.20	3.3 ± 0.5
7 - $Pt_c/PPD/[Glyc(1\%)/AOx]_{10}/PU(1\%)$	20	0.02 ± 0.01	0.91	2.80 ± 0.30	8.4 ± 0.7
8 - $Pt_c/PPD/[\{PEI(1\%)+Glyc(1\%)\}/AOx]_{10}/PU(1\%)$	40	1.73 ± 0.08	0.99	0.09 ± 0.03	0.27 ± 0.1
9 - $Pt_c/PPD/[PEI(1\%)/AOx]_{10}/BSA(10\%)/GA(1\%)$	40	0.78 ± 0.04	0.97	0.57 ± 0.14	1.7 ± 0.4
10 - $Pt_c/PPD/[\{PEI(1\%)+Glyc(1\%)\}/AOx]_{10}/BSA(10\%)/GA(1\%)$	50	0.76 ± 0.04	0.97	0.35 ± 0.23	1.0 ± 0.7

Table 3: *In vitro* ethanol sensitivity of ten different biosensor designs at day 1 in terms of linear region slope (LRS), LOD and LOQ

A further step in order to increase the performance obtained up to this stage was to include the two enzyme stabilizers together (Section 3.5). So, a 1% mixed solution of PEI and glycerol was deposited over the nanometer thick layer of PPD. For design 8 the sensors where alternately dipped 10 times, firstly in the enzyme stabilizers mix solution, and then in the 200 U/mL AOx solution. This multilayers pattern, represented in Figure 10 was trapped by mean of a quick dip into a 1% PU solution deposited by dip-evaporation:

8 - $Ptc/PPD/[\{PEI(1\%)+Glyc(1\%)\}/AOx]_{10}/PU(1\%)$

The mix of PEI and glycerol led to a very remarkable enhancement of biosensors performance, resulting in a significant increase in I_{MAX} (115 ± 6 nA, R^2= 0.978), LRS (1.73 ± 0.08 nA mM^{-1}, R^2= 0.996) and K_M (41 ± 5 mM) compared to the best designs obtained up to this stage (designs 4 and 5) with PEI alone (Tables 2).
The response to AA was similar to other designs (Table 3), with shielding properties for 1 mM AA (1.72 ± 0.36 nA and a ΔI of 0.55 ± 0.12 nA).

Designs 9 and 10 maintain basically the same scheme as designs 4 and 8, except for the substitution of PU with BSA cross-linked with GA as the "containment net" (Figure 11):

9 - Ptc/PPD/$[PEI(1\%)/AOx]_{10}$/BSA(10%)/GA(1%)
10 - Ptc/PPD/$[\{PEI(1\%)+Glyc(1\%)\}/AOx]_{10}$/BSA(10%)/GA(1%)

Although having the new well-performing mix of enzyme stabilizers, design 10 did not reproduce the very good results of design 8. It is possible that the addition of the protein BSA reduced the enzymatic activity, as well as the process of cross-linking by GA could inactivate AOx, reducing the number of active enzymes molecules.
The results for designs 9 and 10 shown in Tables 2 and 3 are comparable with design 5 in terms of K_M and LRS, while producing a slightly higher I_{MAX} and a lower response to AA interference.

As for the apparent enzymatic kinetic values, biosensor response in terms of limits of sensitivity was also tested at day 1. The LOD and LOQ values (eqs 12 and 13) are shown in Table 3.
The first design of biosensor that we have characterized (design 1) had a LOD of 2.7 ± 1.1 mM and a LOQ of 8.1 ± 3.3 mM. Design 2 showed similar values despite a variation of biosensor configuration, as previously described.

The introduction of PEI (designs 3–5) led to an increase in ethanol sensitivity. Data showed a proportionality between the number of dips in PEI and AOx solution and the sensitivity, passing from 5 to 15 dips. The higher concentration of enzyme deposited on the biosensor considerably reduced the LOD and LOQ down to 182 ± 62 µM and 551 ± 186 µM, respectively (design 5). This result can be quantified as a decrease of the LOD value of –38 ± 5 µM *per* dip (R^2 = 0.980, n = 4) and an increase in the LRS (+44 ± 5 pA mM^{-1} *per* dip; R^2 = 0.989, n = 4), as shown in Table 3.

Mixing PEI and Alcohol Oxidase together as in design 6 and the deposition of glycerol instead of PEI in design 7 led to a worsening in biosensor' sensitivity. In fact, the limits of detection and quantification increased (Table 3) when compared with designs where PEI was immobilized alone, as in design 4 (10 dips) and design 5 (15 dips). The best results in terms of sensitivity values were obtained by dipping the sensors of design 8 in the 1% mix solution of PEI and glycerol. This strategy of immobilization yielded the best design of biosensor, providing a consistent increase in ethanol sensitivity demonstrated by the lowest values observed for LOD (88 ± 28 µM) and LOQ (265 ± 86 µM, Table 3).

Finally, investigating the effect of substitution BSA cross-linked with GA instead of the 1% PU solution as "containing net" (designs 9 and 10), a doubling of LOD and LOQ values was observed, comparing the corresponding data from designs 4 and 8. The possible causes of this behavior have been discussed above.

4.1.2 Study of biosensor stability over time

The stability of biosensors performance over time was determined through a study on aging. Among all the 10 designs developed in the first part of the study, the 4 more promising designs were selected, on the basis of their best values of apparent enzymatic kinetic parameters, sensitivity and AA shielding properties shown at day 1 (Tables 2 and 3 Section 4.1.1).

For that purpose, biosensors that were calibrated immediately after their manufacture on day 0 (corresponding to the time of *in vivo* implantation), and at days 1–2 (which represent the first and second day of data recording) were then further calibrated once at week (day 7, day 14, day 21) up to day 28. The purpose of this experiment was to know the temporal limit of each biosensor design for a reliable *in vivo* use, investigating the stability of the enzymatic activity and polymer shielding efficacy before biosensor performances decrease.

Thus, ethanol and ascorbic biosensor response was assessed every 7 days, and Michaelis–Menten kinetic parameters I_{MAX} (Figure 21) and K_M (Figure 23) sensitivity (LRS, Figure 22), as well as the shielding power against AA (Figure 24) were analyzed.

After each calibration, biosensors were rinsed with deionized water and then stored dry in a fridge at temperature of 4 ^{o}C.

The four selected designs were:

5 - Ptc/PPD/[PEI(1%)/AOx]$_{15}$/PU(1%)

8 - Ptc/PPD/[{PEI(1%)+Glyc(1%)}/AOx]$_{10}$/PU(1%)

9 - Ptc/PPD/[PEI(1%)/AOx]$_{10}$/BSA(10%)/GA(1%)

10 - Ptc/PPD/[{PEI(1%)+Glyc(1%)}/AOx]$_{10}$/BSA(10%)/GA(1%)

The trend for these four selected designs was a quite homogeneous decay in terms of I_{MAX} (Figure 21) and LRS (Figure 22) as biosensors got older. An interesting difference was evidenced in design 8. Until the seventh day after its manufacture, design-8 I_{MAX} and LRS values were statistically superior with respect to the other designs. After this time the performances decreased, showing an analog trend compared with the other designs, up to day 28 (* = $p < 0.05$ vs. other designs on the same day (unpaired t-test). # = $p < 0.05$ vs. days 0–7 (ANOVA followed by Newman-Keuls post test).

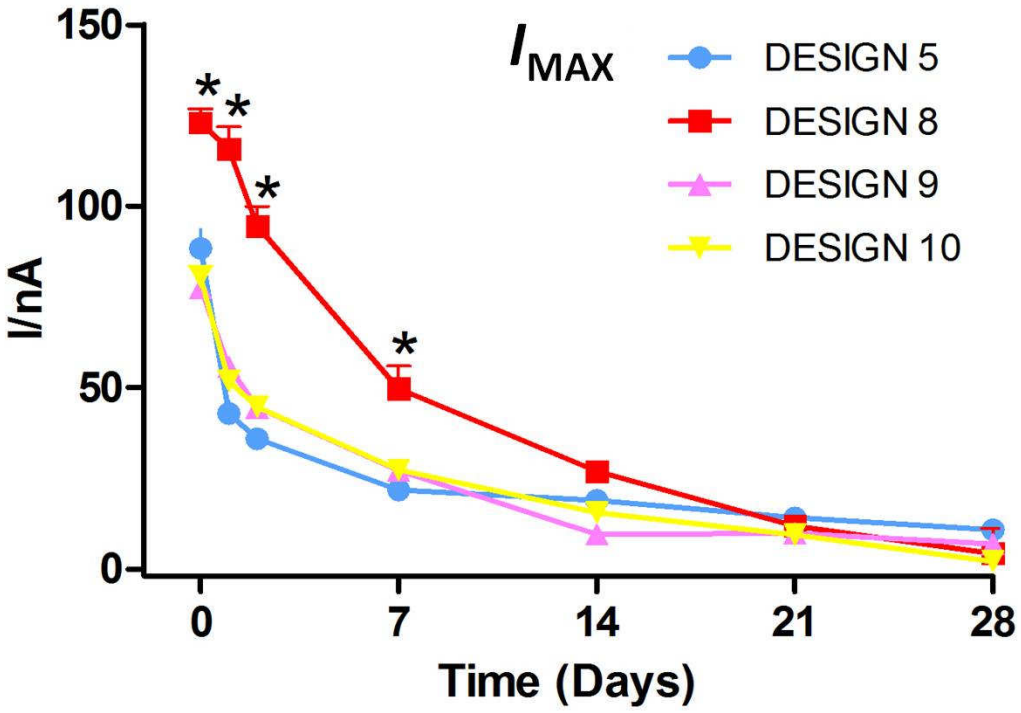

Figure 21 Aging (28-day *in vitro* study) of the four most promising biosensor designs (n = 4 for each group) for I_{MAX}. * = $p < 0.05$ vs. other designs on the same day (unpaired *t*-test). # = $p < 0.05$ vs. days 0–7 (ANOVA followed by Newman-Keuls post test).

Designs 9 and 10 showed basically the same results from day 0 to day 7 (Figures 21 and 22), even if lower than design 8. As already discussed, the difference in the "trapping net" deeply differentiated their behavior.

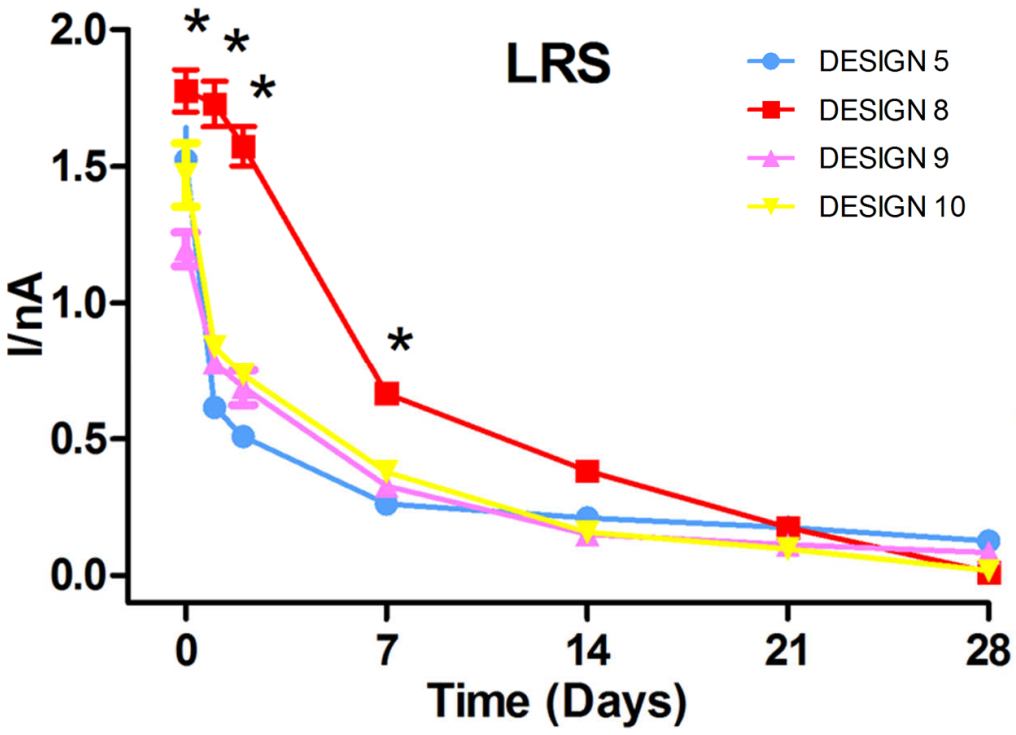

Figure 22: Aging for LRS. * = $p < 0.05$ vs. other designs on the same day (unpaired *t*-test). # = $p < 0.05$ vs. days 0–7 (ANOVA followed by Newman-Keuls post test).

Design 5 demonstrated the worst performances, early decreasing in sensibility at day 1 and day 2. Nevertheless, values obtained at day 28 were similar to the others. The main difference between designs 5 and 8 was the co-presence of glycerol in the mixed enzyme enhancer solution in the more performing design versus PEI alone in design 5, which clearly played an important role in design 8 performances.

The trend in K_M values showed a rather uniform behavior in all studied designs (Figure 23). The values of this enzymatic kinetic parameter increased from day 0 to day 2 for all biosensors, and then remained quite stable until the end of the study. The K_M values of design 8 were the lowest, meaning that the substrate had a higher affinity for the enzyme, resulting in a faster turnover of ethanol molecules catalyzed by each protein. As a consequence, design 8 showed the best I_{MAX} and LRS values discussed above (Figures 21 and 22).

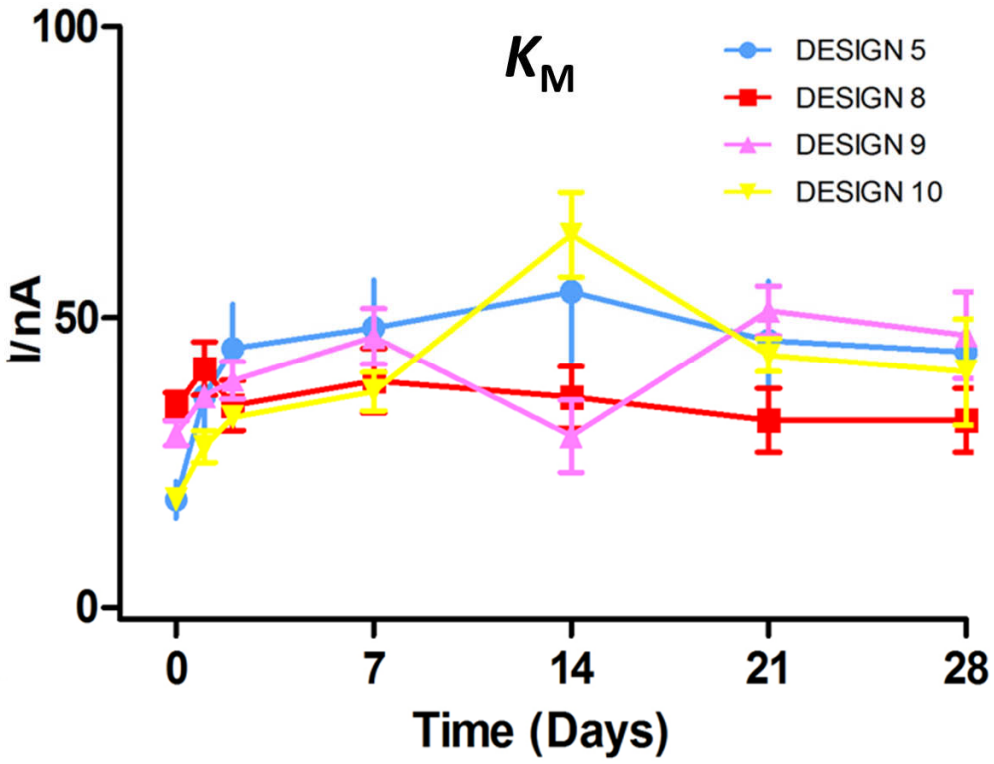

Figure 23: Aging for K_M. * = $p < 0.05$ vs. other designs on the same day (unpaired *t*-test). # = $p < 0.05$ vs. days 0–7 (ANOVA followed by Newman-Keuls post test).

Otherwise, the shielding efficacy for the ascorbic acid was quite different, depending on the structure of the considered design, even if basically they are all based on the same strategy of electro-deposition of the PPD polymeric layer.

A very important parameter in the aging biosensor study is the PPD polymer effectiveness over time. In a multilayer, pattern-based biosensor, AA shielding efficacy could even be affected by the different components added over the PPD coating. Once again it seemed to be that the BSA-GA cross linking contributed to a deterioration of designs 9 and 10. As a matter of fact, those designs showed the worst capacity in AA shielding (Figure 24).

On the other hand, the final quick dip in the 1% PU solution (strong THF solvent, see Section 3.1) did not affect the PPD polymer consistency, and guaranteed a better AA interference rejection over the first week for both designs 5 and 8. From day 7 up to day 28, the biosensors ability to prevent AA interference decreased. This suggested that one week was the limit of reliability of the biosensor for *in vivo* implantation.

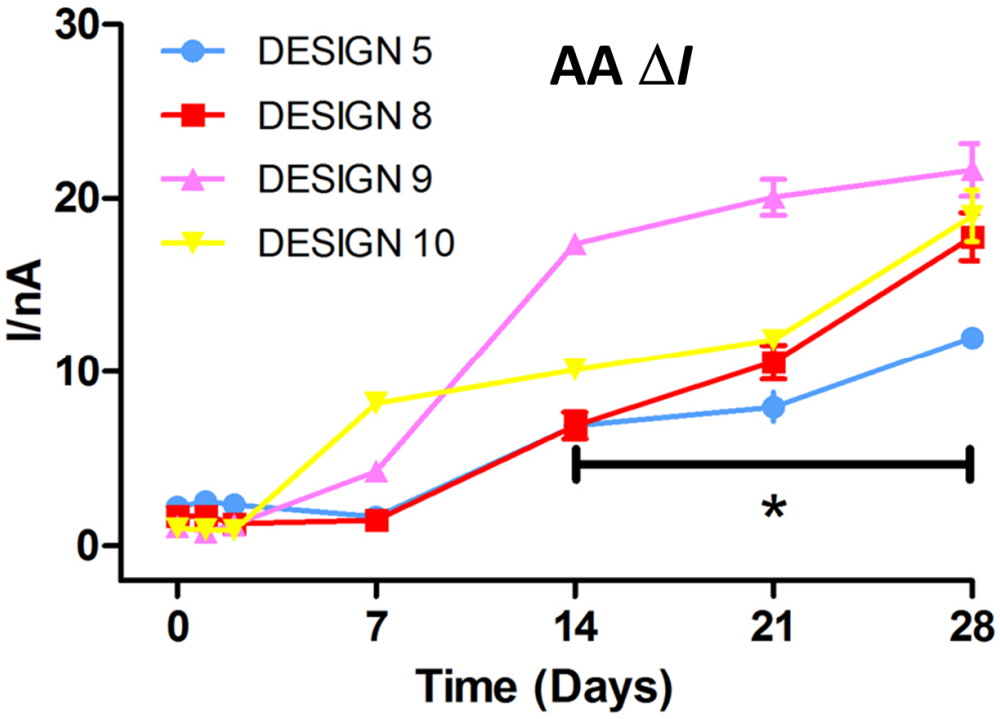

Figure 24: Aging for AA Δ*I*. * = $p < 0.05$ vs. other designs on the same day (unpaired *t*-test). # = $p < 0.05$ vs. days 0–7 (ANOVA followed by Newman-Keuls post test).

This finding has been confirmed by calculating the AA percentage interference on the 30 mM EtOH current (*i.e.*, in the linear response region). The evidence that ethanol could reach a concentration of about 30 mM in the CNS after intraperitoneal injection (Adalsteinsson et al., 2006; Jamal et al., 2003) led us to monitor the response of the selected designs (5, 8, 9 and 10) when exposed to that concentration of ethyl alcohol.

Figure 25 shows the limiting currents values for 30 mM EtOH detected for each different design. Furthermore, the AA Δ*I* currents studied over 28 days were plotted. The trend of I_{MAX} and LRS values discussed above for the stability study of design 8 (Figures 21 and 22), together with the best AA rejection property, resulted in interference equivalent to only 1% after 2 days, which increased to just 2% at day 7 (*, # = $p < 0.05$ vs. the corresponding day 0 (ANOVA followed by Newman-Keuls post test).

In fact, by observing the limiting currents resulting from the oxidation of 30 mM ethanol, and the shielding power for ascorbic acid (AA Δ*I*), design 8 showed once again the best range of performance.

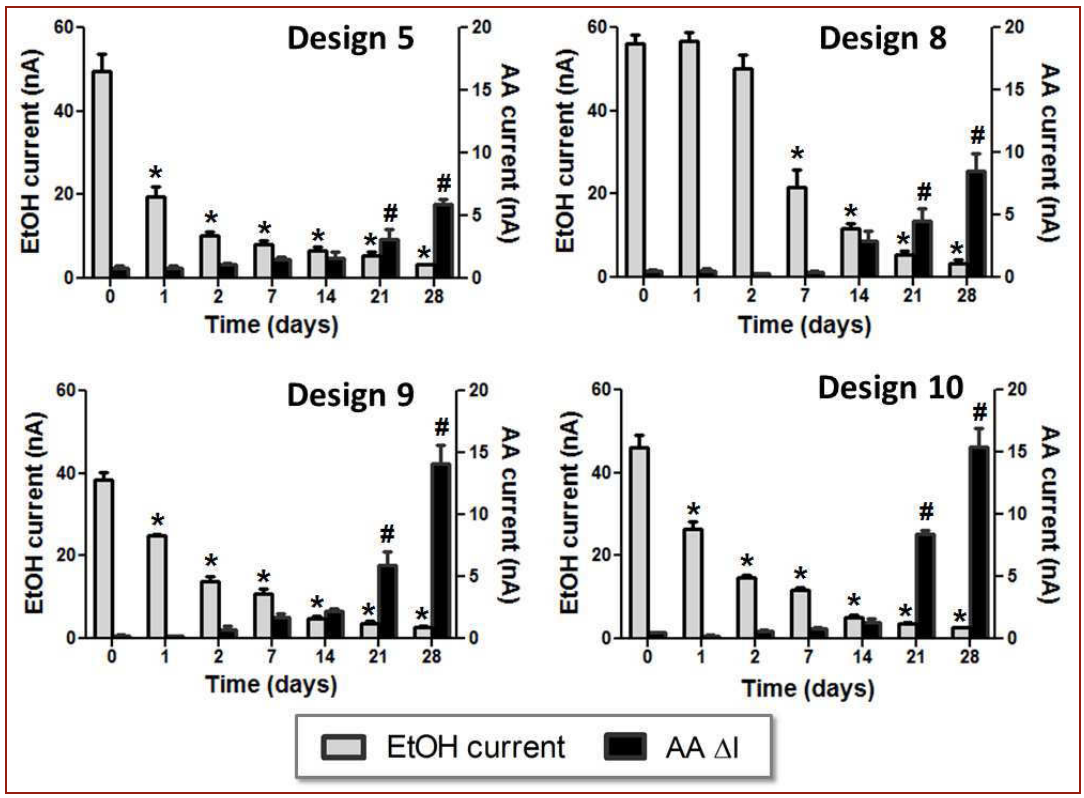

Figure 25: Evolution over 28 days of the *in vitro* ethanol response (30 mM) and AA interference (0.5→ 1 mM Δ*I*) of the four most promising biosensor designs.

4.2 Effects of enzyme loading on biosensor performance

Based on the findings that design 8 was demonstrated to be the best performing and stable biosensor among all those developed, our study re-focused on investigating what the effects may be of depositing a different concentration of the enzyme AOx compared to the 200 U/mL solution used until this stage of the project. Thus, the only variable considered to further optimize the biosensor was to change the AOx solution concentration. Having established the benefits of design 8, however, the multilayered disposition of this configuration (see Figure 10, Section 3.6) was not varied, nor was the deposition sequence.

In order to enhance ethanol biosensor performance and sensitivity, four fresh different AOx solutions were prepared, dissolving different amounts of enzyme in 1 mL of PBS buffer:

- AOx (100 U/mL)
- AOx (400 U/mL)
- AOx (600 U/mL)
- AOx (800 U/mL)

Then, AOx was deposited by dip-evaporation (10 quick dips) on the biosensor surface (in the configuration of design 8), resulting in four news designs, designated as follow:

Ptc/PPD/[{PEI(1%)+Glyc(1%)}/AOx(100 U/mL)$_{10}$/PU(1%)
Ptc/PPD/[{PEI(1%)+Glyc(1%)}/AOx(400 U/mL)$_{10}$/PU(1%)
Ptc/PPD/[{PEI(1%)+Glyc(1%)}/AOx(600 U/mL)$_{10}$/PU(1%)
Ptc/PPD/[{PEI(1%)+Glyc(1%)}/AOx(800 U/mL)$_{10}$/PU(1%)

Similarly, the scheme of the original design 8 will be indicated now as:

Ptc/PPD/[{PEI(1%)+Glyc(1%)}/AOx(200 U/mL]$_{10}$/PU(1%)

Furthermore, because the enzymatic concentration variation is the core of this part of dissertation, it is opportune now to specify that design 8 will be named as “design 8-200”, indicating the AOx concentration. Similarly, “design 8-100” and “design 8-400” refers to the biosensors set obtained by 10 dips into the 100 and 400 U/mL AOx solutions, while “design 8-600” and “design 8-800” nomenclature will be use for biosensors made with the most concentrated enzymes solutions.

4.2.1 Comparison of new designs at day 1

For the four new designs (n = 4 for each group), the sensitivity to ethanol and AA at day 0 and day 1 was assessed. These were then compared with results already obtained by design 8-200, in order to evaluate and quantify how the difference in AOx loading affected biosensor performance. In the same way, a study of their stability over time (day 0 to day 28) was conducted.

The apparent Michaelis–Menten kinetic parameters (I_{MAX} and K_M) and the linear region slope (LRS) in the reference linear range were analyzed (Table 4), as well as LOD and LOQ values, and the efficiency in rejecting AA interference (Table 5).

Table 4 shows the response parameters of the different designs at day 1. These data revealed that halving the enzyme concentration with respect to design 8-200 reduced the number of ethanol molecule oxidized at the biosensor surface per unit time, resulting in a lower I_{MAX} (75 ± 6 nA) for design 8-100. On the other hand, when the AOx concentration was doubled (design 8-400), this led to higher I_{MAX} values, equal to 308 ± 10 nA.
So, I_{MAX} values increased quite linearly with the augmentation of the enzyme loading from 100 to 200 and 400 U/mL solutions, ranging between 75 ± 6 and 308 ± 10 nA.
This increase has been quantified as 0.80 ± 0.14 nA of limiting current for each unit of enzyme dissolved in 1 mL of solution (R^2 =0.975; n = 4).

AOx loading solution (U/mL)	Michaelis–Menten kinetics			Linear regression		
	EtOH I_{MAX} (nA)	EtOH K_M (mM)	R^2	EtOH concentration limit (mM)	EtOH LRS (nA mM^{-1})	R^2
100	75 ± 6	34 ± 7	0.97	30	1.09 ± 0.06	0.99
200	114 ± 7	44 ± 4	0.98	40	1.77 ± 0.08	0.99
400	308 ± 10	56 ± 6	0.98	40	3.94 ± 0.12	0.99
600	67 ± 13	52 ± 11	0.97	40	0.92 ± 0.09	0.99
800	46 ± 10	59 ± 9	0.98	40	0.67 ± 0.15	0.99

Table 4: *In-vitro* characterization at Day 1 (n = 4 for each group) of different biosensor designs with different enzyme loading

When even higher concentrations of Alcohol Oxidase were used in the enzyme solution, as in designs 8-600 and 8-800, sensitivity decreased with respect to design 8-400 and I_{MAX} values tended to decay exponentially (R^2 = 0.983; n = 4) with a halving of the current every 57 U/mL and a plateau of 44 ± 13 nA.

This is unlikely due to fewer AOx molecules being deposited on the electrode surface, but could be partially related to the decrease in H_2O_2 sensitivity observed for these biosensors (see Table 5, and reactions 6–8 of Section 3.4).

The LRS trend reflected that seen in I_{MAX}. In fact, the LRS in the reference linear range also tended to increase with the concentration of enzyme in the dipping solution from designs 8-100 up to 8-400 (10 ± 2 pA mM^{-1} U^{-1} mL; R^2 = 0.989; n = 20), reaching the maximum value of 3.94 ± 0.12 nA mM^{-1}. Again, a worsening in biosensors performance was found for designs 8-600 and 8-800, both relative to the original design (8-200) as well as to the best performing configuration at day 1, namely design 8-400 (Table 4).

Specifically, excessive levels of AOx in loading solution led to an exponential decay in ethanol sensitivity (R^2 = 0.981; n = 20) with a halving of the resulting current every 56 U/mL of AOx and a plateau of 0.65 ± 0.15 nA mM^{-1}.

All the new designs showed the same linear response region (<K_M) to ethanol as design 8-200, in a range between 0 and 40 mM. The only exception was design 8-100 that showed a smaller linear response span (0–30 mM) because these biosensors exhibited the lowest apparent K_M value, corresponding to 34 ± 7 mM (Table 4).

Then passing from design 8-100 to design 8-400, a linear increase was observed in K_M (0.074 ± 0.009 mM U^{-1} mL; R^2 = 0.987; n = 20), whereas no significant differences were found for further increases in AOx solution concentration.

The sensitivity parameters displayed by the four new designs were compared with design 8-200. Increasing enzyme concentration also influenced the LOD and LOQ (eqs 12-13, Section 3.12) as illustrated in Table 5. LOD values increased proportionally to the concentration of enzyme, ranging from 0.006 ± 0.004 mM (LOQ = 0.2 ± 0.1 mM) to 0.053 ± 0.014 mM (LOQ = 0.42 ± 0.19 mM).

AOx loading solution (U/mL)	LOD ± SEM (µmol L^{-1})	LOQ ± SEM (µmol L^{-1})	H_2O_2 sensitivity drop (% *vs* AOx-free design)	1 mM AA (nA)
100	6 ± 4	20 ± 6	−10 ± 5 %	1.32 ± 0.31
200	11 ± 3	30 ± 10	−19 ± 4 %	1.73 ± 0.13
400	17 ± 6	56 ± 16	−28 ± 5 %	0.98 ± 0.27
600	32 ± 18	106 ± 31	−39 ± 5 %	1.64 ± 0.42
800	53 ± 14	164 ± 59	−46 ± 5 %	1.03 ± 0.29

Table 5: *In-vitro* characterization at day 1 (*n* = 4 for each group) in terms of LOD and LOQ, H_2O_2 sensitivity decrease, and 1 mM AA interference.

Hydrogen peroxide sensitivity (Table 5) decreased with solution enzyme concentration in a linear manner (–5.6 ± 0.4 % for every 100 U/mL increase of AOx in the dipping solution; R^2 = 0.976; n = 20). Taken together, these results suggest that increasing the concentration of AOx in the dipping solution enhanced biosensor enzyme loading. The extra protein on the biosensor surface, however, progressively lowered the Pt sensitivity to H_2O_2, ultimately leading to lower EtOH responses (see reactions 6–8 of Section 3.4).

Finally, no substantial difference among all the new designs at day 1 was found in terms of AA rejection (Table 5). As a matter of fact, the 1 mM limiting currents ranged from a minimum of 0.98 ± 0.27 nA (400 U/mL) to a maximum of 1.73 ± 0.13 (200 U/mL).

4.2.2 Study of the new designs' stability over time

A study of biosensor stability over time was conducted for the new designs, monitoring the responses to ethanol and AA over a period of 28 days from their manufacture. Apparent Michaelis–Menten kinetic parameters (I_{MAX} and K_M) and LRS values determined for biosensors at day 2, day 7, day 14, day 21 and day 28 were analyzed and compared to design 8-200 (as stated in Section 4.1.2), as well as LOD and LOQ values and the efficiency in rejecting AA interferences.

All new designs showed a homogeneous decay in terms of I_{MAX} (Figure 26) from day 0 to day 28, and followed the same trend observed during design 8-200 aging study (see Figure 21).

A significant improvement in terms of stability was shown by design 8-400; in fact, its better sensitivity and sensibility showed at day 1 was confirmed over time, resulting in higher I_{MAX} values respect with the biosensor loaded with 200 U/mL.

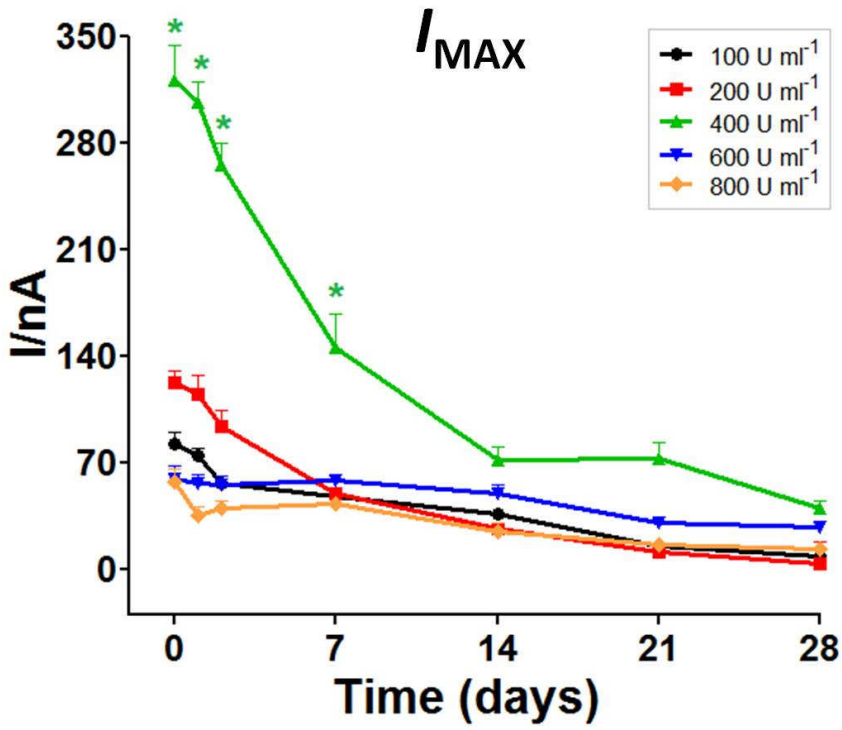

Figure 26: *In-vitro* stability study: evolution of the I_{MAX} over a 28-day monitoring period for biosensors fabricated from different enzyme loading solutions (n = 4 for each group; * $p < 0.05$ vs other groups).

Trends shown in Figure 26 illustrate how I_{MAX} values of design 8-400 were statistically higher than for the others from day 0 to day 7 ($p < 0.05$ vs other designs), remaining superiors until day 21. Finally, at day 28, the gap between all designs tended to be smaller.

The aging effect for design 8-600 and design 8-800 was quite different compared with the other configurations, in that they showed the worst performance at day 1, but the decrease in I_{MAX} values was less pronounced over time.

Mean values of K_M were found to be not significantly dependent on enzyme loading up to 800 U/mL (Figure 27). K_M values showed a rather homogeneous behavior for all designs over time, tending to slowly increase over the entire monitoring period.

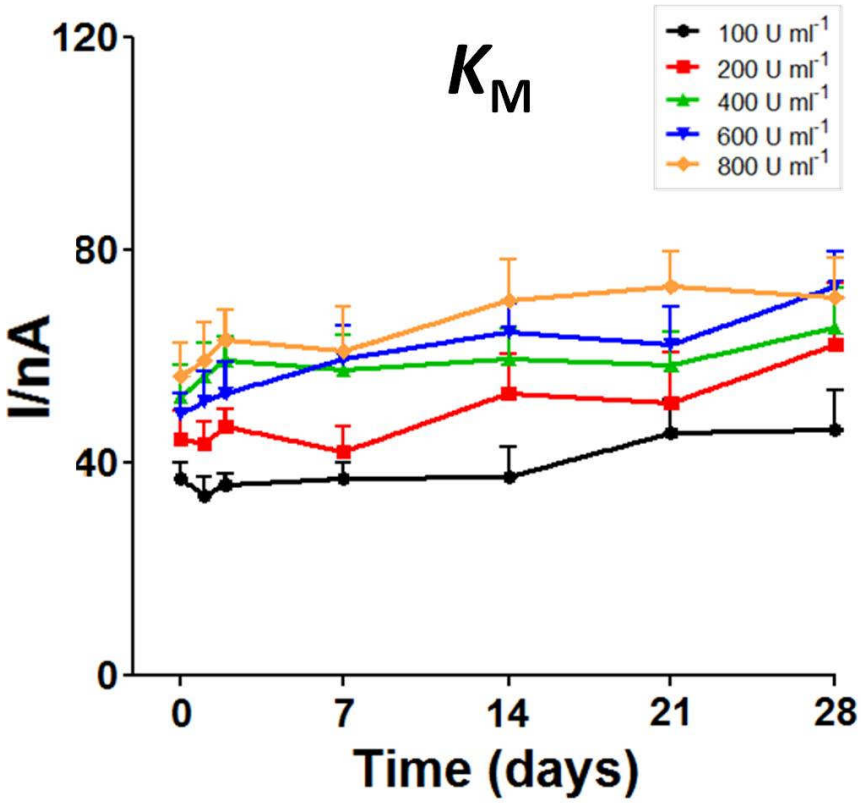

Figure 27: *In-vitro* stability study: evolution of K_M over a 28-day monitoring period for biosensors fabricated from different enzyme loading solutions (n = 4 for each group).

Figure 28 illustrates the trend of LRS values. It was observed to be similar to those previously described for I_{MAX}. As a matter of fact, the LRS values of design 8-400 biosensors were higher (* $p < 0.05$ vs other designs) than for other designs from day 0 up to day 28.

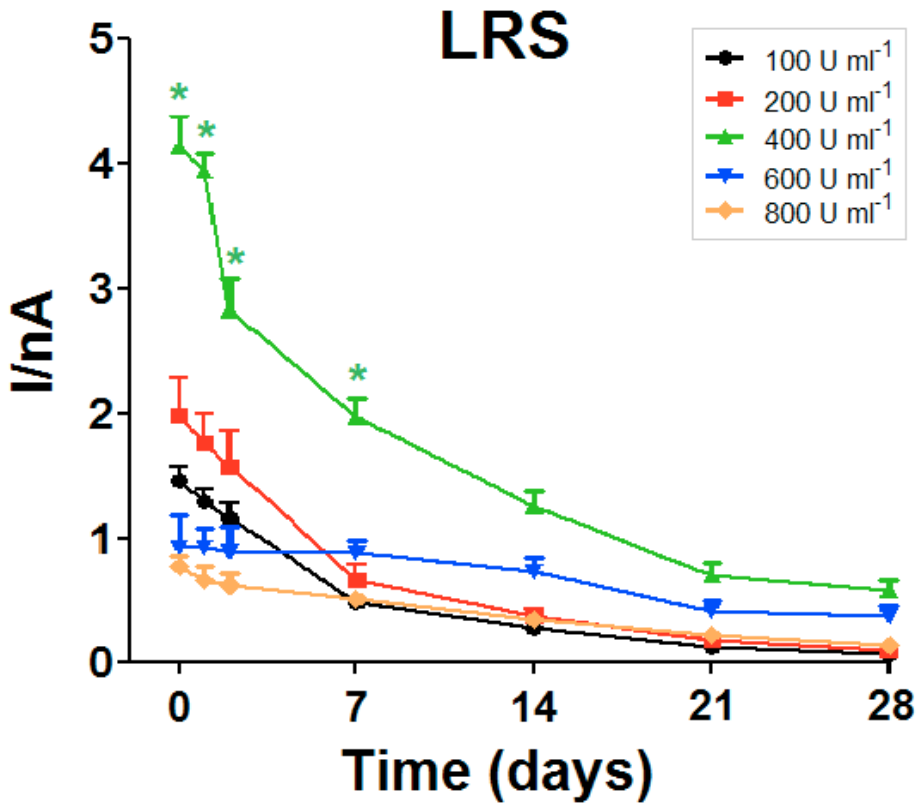

Figure 28 *In-vitro* stability study: evolution of the LRS over a 28-day monitoring period for biosensors fabricated from different enzyme loading solutions (n = 4 for each group).

The biosensors effectiveness to reject AA interference was monitored throughout the aging study and expressed as AA Δ*I*, as shown in Figure 29.

Comparable values were obtained up to day 7 for all designs (0.47 ± 0.04 nA; *n* = 20). Then, due to the deterioration of PPD polymer, a homogeneous increase in AA sensitivity was observed after day 7. The lowest observed slope belonged to design 8-600 (0.21 ± 0.03 nA day^{-1}), while the higher as been observed in design 8-100 (0.34 ± 0.06 nA day^{-1}).

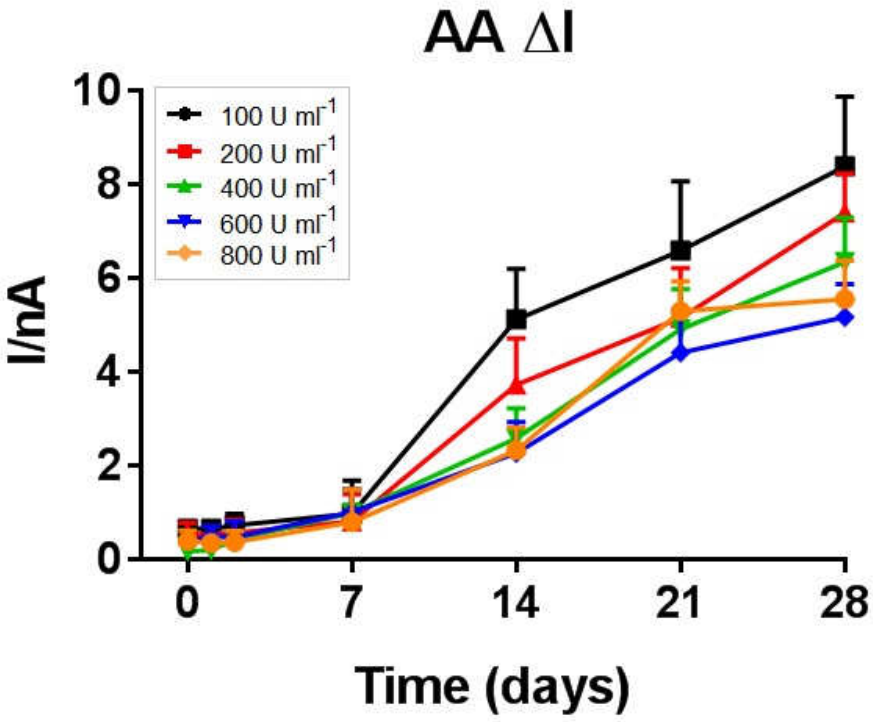

Figure 29. *In-vitro* stability study: evolution of the AA Δ*I*, over a 28 days monitoring period for biosensors fabricated from different enzyme loading solutions (n = 4 for each group).

4.3 Oxygen dependence of biosensor responses

The oxygen dependence of the biosensor response to ethanol was tested for all designs. As shown in Table 6, oxygen I_{MAX} increased almost linearly when higher concentrations of AOx solution were deposited on the biosensor surface, passing from design 8-100 (19.1 ± 3.5 nA) to design 8-200 (27.4 ± 3.5 nA) and design 8-400 (64.2 ± 4.3 nA). The enhancement has been quantified as 0.16 ± 0.03 nA per each enzyme unit dissolved in PBS buffer ($R^2 = 0.974$; $n = 20$).

For further increases of immobilized AOx molecules, I_{MAX} values tended to exponentially decay ($R^2 = 0.924$; $n = 20$) when the enzyme loading solution varied from 400 up to 800 U/mL with a halving of the current every 55 U/mL and a plateau of 13.4 ± 4.6 nA.

AOx loading solution (U/mL)	Apparent Michaelis–Menten kinetic parameters for oxygen		
	O_2 I_{MAX} (nA)	O_2 K_M (µM)	R^2
100	19.1 ± 3.5	11.1 ± 2.3	0.98
200	27.4 ± 5.2	17.3 ± 4.4	0.98
400	64.2 ± 4.3	37.7 ± 5.1	0.99
600	17.4 ± 3.4	57.2 ± 8.3	0.98
800	13.7 ± 3.7	72.3 ± 11.2	0.97

Table 6: Oxygen dependence study at Day 1.

An increased oxygen dependence of the biosensor response, expressed as K_M for O_2, was observed for variation of AOx solution concentration from 100 to 400 U/mL, in parallel with I_{MAX} (Table 6). In particular, design 8-200 oxygen dependence was quantified as 17.3 ± 4.4 μM, while design 8-400 showed a value of 37.7 ± 5.1 μM. Surprisingly, an opposite trend compared with what emerged from I_{MAX} values was observed for further increases of AOx loading. As a matter of fact, oxygen dependence continued to increase for designs 8-600 and 8-800. Thus, a linear increase in oxygen dependence ($K_M(O_2)$ = 0.091 ± 0.003 μM U^{-1} mL; R^2 = 0.997; n = 20) was observed with the increase of the enzyme concentration in the loading solution from 100 to 800 U/mL.

The results emerged from the oxygen dependence study were critical to establish which design among all those characterized was the most reliable for *in vivo* applications. The estimated average oxygen concentration dissolved in the extracellular fluids in the brain has been quantified as ~50 μM from previous findings (Zauner et al., 1995; Murr et al., 1994; Nair et al., 1987).

To monitor the variation in ethanol concentration in extracellular fluids, and particularly in the brain, independently from physiological oscillations in oxygen levels, the biosensor $K_M(O_2)$ needs to be lower than one half of the oxygen concentration dissolved in the brain ECF.

In this way, the biosensor would be saturated with oxygen, which is the electron acceptor involved in AOx catalysis (see reactions 6–8), so that ethanol oxidation would be based just on the apparent Michaelis–Menten parameters for ethanol. Design 8-400, while demonstrated to be more sensitive and stable up to 1 week among all designs developed, displayed an excessive oxygen dependence ($K_M(O_2)$ = 38 ± 5 μM; see Table 8) which could undermine its *in vivo* performance.

On the other hand, design 8-100 and design 8-200 fulfill the $K_M(O_2)$ requirement. Among these two designs, biosensors loaded with 200 U/mL AOx concentration was demonstrated here to be the best performing in terms of the analytically most important parameter (LRS) on day 1, as well as of stability over time, and was therefore considered the most reliable design to monitor ethanol concentration in the brain for up to 7 days.

4.4 Biosensor response time

Rapid detection is a critical characteristic for biosensors targeting molecules whose concentration could change rapidly, such as neurotransmitters and other biological compounds. As discussed in Section 1.5.3, a fast monitoring of ethanol brain level variations is a pivotal factor to better establish and understand the basis of its mechanism of action and its neurobiological effects on the CNS.

For evaluating the response time of biosensors, ethanol and AA calibrations were performed in stirred condition, using a data acquisition rate of >100 Hz. A $t_{90\%}$ parameter was previously defined (Rothwell et al., 2010) as the time needed for the signal to reach the 90% of its maximum response value, starting from its baseline current.

In particular, we were interested to ascertain the response time for ethanol of design 8-200 which, as previously discussed, showed the best performance of stability and sensitivity, being the most reliable candidate for use in *in-vivo* studies.

The time required for design 8-200 to reach the $t_{90\%}$ following the addition of ethanol aliquots in the electrochemical cell was quite fast (1.6 ± 0.7 s, n = 20; 4 biosensors × 5 determinations; mean ± SD). This compares favourably with other PPD/PEI-based biosensor designs, such as that for glutamate of ~2 s (McMahon et al., 2007), and demonstrates one of the benefits of the ultra-thin nature of the PPD polymer–enzyme composite matrix. What is even more interesting is that the final layer of PU, not present in the 2007 design, did not increase the time response of these ethanol biosensors.

This critical parameter suggests that design 8-200 was surely suitable for real-time monitoring of variations in ethanol concentration in brain extracellular fluids.

4.5 pH dependence of the biosensor response

The final part of design 8-200 characterization consisted of the study of the pH influence on biosensor performance. The experiment was performed by addition of 15 mM ethanol in each different pH solution tested, corresponding to the concentration could be reached in brain ECF after a single intra gastric administration of 1 g $kg^{-1}$of ethanol (Rocchitta et al., 2012).

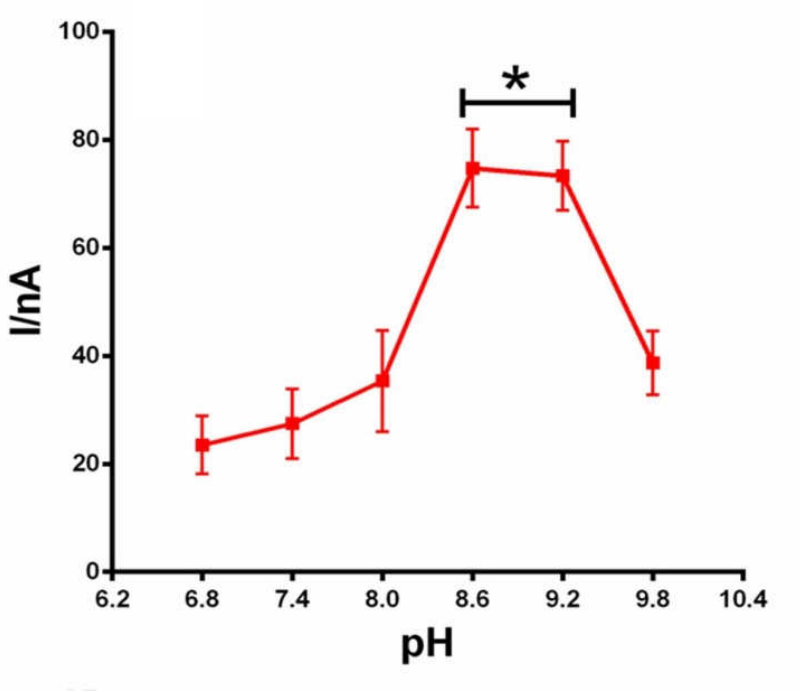

Figure 30: The influence of pH on the 15 mM ethanol response of the design 8 biosensor. * $p < 0.05$ vs pH 6.8 – 8.0.

The biosensor response for 15 mM ethanol of design 8-200 after varying the pH from 6.8 up to 9.8 is plotted in Figure 30. Results showed an increase in current signal passing from pH 6.8 to 8.6. The optimum in biosensor performance was obtained between pH 8.6 and 9.2, where the response was about 300% higher than at pH 7.4 ($p<0.05$ *vs* pH 6.8 – 8.0). The response at pH 9.8 decreased, indicating no further improvement. Biosensor response at physiological pH 7.4 was considered adequate for *in vivo* studies.

4.6 Temperature dependence of the biosensor response

Finally, a temperature dependence study on design 8-200 was conducted at physiological pH 7.4. Figure 31 shows the plot of biosensor response for 15 mM EtOH at different working temperatures.

Although a small temperature dependence was observed, this was considerably less than that observed for the enzyme in solution (Kato et al., 1976). Specifically, the biosensor response was only 18% less at 20 ^{o}C compared with the maximum responses observed between 35 and 40 ^{o}C. Thus, the difference in oxygen demand at the two temperatures is not likely to have a major impact on the biosensors' oxygen tolerance *in vivo* (37 ^{o}C).

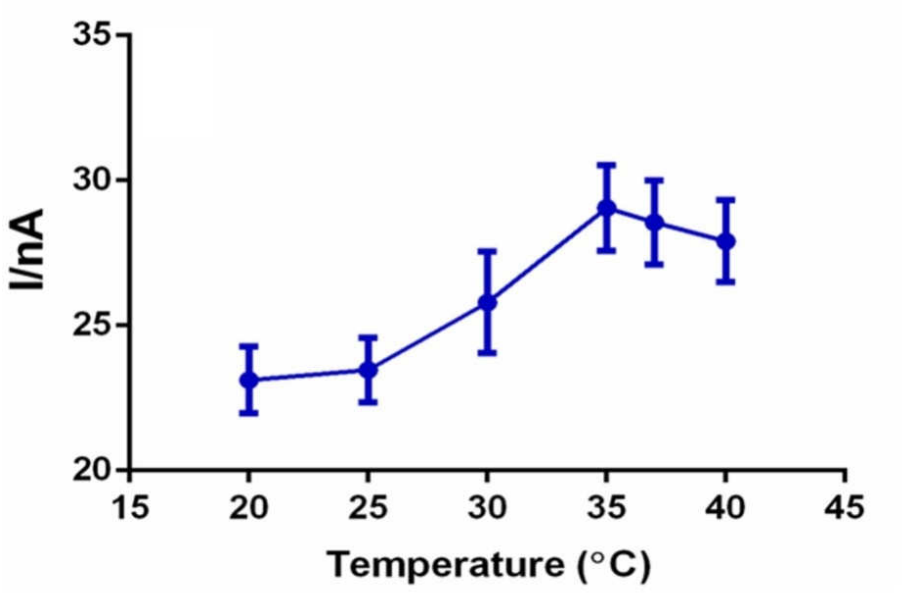

Figure 31: Temperature dependence study on the 15 mM ethanol response of the design 8 biosensor.

4.7 *In vivo* response of the biosensor to systemic administration of ethanol, and effect of ranitidine

Biosensor design 8-200 was selected for implantation in the *nucleus accumbens* of Sprague-Dawley rats. New biosensors were freshly made and calibrated immediately before their implantation by means of stereotaxic neurosurgery.

Figure 32 shows the result of *in vitro* calibration of ethanol biosensors at day 0 before implantation. The resulting calibration curve showed reasonable Michaelis–Menten kinetics ($R^2 = 0.965$) with an I_{MAX} of 126 ± 10 nA and a K_M of 38 ± 7 mM (n = 4). The response to pharmacologically relevant concentrations of ethanol (0–40 mM) revealed good linearity ($R^2 = 0.992$) with a slope of 1.78 ± 0.44 nA mM^{-1}.

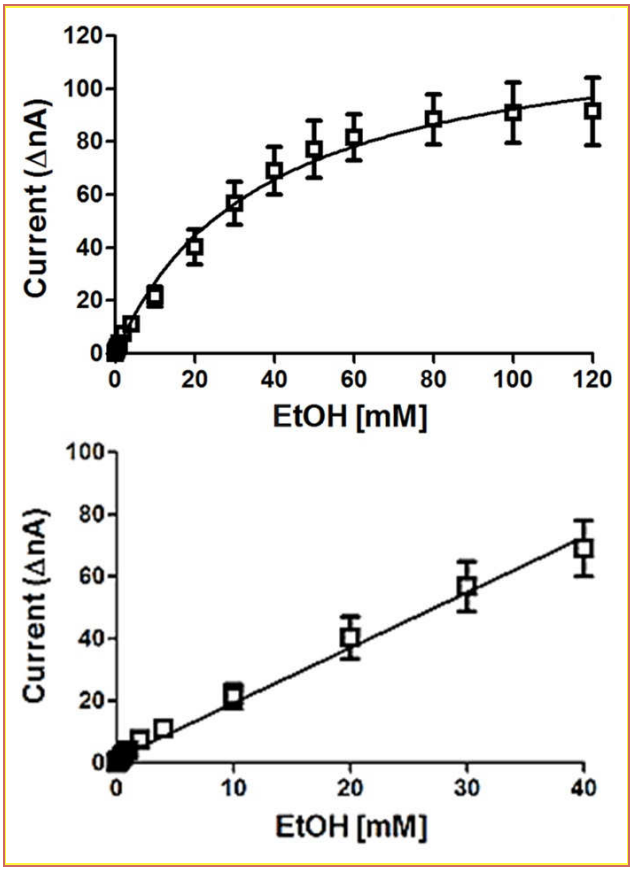

Figure 32: ***In vitro*** **calibration of ethanol biosensors performed immediately before neurosurgery.**

In a separate series of experiments, the potential electrochemical interference of ranitidine was studied *in vitro* on a design 8-200 biosensor (indicated as "b", red line, in Figure 33) and on an enzyme-free sentinel microsensor (Ptc/PPD/[PEI+Glyc]10/PU(1%) indicated as "s", blue line in Figure 33. The aim of these experiments was to demonstrate that ranitidine, known to inhibit alcohol metabolizing enzymes (ADH, ALDH, MEOS as discussed in Section 1.2.1) does not interfere with immobilized AOx activity. Moreover, the test was required to exclude electroactive properties of the molecule at the concentrations used, because of ranitidine does cross the blood brain barrier in small quantities, estimated as 1–20 ng mL^{-1} (Walt et al., 1981).

For this purpose, three successive injections of ethanol (10, 20 and 30 mM, red arrows 1 Figure 33) were made in PBS, succeeded by two injections of ranitidine hydrochloride (1 and 10 µM at green arrows 2 and 3, respectively). Results shown in Figure 33 demonstrated that ranitidine did not interfere with Alcohol Oxidase activity or exhibited any detectable electroactive properties (at +0.7 V *vs.* Ag/AgCl). Biosensors were also exposed to AA (0.5 mM and 1 mM) to confirm their AA blocking properties (data not shown).

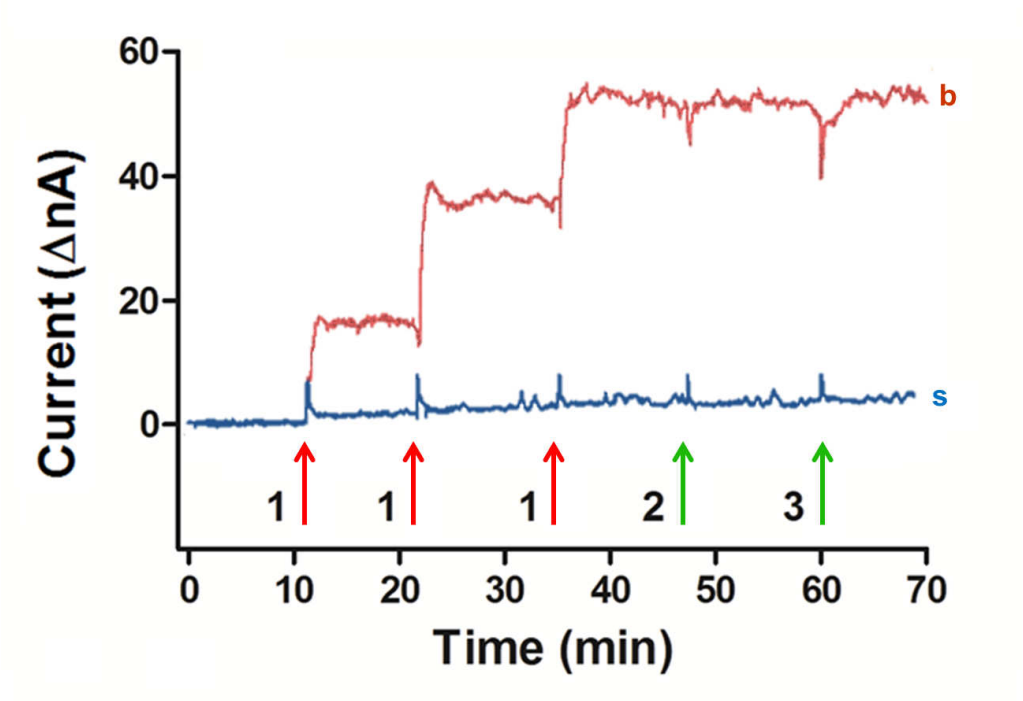

Figure 33: Tests of the potential electrochemical interference of ranitidine performed by two injections of ranitidine hydrochloride in the presence of a biosensor and 'sentinel' sensor. The potential interference of ranitidine was studied *in vitro* on a design 8-200 biosensor (indicated as "b") and on an enzyme-free sentinel microsensor (Ptc/PPD/[PEI(1%)+Glyc(1%)]$_{10}$/PU(1%), indicated as "s") by means of three successive injections of ethanol (10, 20 and 30 mM, red arrows 1) were made in PBS succeeded by two injections of ranitidine hydrochloride (1 and 10 µM, green arrows 2 and 3, respectively).

The *in vivo* experiments started 24 h after surgery (day 1) by polarizing the ethanol biosensor at +0.7 V *versus* the implanted Ag/AgCl reference electrode, and recording the telemetric signal until a stable baseline was reached (by 40–50 min).

The control group of animals (n = 3) was pretreated with an injection of saline solution (1.5 mL i.p; Figure 34, arrow 1). After 20 minutes, the ethanol was administered (1 g kg^{-1} i.g.; Figure 34, arrow 2) and resulted in an increase of the biosensor current that reached its maximum amplitude (23.4 ± 3.2 nA) about 30 minutes after ethanol administration (*i.e.*, at 60–80 min; see Section 1.2 for more informations about ethanol pharmacokynetics). The biosensor current was recorded for 2 hours after the ethanol injection, and decreased to 11.8 ± 3.1 nA.

In a second group of rats (n = 3), ranitidine at dose of 30 mg kg^{-1} dissolved in 1.5 mL of saline was administered i.p. 20 minutes before the intra-gastric administration of ethanol (arrow 1, Figure 34).

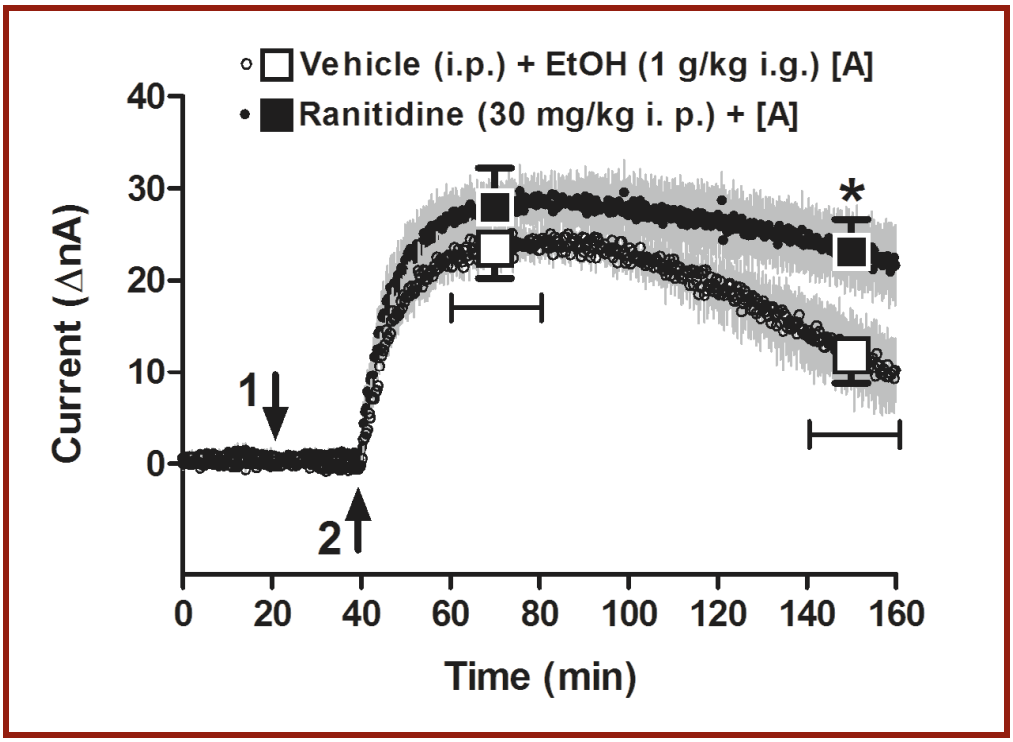

Figure 34: ***In vivo*** **response of ethanol biosensors implanted in the right** ***nucleus accumbens***

The peak of biosensor current appeared about 30 minutes after ethanol administration, and maintained quite a high level (27.9 ± 4.3 nA at 60–80 min). As expected, due to the ranitidine effect on catabolic ethanol enzymes of rats, the subsequent decrease was less pronounced in ranitidine-pretreated animals (23.2 ± 3.5 nA at 140–160 min) and statistically different from the control group ($p < 0.05$). Following the experiments, rats were sacrificed and *post-mortem* histology performed demonstrating that all biosensors were located in the shell of the *nucleus accumbens* (data not shown).

4.8 PPD polymer properties

As stated in Section 3.3, a further investigation of polymer deposition strategies was conducted in a different experimental environment, carried out in the *Biosensors & Electrochemistry Laboratory* of the *School of Chemistry & Chemical Biology* at University College Dublin.

The main purpose was to examine the behavior and the efficiency of the PPD polymer when the *ortho*-phenylenediamine monomer (weak base electrolyte) was dissolved in media other than PBS, which had been used up to this point in our laboratory in Sassari. For each monomer solution, the pH and conductivity (κ) parameters were checked immediately after the electropolymerization procedure. Electro-deposition conditions used in this study are shown in Table 7.

Solution	pH	κ µS cm^{-1}
PBS		
PBS + 300 mM oPD	7.58	12,900
Milli-Q water		
water + 300 mM oPD	7.65	11
100 mM HCl (Milli-Q W)		
100 mM HCl + 300 mM oPD	4.54	6,400
10 mM HCl (Milli-Q W)		
10 mM HCl + 300 mM oPD	5.88	711
10 mM HCl + 100 mM oPD	5.51	885
10 mM HCl + 50 mM oPD	5.20	835

Table 7: pH and conductivity data for the solutions used in the Dublin work. All media were aqueous.

The highest pH value was obtained from the monomer solution made by dissolving 300 mM oPD powder in MilliQ water (pH 7.65). The basicity of the oPD amine groups contribute to increase the alkalinity of the solution. For the same reason, the value of the same high concentration of oPD increased to pH 7.58 the normal value of the PBS buffer pH (7.4). The lowest pH value was obtained for 300 mM oPD dissolved in a100 mM HCl aqueous solution, pH 4.54, due to the amount of acid present. Then, three different monomer solutions were prepared, by dissolving 50, 100 and 300 mM oPD in a 10 mM HCl aqueous solution. pH values progressed from 5.20 to 5.51 and 5.88, respectively, when increasing the dissolved monomer concentration.

Conductivity values (κ) ranged from 11 μS cm^{-1} for 300 mM oPD dissolved in Milli-Q water (illustrating the very weak nature of this electrolyte monomer) to 12.9 mS cm^{-1} when dissolving the monomer in PBS. This latter value was due to the higher ion concentration in PBS buffer compared with the other solutions (Table 7).

The further analysis of electropolymerization values of Q_{poly}, $t_{½}$(poly), I_{max}(AA) and t_{max}(AA) is shown in Table 8 (see Section 3.3 for further details).

Q_{poly} values (the amount of charge passed during the 30 min of the electropolymerization procedure) did not show any particular trend or difference among the various polymers.

Values of $t_{½}$(poly), *i.e.*, the half-life of the exponentially decaying electropolymerization current associated with the self-sealing electro-deposition of the insulating PPD layer, and therefore a measure of the time required by the polymer to form, was faster for monomer solutions containing high ion concentration. In particular, polymers made in PBS medium had a half-life of only 0.35 ± 0.04 s (n=12) while, in contrast, the MilliQ water system needed 480 ± 60 s (n=16). For other polymers, the $t_{½}$(poly) values were rather homogeneous, and not really useful in predicting permselectivity polymer properties.

Values of I_{max}(AA) indicated the highest current (nA) reached by the sensors for 0.5 mM AA in the cell during AA calibrations on day 1 (*i.e.*, the day after polymer deposition).

When this concentration was injected, the naive polymer experienced AA for the first time, and represents a basic model of biosensor implantation in the brain (Figure 35), where a baseline of 0.5 mM AA has been estimated (Miele and Fillenz, 1996; Boutelle et al., 1989; O'Neill and Fillenz, 1985). Thus, I_{max}(AA) was used as a predictive parameter of biosensors behaviour immediately following implantation, but not as discriminative value of the polymer's effective shielding efficiency during LIVE (long-term *in-vivo* electrochemical) recordings.

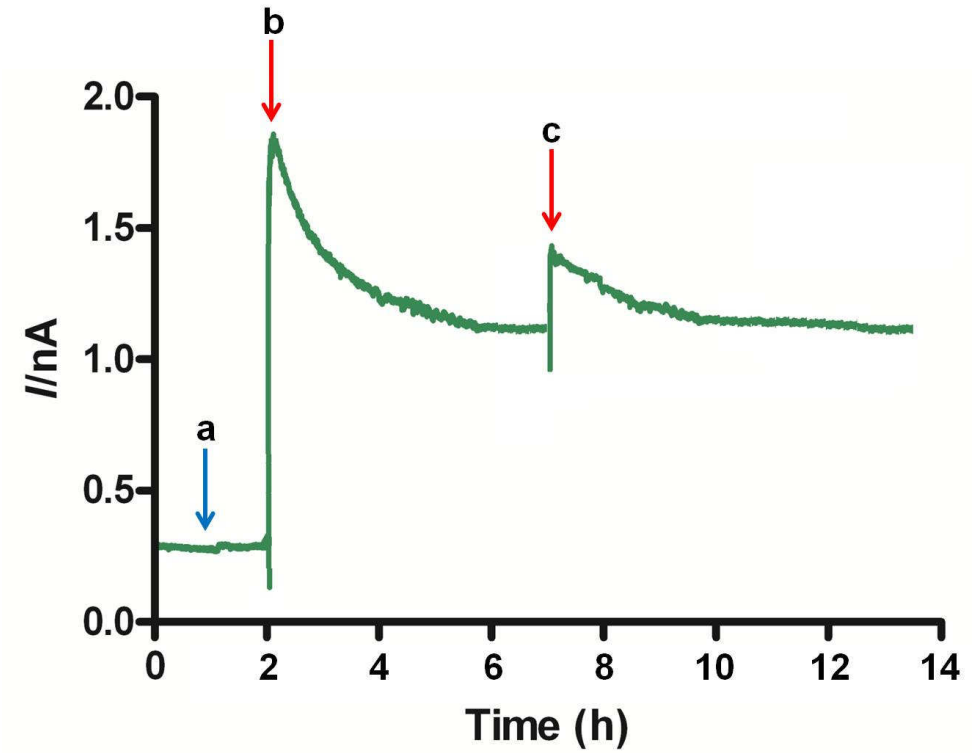

Figure 35: A typical AA time course. Blue arrow (a) indicates the flat baseline current reached by the biosensors following their immersion in PBS overnight. Red arrows correspond to the two injections of 100 mM AA stock solution needed to expose the biosensors to 0.5 mM (b) and 1 mM AA.

Although some I_{max}(AA) values were high compared with the 1 mM AA current (see Table 8), many PPD-coated sensor designs showed a progressive decrease in 0.5 mM AA limiting current, reaching a flat baseline (Figure 35, data not shown).

The best results in terms of I_{max}(AA) were provided by polymer made with 300 mM oPD solved in PBS (1.1 ± 0.1 nA, n=12). Nevertheless, the time needed to reach the peak of the current was long, because of the time course tended to widen over the calibration, as indicated by the t_{max}(AA) value in Table 8 (66 ± 9 min, n=12). In this way, the time required for the current to decrease and reach a 0.5 mM plateau was quite long (Figure 35).

Condition (n-value)	[PPD] mM	Q_{poly} mC	$t_{½}$(poly) s	I_{max}(AA) nA	t_{max}(AA) min	I_L(AA) nA
PBS (12)	300	0.6 ± 0.1	0.35 ± 0.04	1.1 ± 0.1	66 ± 9	0.58 ± 0.09
MilliQWater (16)	300	1.1 ± 0.1	480 ± 60	6.0 ± 0.3	65 ± 8	0.69 ± 0.22
100 mM HCl (12)	300	1.2 ± 0.1	7 ± 0.8	7.6 ± 1.2	200 ± 9	0.66 ± 0.11
10 mM HCl (16)	300	2.1 ± 0.3	13 ± 1	4.0 ± 0.5	34 ± 2	0.39 ± 0.25
10 mM HCl (8)	100	1.0 ± 0.1	9 ± 1	4.3 ± 0.3	600 ± 40	2.68 ± 0.84
10 mM HCl (8)	50	0.8 ± 0.5	8.4 ± 1	4.0 ± 0.3	700 ± 40	2.32 ± 0.26

Table 8: Some PPD electropolymerization and AA calibration parameters

On the other hand, even if polymer made by deposition in 10 mM HCl+300 mM oPD showed the highest I_{max}(AA) value (4.0 ± 0.5 nA, n=16) compared with PBS, the peak was reached in a shorter time (t_{max}(AA) = 34 ± 2 min, n=16), soon beginning to decrease and stabilizing its 0.5 AA limiting current (data not shown). The polymers electro-deposited in the presence of the lower oPD concentrations investigated (100 and 50 mM) gave essentially the same results in terms of I_{max}(AA) value compared with 300 mM oPD, but showed a drastic worsening of t_{max}(AA) values (Table 8).

The MilliQ Water+300 mM oPD polymer showed a I_{max}(AA) value of 6.0 ± 0.3 nA (n=16) and a t_{max}(AA) of 65 ± 8 min. Finally, the polymer made by deposition in 100 mM HCl+300 mM oPD resulted in the worst I_{max}(AA) value and longest t_{max}(AA) values.

Unlike the data discussed above, results obtained by evaluating the analytical performance of the different polymers studied represent the main discriminative data, indicating the apparent permeability and selectivity parameters of the novel polymers: P(HP)%, P(AA)% and S% (see Table 9).

Condition (*n*-value)	[PPD]/mM	P(HP)%	P(AA)%	S%
PBS (12)	300	72 ± 11	0.15 ± 0.03	0.17 ± 0.03
MilliQWater (16)	300	46 ± 7	0.55 ± 0.8	0.74 ± 0.8
100 mM HCl (12)	300	93 ± 5	0.82 ± 0.2	0.36 ± 0.2
10 mM HCl (16)	300	81 ± 4	0.09 ± 0.2	0.07 ± 0.2
10 mM HCl (8)	100	56 ± 5	0.45 ± 0.1	0.62 ± 0.1
10 mM HCl (8)	50	75 ± 5	0.50 ±0.1	0.36 ±0.1

Table 9: apparent permeability parameters. Values of parameters are presented as mean ± standard error (SEM). All electropolymerization were performed at + 0.7 V vs a pseudo Ag reference electrode.

Values obtained for the new polymers were compared with those from the classic medium commonly used for the polymer coating, or by dissolving 300 mM oPD in

PBS buffer, where the apparent permeability to hydrogen peroxide, P(HP)%, was 72 ± 11% (n=12).

An improvement in hydrogen peroxide permeability was achieved by polymerizing the platinum wires with a 100 mM HCl+300 mM oPD solution (93 ± 5%; n=12). The difference in the slopes (nA mM^{-1}) obtained for the hydrogen peroxide calibration performed before and after the polymer deposition was really marginal.

A higher P(HP)% value respect to the PBS condition was also reached by polymerizing the sensors using a 10 mM HCl+300 mM solution, corresponding to 81 ± 4% (n=16), while no improvement was observed by electro-deposition in a 10 mM HCl 100 mM oPD solution.

Comparable results of hydrogen peroxide permeability were obtained between polymers made of 50 mM oPD in 10 mM HCl (75 ± 5%) and the classic PBS+300 mM oPD condition. No improvement was observed by dissolving 300 mM oPD into MilliQ water, not even with 10 mM HCl 100 mM oPD (46 ± 7% and 56 ± 5%, respectively, n=8).

Because the incorporation of a permselective membrane such as PPD on the implantable biosensor surface is required to reject electrochemical interference by reducing agents present in the tissue (McMahon et al., 2006), the values of P(AA)% plays the very key role in determining what is the best performing polymer (O'Neill et al., 2008; Kirwan et al., 2007). The reference PBS conditions of deposition resulted in an excellent AA-rejection value of 0.15 ± 0.03% (n=12). The only improvement was seen following the electro-deposition procedure in the 10 mM HCl+300 mM oPD medium, leading to a value of 0.09 ± 0.02% (n=16). All the other polymers displayed a worsening in AA shielding efficiency, even the one obtained by 100 mM HCl+300 mM oPD medium, that exhibited the best P(HP)% value described above.

Polymer selectivity (S%) defined by eq 5 (Section 3.3) represents the percentage interference by AA in H_2O_2 detection for equimolar concentrations, and for biosensor applications the ideal value would be zero (O'Neill et al., 2008; Kirwan et al.; 2007).

By virtue of the good hydrogen peroxide permeability (81 ± 4%) and the excellent AA rejection properties (P(AA)%, 0.09 ± 0.02%), the polymer obtained by polymerizing at +0.7 V vs Ag in the 300 mM oPD monomer dissolved 10 mM HCl solution resulted in the best selectivity value (S%, 0.07 ± 0.02%, n=16).

Surprisingly, wide variations in PPD electrosynthesis conditions only marginally affected the ability of this polymer to transport H_2O_2 to the metal surface, while demonstrating an efficient AA interference rejection. For example, even a three orders of magnitude difference in the half-life of the electropolymerization self-sealing process observed between the pure water and PBS systems (Table 8), only gave rise to a factor of four difference in their resulting permselectivity (S%) values.

Thus, the correspondent value of S% obtained by dissolving the monomer in PBS buffer was 0.17 ± 0.03% (n=12). This result revealed that the novel polymer improved the permselectivity by a factor of 2.4.

All the other polymers investigated showed a poorer (higher) value of S% (Table 9).

5 - Discussion and conclusions

5.1 Background

Ethanol, is the main non-aqueous component of alcoholic drinks, whose consumption is a legal, commonly-accepted and widespread practice in nearly all societies, particularly in western cultures. As a consequence, alcohol is the most consumed psychoactive drug in the world, due to its abilities to change human consciousness and to its easy availability.

Although there is evidence that a moderate consumption of ethanol could be helpful to the heart (Carrizzo et al., 2013; Tung et al., 2013), an unregulated use of alcohol is truly unsafe: its toxic action on organs, chiefly the liver, coupled with its teratogenic properties and psychoactive effects, make it a dangerous drug for human health.
Alcohol is able to induce cirrhosis and steatosis (Fickert and Zatloukal, 2000), as well as pass through the placental barrier and inhibit fetal growth or weight, creating typical facial stigmata and a series of mental and physical damage, producing the so-called fetal alcohol syndrome or FAS (Lemoine et al., 2003).
Moreover, high levels of ethanol found in drivers' blood is the major cause of death from car crashes, especially among young drivers (Voas et al., 2013; Voas and Fell, 2013).

Acute ethanol effects are due to its pharmacokinetic profiles of absorption, distribution and elimination which determine the level of systemic exposure.
Ethanol crosses the blood–brain barrier and acts as a psychoactive drug primarily affecting brain functions altering perception, mood, consciousness, cognition, and behavior. Ethanol exerts a biphasic effect on the CNS, inducing prevalently euphoric effects at low doses, while depressing its function when BALs increase.

Alcohol affects the physiological action of a wide range of brain neurotransmitters and signaling molecules.

Acute ethanol chiefly enhances inhibitory GABAergic transmission (binding to its specific site at GABA-A receptors, see Figure 3 in Section 1.3.1), and decreases glutamatergic excitatory systems leading to a general weakening of brain functions.
The acute ethanol-derived increase of GABAergic transmission, together with the disruption of the glutamatergic tone in the CNS, are responsible for the euphoric, sedative, tranquilizing and anesthetic properties of beverage alcohol at low–medium concentrations (Lovinger et al., 1989). The dual effect of alcohol manifests when BALs increase further. The alteration of the glutamate system is responsible for staggering, slurred speech, and memory blackouts, while the further contribution of GABA effects, related to high ethanol doses, leads to a severe depressant effect on brain functionality, which in extreme cases can lead to loss of consciousness, coma and even death as a result of respiratory depression (De Witte, 2004).
Moreover, alcohol affects the physiological action of other neurotransmitters and signaling molecules, such as dopamine, serotonin, opioids, acetylcholine, norepinephrine, neuropeptide Y, *etc.*

In particular, opioid systems and serotonin appear to contribute to influence alcohol drinking behavior by interacting with the mesocorticolimbic dopaminergic system (Hyman et al., 2006; Janecka et al., 2004), a specific brain neuronal reward system which uses dopamine as neurotransmitter (see Figure 4 and Section 1.3.7 for further information) involved in movement, motivation, learning, arousal and orgasm, emotion and attention (Gonzales et al., 2004), and demonstrated to play a key role in modulating fundamental survival mechanism of species, such as how to obtain food, water or mating, defined as reward-motivated behaviors (Hyman et al., 2006). Both responses to natural rewards and various drugs of abuse have been found to show several similarities and shared pathways, increasing the level of released dopamine in the associated brain areas (Avena and Hoebel, 2003).

Ethanol acts in the same way, by promoting an increase of activity in the mesolimbic dopamine system (VTA) and of the multisynaptic dopaminergic reward circuitry, resulting (at least acutely) in higher levels of dopamine released in the neuronal dopaminergic projections, predominantly *nucleus accumbens* (Di Chiara and Imperato, 1986; Koob and Bloom. 1988).

Thus, dopamine seems to play a very key role, being involved in those ethanol positive reinforcing properties demonstrated to be crucial in first stages of alcohol addiction. A sensitization phenomenon seems to be the first step leading a subject from alcohol use to abuse, due to an increment in the reinforcement value of ethanol after repeated exposure, when an individual associates the liking effects of alcohol with the positive stimulus of wanting (Robinson and Berridge, 1993). After repeated consumption of alcohol, the wanting is amplified into a pathological status characterized by craving for the drug.

The continual consumption of ethanol can cause alcoholism, a severe pathological chronic relapsing disorder characterized by the high and compulsive ingestion of alcohol, and loss of control over intake (Section 1.4).

The long-term abuse of alcohol produces physiological changes in the brain. The neurotransmitter systems disrupted by acute ethanol, such as those of GABA and glutamate, are even more deeply altered during chronic exposure, generating adaptive processes resulting in a compensatory balance that concur to develop neuroadaptive phenomena such as tolerance (Leblanc et al., 1975) and psychophysical dependence. This dysregulation also involves neural circuits implicated in the control of motivational processes (arousal, reward, stress, *etc*.), such as those involving serotonin, opioids and norepinephrine. The impairment of these systems deeply contributes to the allostatic state that characterizes the development of alcohol dependence (Hardman and Limbird, 2005; Volkow et al., 2007), such as to the onset of withdrawal syndrome, the irrefutable signal of physical dependence characterized by a state of hyperexcitation, anxiety and *delirium tremens* (O'Brien, 2005; Sullivan et al., 1989).

In attempting to restore the "pathological neurotransmitter equilibrium" and avoid the negative psychophysical effects related to further withdrawal episodes (negative reinforcement; Rassnick et al., 1993), the addicted individual needs a continuous assumption of ethanol (Valenzuela and Harris, 1997).

Although subjected to diverse studies, the molecular mechanisms through which ethanol alters the function of the mesolimbic dopamine system have still not been entirely elucidated (Karahanian et al., 2011; Mostofa et al., 2003; Munson et al., 1995). Moreover, the varied and complicated set of interactions with several neuronal pathways makes the investigation of ethanol pharmacodynamics quite difficult. Several researchers focused their efforts to better understand the causes and the mechanisms involved in this very complex disorder, and even if much progress has been made, many other unsolved questions and issues remain for further investigation.

5.2 Approaches to ethanol detection

Ethanol detection in the brain kindles a particular interest, especially the monitoring of its concentration dynamics. New technologies are being combined with traditional approaches to study the effects of acute alcohol as well as the delicate transition from alcohol use and abuse to dependence.

Using the most appropriate methods it is possible to investigate its effects on humans as well as in animal models which recreate the specific symptoms of alcohol dependence (Loos et al., 2013).

Non-invasive approaches such as magnetic resonance spectroscopy (MRS), magnetic resonance imaging (MRI) or positron emission tomography (PET) have been used to monitor directly alcohol and its metabolites, in the CNS of both animals and humans (Adalsteinsson et al., 2006; Ross and Bluml, 2001; Sammi et al., 2000; Hetherington et al., 1999; Mushahwar and Koeppe,1972), while microdialysis demonstrated to be a reliable technique in preclinical studies to investigate the relationship between ethanol-related behaviors and neurochemical variations (Gonzales et al., 1998) and to assess the effects of some therapies for alcoholism (Nurmi et al., 1994).

Nevertheless, all the above-cited techniques possess temporal resolution and detection limits (see Sections 1.5.1–1.5.2 for a further detailed description), yet ethanol concentrations in the brain can vary dynamically, as well as those of the neurotransmitters it affects. As a consequence, their optimal study would require a real-time approach, such as the employment of a biosensing technique, which has already been demonstrated to be a reliable tool in the dynamic detection of a number of neurobiological molecules, with high temporal and spatial resolution (Rocchitta et al., 2013; Secchi et al., 2013; Rocchitta et al., 2012; Mohd Zain et al., 2012; Calia et al., 2009; McMahon and O'Neill, 2006; Lowry et al., 1988).

The desire for monitoring of fast ethanol concentration dynamics focused our research to develop, characterize and optimize an implantable amperometric biosensor capable of real-time monitoring ethanol concentration changes in brain extracellular fluids of animals (Secchi et al., 2013; Rocchitta et al., 2012).

A biosensor is an analytical tool in the form of a self-contained integrated device which is capable of providing a specific, often quantitative, measure of the concentration of a target substrate, using a biological recognition element, usually an enzyme, which is in direct spatial contact with a suitable transducer element (see Section 1.5.3 for a more detailed description).

The flavoprotein Alcohol Oxidase from *Hansenula polymorpha* was chosen as biological element to develop our ethanol biosensor (Sections 1.5.3.2 and 3.4). This aspecific enzyme converts ethanol into acetaldehyde and hydrogen peroxide as a by-product. Then, hydrogen peroxide was oxidized at the Pt transducer surface, by applying a constant anodic potential of +0.7 V *vs* Ag/AgCl, producing a detectable electric current related to ethanol concentration (eqs 6-8 in Section 3.4). Based on the mechanism of how the response is generated, this amperometric ethanol biosensor belongs to the first-generation biosensor category, as discussed in Section 1.5.3.

Five different enzyme solutions were prepared by dissolving the enzyme powder in 1 mL of PBS buffer (Phosphate Buffered Saline), and the concentration expressed as units of protein dissolved per mL, specifically 100, 200, 400, 600 and 800 U/mL.

Nevertheless, in the first phase of biosensor development only the 200 U/mL concentration was used, and immobilized *via* dip-evaporation, as described in Section 3.4.

5.3 Ethanol biosensor characterization

Ten different miniaturized ethanol biosensor designs were initially developed, all based on the same cylindrical geometry, obtained by cutting away 1 mm of Teflon coating the micrometer (125 μm) Pt wire transducer (Figure 7 in Section 3.4).
The different strategies used to differentiate biosensor designs involved the variation of the sequence of PPD electrodeposition and of enzyme immobilization, as well as changes in the amount of enzyme loaded (Section 4.2), the addition or co-addition of enzyme stabilizers (Section 3.5), as well as their disposition in the multi-layered pattern (Section 3.6, Figures 8-11). All these approaches aimed to obtain the best performing design, maximizing ethanol sensitivity as well as the biosensor ability to reject the main electroactive interference species present in the brain, chiefly AA.
Because of the electro-deposition of a poly-*ortho*-phenylenediamine (PPD, described in Section 3.2) nanometer-thick membrane has proven to be a reliable procedure to drastically limit the passage of AA trough the biosensor component layers, allowing simultaneously a good hydrogen peroxide permselectivity (Kirwan et al., 2007), all designs manufactured were based on this strategy for blocking interference species (Secchi et al., 2013; Rocchitta et al., 2012).

Immediately after the manufacture, all biosensors were characterized *in vitro* in an electrochemical cell (Section 3.7) at day 0, corresponding to the time of *in vivo* implantation, and at days 1-2, which represent the first and second day of *in vivo* data recording.
Among these ten designs, the four most promising biosensors (5,7,8 and 10; see Tables 2 and 3) were further calibrated once at week (day 7, day 14, day 21) up to day 28 to know the temporal limit of each biosensor design for a reliable *in vivo* use, investigating the stability of the enzymatic activity and polymer shielding efficacy before biosensor performances decrease (Section 4.1.2).

Ethanol and AA calibrations were performed using CPA technique (see Section 1.5.3.1) and biosensors performance analyzed in terms of I_{MAX}, K_M, LRS and AA shielding power (eq.9, Section 3.4) as well as by evaluating LOD and LOD values (eqs 12 and 13). These are fundamental parameters in order to evaluate the sensitivity to ethanol versus interference species (O'Neill et al, 2008), and are critical to select the best performing design for *in vivo* implantation (Secchi et al., 2013; Rocchitta et al., 2012).

The first step was to establish the best strategy to immobilize the enzyme relative to PPD polymer deposition, in order to achieve the highest number of active AOx molecules on the biosensor surface.
The amount of active enzyme on related biosensor surfaces is quantified by I_{MAX} parameter (eq 9), provided the sensitivity of the biosensor to the hydrogen peroxide is similar across the designs (Kirwan et al., 2007; Rothwell et al., 2010).
Comparison of results obtained at day 1 shows that the first biosensor developed (design 1) had the worst sensitivity (Tables 2-3, Section 4.1.1). Evidently, immobilization of the enzyme on the metal bare and the electropolymerization of PPD over the biological component layer was not advantageous (Figure 8).

As shown in Table 2, an increase in I_{MAX} was observed in design 2, where PPD was directly deposited on the transducer surface while Alcohol Oxidase was immobilized over the PPD nanometer-thick layer. Moreover, 1% PU was introduced as a "trapping net" (Figure 9).
The further addition of PEI (Figure 10) led to an increase in biosensor I_{MAX} value, compared with both designs 1 and 2 (Table 2). PEI is a positively-charged macromolecule usually known to act as an enzyme stabilizer (Bolivar et al., 2009; Qian et al., 2004) that interacts with the negative charges of the oxidase enzymes (at pH 7.4), enhancing their catalytic activity (Section 3.5). However, in our study, PEI acted more as an "enzyme activity enhancer", as previously described (Secchi et al., 2013; Rocchitta et al., 2012; McMahon et al., 2006).

On the other hand, the presence of glycerol gave greater stability to the biosensor.
Then, mixing together both PEI and glycerol (1% solution), we obtained an additive effect evidenced by the increased number of active enzyme molecules demonstrated by the enhanced I_{MAX} and decrease of LOD and LOQ values (Tables 2 and 3) and by the maintenance of such high I_{MAX} and values over time (Figures 21, Section 4.1.2) due to the glycerol effect in designs 7, 8 and 10 (Rocchitta et al., 2012).

The second apparent Michaelis–Menten parameter, K_M, is the substrate concentration corresponding to the half of I_{MAX} response, and reflects both the affinity and access of the substrate to the enzyme (Moran et al., 2005).
This parameter plays a dual significance in analyzing biosensors performance: it determines the amplitude of linear region slope of the biosensor substrate (LRS = I_{MAX} / K_M), as well as the concentration range of the linear response (~½K_M) (Bazzu et al., 2009; Kirwan et al., 2007). Thus, the higher the K_M value, the smaller the LRS but the wider the linear response region (Rocchitta et al., 2012).
Due to the findings that ethanol in rats CNS could reach a concentration of 30 mM after 1 g/kg i.p. injection (Yoshimoto and Komura. 1993; Adalsteinsson et al., 2006), corresponding to the dose and route of administration we wanted to use in our *in vivo* experiments, all the approaches were aimed to achieve the best I_{MAX} and K_M values, in order to obtain the highest ethanol LRS up to 30 mM (Rocchitta et al., 2013).
The K_M values of design 8 were the lowest, meaning that the substrate had a higher affinity for the enzyme, resulting in a faster turnover of ethanol molecules catalyzed by each protein.
Thus, the introduction of the enzyme enhancer PEI provided a sustained increase in LRS values. Even though LRS is generally valid only up to half the K_M value (Kirwan et al., 2007; Rothwell et al.; 2010) design 8 showed a good linearity up to 40 mM with R^2 = 0.996 (Table 3) because of slight deviations from Michaelis–Menten behavior (R^2 < 0.98, Table 2) in the form of a flattening of the calibration plot at low concentrations (see Figures 12A-C and 32). Moreover, due also to the glycerol effect, design 8 I_{MAX} and LRS values were statistically superior respect to the other designs

until the seventh day after its manufacture, as discussed in Section 4.1.2 and shown in Figures 21-22.

Although having the same mix of enzyme stabilizers (PEI+Gly, 1%), design 10 did not reproduce the very good results of design 8. It is possible that the addition of the protein BSA reduced the enzymatic activity, as well as the process of cross-linking by GA could inactivate AOx, reducing the number of active molecules.

As described before, following the failure shown by PPD coating procedure used for design 1, the common strategy used for blocking electroactive species was the electrodeposition of a PPD polymeric layer onto the bare metal surface. Nevertheless, the shielding efficacy for AA among all the sensors was quite different, depending on the structure of the particular design, ranging from 0.8 up to 2.6 nA at day 1 (Table 3 on Section 4.1.1).

The gap improved during the study of PPD polymer effectiveness over time. In a multilayer, pattern-based biosensor, AA shielding efficacy could even be affected by the different components added over the PPD coating. The final quick dip in the 1% PU solution (strong THF solvent, see Section 3.1) did not affect the PPD polymer consistency, and guaranteed a better AA interference rejection over the first week for both designs 5 and 8, while on the other hand it seemed to be that the BSA-GA cross linking contributed to a deterioration of designs 9 and 10, which showed the worst capacity in AA shielding (Figure 24 in Section 4.1.2). This suggested that one week was the limit of reliability of those biosensor for *in vivo* implantation.

Furthermore, no significant interference signals were observed on exposing biosensors to other electroactive molecules (dopamine, 3,4-dihydroxyphenylacetic acid, and uric acid) present in the CNS extracellular fluids, even at pharmacologically relevant concentrations (data not shown), as reported previously for other PPD-based biosensor designs (Ryan et al., 1997).

Indeed, another important parameter was determined from calibration data obtained from EtOH and AA responses over time.

Because evidence in literature suggests that ethanol could reach a concentration of about 30 mM in the CNS after intraperitoneal injection (Adalsteinsson et al., 2006; Jamal et al., 2003) as well as its administration i.p. can increase AA levels (about 0.5 mM) by about 200% in the *striatum* (Liu et al., 1999; Hou et al., 2005; Hou et al., 2007; Dai et al., 2006), we decided to quantify the percentage interference by AA relative to the measured biosensor current for 30 mM ethanol.
Although the response of AA in some brain areas, such as the *hippocampus*, can be markedly different from that in the *striatum* (Grünewald et al., 1983), AA baseline levels and responses in the *striatum* and *nucleus accumbens* are often quite similar (Brose et al., 1989; Fillenz and O'Neill RD. 1986). This knowledge of AA levels is important in which *nucleus accumbens* is the brain area where our ethanol biosensor would be implanted, being this neuronal termination widely accepted to be the epicenter of reward in the brain and where higher levels of dopamine are released after ethanol intake (Di Chiara and Imperato, 1986; Koob and Bloom, 1988). Moreover, as discussed above and widely in Sections 1.3.7 and 1.4, the *nucleus accumbens* is involved in those ethanol positive reinforcing properties and sensitization phenomenon demonstrated to be crucial in first stages of alcohol addiction (Robinson and Berridge, 1993), as well as in the pathological status characterized by craving for the drug (Gilpin and Koob, 2008).

So, variations in the AA current when its concentration changed from 0.5 (striatal and *nucleus accumbes* ECF baseline level) to 1 mM where evaluated, expressed in nA as AA ΔI. The impact of AA ΔI on the current resulting from 30 mM ethanol is shown in Figure 25.
For design 8, the percentage interference was estimated to be less than 1% up to day 2, and about 2% up to a week after the biosensor manufacture.

Then it reached a value of 25% at day 14, increasing week by week in conjunction with the worsening of polymer shielding ability (Rocchitta et al., 2012).
These results confirmed that design 8 could not be implanted for more than one week because of the decrease in its sensitivity (worsening of I_{MAX} and LRS values) and selectivity, associated with the increase in AA interference (Secchi et al., 2013; Rocchitta et al., 2012).
Nevertheless, these data also assessed that the predictable variations in AA concentrations *in vivo* in our target CNS area are unable to interfere significantly with the currents produced by 30 mM ethanol during the first 7 days in design 8, confirming that the best biosensor design developed among the ten original designs could be a reliable tool for short-time monitoring of ethanol *in vivo* (see Section 4.1.2 for all detailed results and comparison among the different designs).

Based on the findings that design 8 was demonstrated to be the best performing and stable biosensor among all those developed, our study re-focused on investigating what the effects might be of depositing a different concentration of the enzyme AOx compared to the 200 U/mL solution used until this stage of the project (see Section 4.2 and subheadings, and Secchi et al., 2013; Rocchitta et al., 2012).

Our goal was to achieve an improvement of active enzyme loading on the biosensor surface, in order to obtain higher I_{MAX} values, as well as to extend its stability over time, decisive in evaluating the limit of *in vivo* reliable use ascertained as 7 days for design 8.
Having established the benefits of design 8, however, the multilayered disposition of this configuration (see Figure 10, Section 3.6) was not varied, nor was the deposition sequence; at this stage, the only variable considered to further optimize the biosensor was to change the Alcohol Oxidase solution concentration. Four fresh different Alcohol Oxidase solutions were prepared, dissolving respectively 100, 400, 600 and 800 enzyme units in 1 mL of PBS buffer in order to enhance ethanol biosensor performance and sensitivity.

Thus, four new ethanol biosensor designs were generated by dip-evaporation into the fresh solutions. Because the enzymatic concentration variation of these different designs 8 assumed a critical relevance, it is necessary now to specify it for each of design 8. So, the original design 8 was re-named as “design 8-200”, indicating the AOx concentration of 200 U/mL. Similarly, “design 8-100” refers to the biosensor set obtained by 10 dips into the 100 U/mL AOx solution, as well as “design 8-400”, “design 8-600” and “design 8-800” nomenclature will be used for biosensors made with the most concentrated enzymes solutions, as described on Section 4.2.

For the four new designs (n = 4 for each group), the sensitivity to ethanol and AA at day 0 and days 1-2 was assessed. In the same way, a study of their stability over time (day 0 to day 28) was conducted, by analyzing the apparent Michaelis–Menten kinetic parameters (I_{MAX} and K_M) and the linear region slope (LRS) in the reference linear range (Table 4), as well as LOD and LOQ values, and the efficiency in rejecting AA interference (Table 5). Results were then compared with results already obtained by design 8-200, in order to evaluate and quantify how the difference in AOx loading affected biosensor performance (Secchi et al., 2013; Rocchitta et al., 2012).

Table 4 of Section 4.2.1 shows the trend of I_{MAX} values obtained at day 1: the increase in Alcohol Oxidase concentration loading from 100 to 200 and 400 units per mL led to a linear increase of I_{MAX} values. The highest I_{MAX} values (308 ± 10 nA) were obtained with an AOx loading solution of 400 U/mL (design 8-400). After this peak, the response exponentially decreased for the more concentrated AOx solutions (designs 8-600 and 8-800).

A similar trend was observed for LRS (Table 4). It is surprising to observe a decrease in ethanol response for the more concentrated enzyme solutions. This phenomenon could be explained by the reduction of the number of active enzyme molecules on the biosensor surface.

This hypothesis is not consistent with oxygen dependence results: the fact that the $K_M(O_2)$ increased monotonically as the concentration of enzyme in solution increased, suggests that the loading of active enzyme is also increasing monotonically and producing more H_2O_2. An alternative explanation is that the excessive loading of macromolecules on the surface has decreased the electrodes' sensitivity to H_2O_2 (O'Neill et al, 2008) as confirmed by the hydrogen peroxide calibration results showed in Table 5 (Secchi et al., 2013).

Even the presence of PEI and glycerol may affect the response of AOx. As previously described, PEI led to an increase in I_{MAX} and LRS on design 8-200 acting as enzyme activity enhancer while glycerol gave greater stability to the biosensor over time (see also Section 4.1.2 and Rocchitta et al., 2012). The enhancement of catalytic activity is related to PEI characteristics: it is a positively-charged molecule able to interact with the negative charges of the oxidase enzymes at pH 7.4 (McMahon et al., 2006). Thus, it is possible that the best combination between enzyme loading and PEI enhancement was obtained at immobilizing at design 8 a 400 U/mL AOx concentration, while a further boost in enzyme loading unbalanced this equilibrium (Secchi et al., 2013).

As already discussed, all our efforts were aimed to increase as much as possible I_{MAX} and K_M values in order to achieve the highest ethanol LRS and linear range (eq. 9). As described for design 8-200, the new designs also showed a good linearity up to 40 mM with $R^2 > 0.996$ (Table 4) because of slight deviations from Michaelis–Menten behavior ($R^2 < 0.984$, Table 4) in the form of a flattening of the calibration plot at low concentrations (Kirwan et al., 2007; Rothwell et al.; 2010). The only exception was design 8-100 that showed a linear response up to 30 mM ethanol (Secchi et al., 2013).

Design 8-400 showed the best performance, in which LRS value of 3.94 ± 0.12 nA mM^{-1}, double the value previously obtained by the original design 8-200 (1.77 ± 0.08 nA mM^{-1}).

Moreover, data emerged from experiments at day 1 revealed that K_M increased linearly with enzyme loading up to 400 U/mL, and remaining at stable values for higher loads on designs 8-600 and 8-800 (Table 4). This trend reflects both a decrease of the affinity of the enzyme to substrate and an increasing difficulty of the substrate to access to enzyme catalytic sites (Moral et al., 2005). The above-discussed enzyme–PEI unbalanced equilibrium and an increase in the number of enzyme molecules on the biosensor surface could be responsible of the K_M increase. This observation is confirmed by the progressive increase of LOD and LOQ values with the enzyme loading, as shown in Table 5 of Section 4.2.1 (Secchi et al., 2013).

Finally, no substantial difference among all the new designs at day 1 was found in terms of AA rejection (Table 5). As a matter of fact, the 1 mM limiting currents ranged from a minimum of 0.98 ± 0.27 nA (400 U/mL) to a maximum of 1.73 ± 0.13 (200 U/mL).

The further study of stability of the new biosensors over a period of 28 days showed that I_{MAX} and LRS values decreased over time(Figures 26 and 28), while K_M slowly increased (Figure 27).

Nevertheless, a significant improvement in terms of stability was shown by design 8-400; in fact, its better sensitivity and sensibility shown at day 1 (Table 4) was confirmed over time, resulting in I_{MAX} and LRS values statistically higher than for the others from day 0 to day 7 ($p < 0.05$ vs other designs), remaining superior until day 21. Finally, at day 28, the gap between all designs tended to be smaller, as stated in Section 4.2.2.

These results ascertained that a considerable improvement with respect to the original design 8-200 was achieved by design 8-400, both at day 1 and over time, particularly after 7 days.

Moreover, the biosensors effectiveness to reject AA interference was monitored throughout the aging study and expressed as AA ΔI, showing an averaged value of 0.47 ± 0.04 nA (n=20) up to the seventh day after manufacture (Figure 29). Although not statistically significant, the increase in enzyme loading progressively improves the shielding performance against AA. The above-hypothesized loss of positive charges and an increase in negative charges could justify this trend as AA is anionic at pH 7.4 (Secchi et al., 2013; Rocchitta et al., 2012).

Unfortunately, after the first week all devices showed an increased sensitivity to AA, confirming what was already found for design 8-200: these ethanol biosensors cannot be implanted chronically for more than one week because of the decrease in their selectivity associated with the increase in AA interference (Sections 4.1.2 and 4.2.2 and Figure 25). So, the study of enzyme loading assessed that design 8-400 was the best performing compared with the original design 8-200 (Secchi et al., 2013), but no further improvement in terms of stability over time was achieved.
To improve AA rejection as well as limit the worsening of PPD polymer over time would be a critical requirement for future *in-vivo* studies, and was therefore the object of further investigation, as described below (see Sections 3.3 and 4.8, Tables 7-9).

5.4 Ethanol biosensor oxygen dependence

Thus, at this stage of ethanol biosensor optimization, two particular designs showed the best performance: design 8-400 and the original design 8-200.

The next study aimed at selecting what design would be the more reliable for *in vivo* monitoring ethanol concentration variations was to assess the reproducibility of biosensors performance under physiological values of oxygen concentration, pH and temperature (Secchi et al., 2013).

As a matter of fact, *in vitro* working conditions are quite different from those biosensors had to face in ECF, mainly in term of air oxygen tension and temperature; so it is fundamental to predict which could be the *in vivo* behavior of biosensors exploiting an oxidase enzyme as biological element.

As discussed before in Sections 1.5.3.2 and 3.4, the flavoprotein Alcohol Oxidase uses oxygen as electron acceptor to catalyze the conversion of ethanol into acetaldehyde and hydrogen peroxide (Figures 7 and 36, eqs. 6-8). As a consequence, an adequate amount of oxygen as co-substrate is required to allow the biosensor to reach its highest enzymatic activity.

A study of the oxygen dependence of biosensors was conducted in PBS in an air-tight electrochemical cell (See Sections 3.8-3.8.1 and 4.3, Figures 13-16), in order to monitor the response of these devices in conditions which simulate striatal oxygen concentrations, estimated as about 50 μM (Zauner et al., 1995; Murr et al., 1994; Nair et al., 1987). This value is significantly different from oxygen concentration in the air (260 μM) present in the laboratory environment for *in vitro* biosensor characterization. An oxygen microsensor was used to monitor the variation in O_2 tension (range from 0 up to 260 μM). Protocol used for this study is shown in Table 1.

As shown in Table 6 of Section 4.3, the oxygen-dependence studies showed that $I_{MAX}(O_2)$ increased with enzyme loading from 100 up to 400 U/mL (64.2 ± 4.3 nA).

The higher I_{MAX} (O_2) values were obtained when loading from an AOx solution of 400 U/mL in design 8-400; after this peak, the response exponentially decreased (Secchi et al., 2013). This trend reflects the above-discussed response to ethanol. The apparent $K_M(O_2)$ increased linearly with enzyme loading reaching the value of 72 ± 11 μM for design 8-800. Dissolved oxygen concentrations in the brain (*striatum*), calculated in a previous study (Bazzu et al., 2009) corresponded to about 37 μM, a value consistent with other results (~50 μM) from international literature (Zauner et al., 1995; Murr et al., 1994; Nair et al., 1987).

Twice the apparent $K_M(O_2)$ value corresponds to the oxygen concentration in enzyme saturation conditions ($I_{MAX}(O_2)$). As a result of this, for monitoring ethanol concentrations in the brain ECF independently from oxygen physiological oscillations, it is necessary that the implanted biosensor $K_M(O_2)$ needs to be lower than one half of the oxygen concentration dissolved in the brain ECF (*i.e.*, < 25-18 μM in relation with previous findings).
In this way, the biosensor would be saturated with oxygen, which is the electron acceptor involved in AOx catalysis (see reactions 6–8), so that ethanol oxidation kinetics would be limited only by the apparent Michaelis–Menten parameters for ethanol.

Unluckily, while design 8-400 demonstrated to be more sensitive and stable up to 1 week among all designs developed, it displayed an excessive oxygen dependence ($K_M(O_2)$ = 38 ± 5 μM; see Table 6 in Section 4.3) which could undermine its *in vivo* performance.

On the other hand, design 8-100 and design 8-200 fulfill the $K_M(O_2)$ requirement, as illustrated in Table 6. Among these two designs, biosensors loaded with 200 U/mL AOx concentration ($K_M(O_2)$ of 17.3 ± 4.4) was demonstrated here to be the best performing in terms of the analytically most important parameter (LRS) on day 1 (Tables 4-5) as well as of stability over time (Figures 26-29 on Section 4.2.2), and was therefore considered the most reliable design to monitor ethanol concentration in the brain for up to 7 days (Secchi et al., 2013; Rocchitta et al., 2012).

Nevertheless, design 8-400 could be suitable for some *in-vivo* experiments when the concentrations of ethanol are not particularly high as in self-administration experiments, where peaks of ethanol are not so pronounced and the consumption of oxygen is not pushed to the extreme as it happens for experimental conditions where ethanol is administrated i.g. (1 g kg^{-1}).
Moreover, our result suggested that design 8-400 could be the best biosensor for *in-vitro* experiments, in terms of its global performance (Secchi et al., 2013).

5.5 Ethanol biosensor response time, pH- and temperature-dependence

Following the crucial findings derived from oxygen dependence studies, the response time for ethanol, and the temperature- and pH-dependence profile of design 8-200 were investigated, in order to complete its *in vitro* characterization.

As discussed in Section 4.4, the response time of ethanol biosensors, corresponding to the time needed for the signal to reach 90% of its maximum response value ($t_{90\%}$) starting from its baseline current following the addition of ethanol aliquots in the electrochemical cell, was quite fast for design 8-200, corresponding to 1.6 ± 0.7 s.

The pH-dependence results demonstrated that the biological element (AOx) exhibited quite a stable response at physiological concentrations of H^+ (in the brain) in a range between pH 7.36 and 7.42, despite the finding that pH values between 8.6 and 9.2 resulted in the optimum of biosensor performance (Figure30, Section 4.5), in agreement with previous studies (Barsan and Brett, 2008).

Finally, temperature-dependence studies revealed a fair stability of biosensor response at physiological temperatures (Figure 31, Section 4.6).

As result of the overall findings obtained after biosensor development, characterization and optimization, design 8-200 was demonstrated to be the best biosensor configuration (among all those studied here) for *in-vivo* applications up to one week after implantation (Secchi et al., 2013; Rocchitta et al., 2012).

5.6 Ethanol biosensor *in vivo* studies

As previously discussed (Section 1.3 and corresponding subheadings), ethanol exerts its psychoactive effects by interacting with several neurotransmitter systems, chiefly enhancing inhibitory GABAergic transmission and decreasing the glutamatergic excitatory systems, while its positive reinforcing properties are related to activation of mesocorticolimbic dopaminergic pathways (Di Chiara and Imperato, 1986).

Because the projections of VTA dopaminergic cell bodies play a pivotal role in mediating ethanol positive reinforcing properties, and were demonstrated to be deeply involved in first stages of alcohol addiction (Sections 1.3.7-1.4), *nucleus accumbens* was chosen as the brain area for real-time monitoring of ethanol concentration dynamics (Rocchitta et al., 2012).

Amperometric biosensors (design 8-200) were implanted in the right *nucleus accumbens* of Sprague-Dawley rats by means of stereotaxic surgery performed under total anesthesia (see Figures 19-20 in Section 3.11.1 and Rocchitta et al., 2012). After the surgery, animals were housed in large plastic bowls, where the *in vivo* experiments were performed at day 1, 24 h after the implant, to allow a full animals' health recovery.
The telemetric device was connected to implanted biosensors for real-time wireless data recording. This arrangement allowed to rats to freely move during the experiments, reducing handling and other forms of stress (Calia et al., 2009; Bazzu et al., 2009). Biosensors were polarized at +0.7 V vs Ag pseudo RE, and the telemetric signal recorded until a stable baseline was obtained (Figures 34 and 36).
The experiments were carried out using two groups of animals, both administered with ethanol i.g. 1 g kg^{-1}. The control group (n=3) was pretreated i.p. with vehicle (1.5 mL saline solution) 20 minutes before ethanol was administrated.

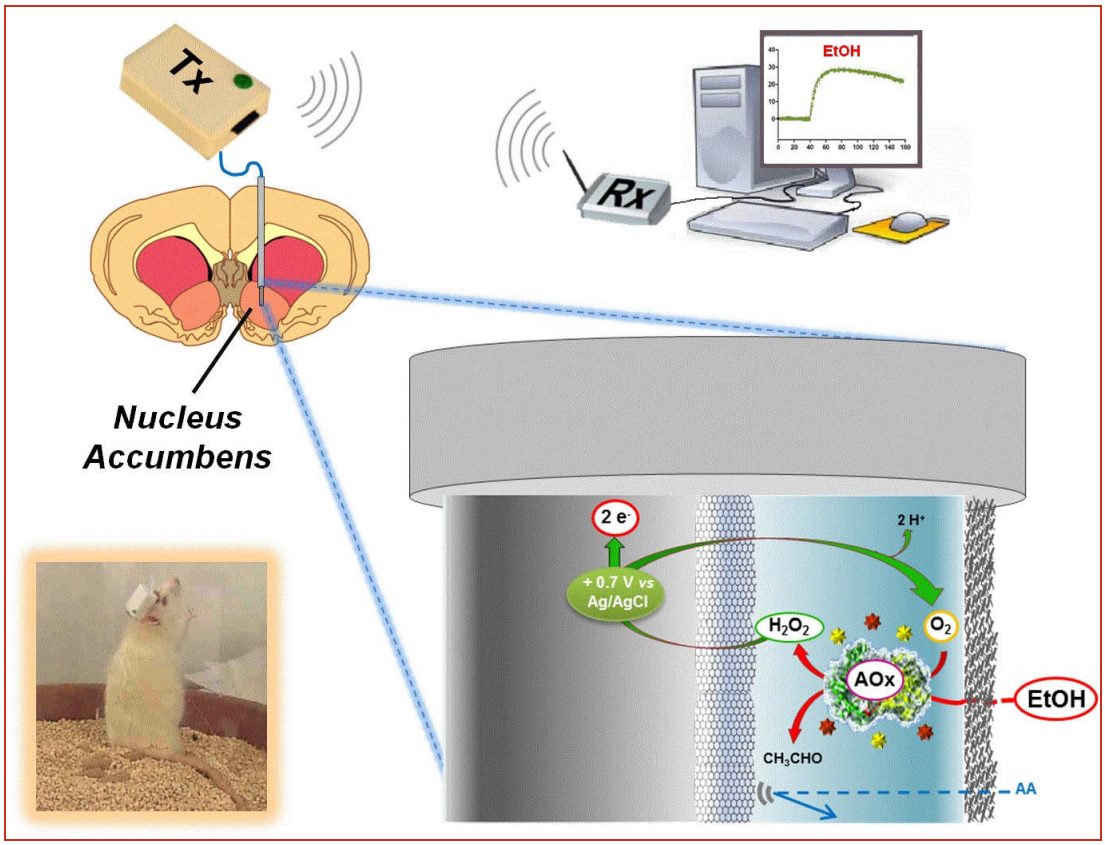

Figure 36: Representation of *in vivo* ethanol real-time telemetric monitoring in the brain of freely moving rats.

Ranitidine at dose of 30 mg kg^{-1} dissolved in 1.5 mL of saline was administered i.p. to the second group of rats (n = 3), 20 minutes before i.g. administration of ethanol. When ethanol reached the brain ECF, there was an increase of its current recorded by the biosensors implanted in the *nucleus accumbens*. Ethanol concentration was detected in real-time and estimated using the pre-implantation calibration shown in Figure 32 (Rocchitta et al., 2012).

The maximum concentration of ethanol in the extracellular compartment (Figure 34, vehicle-treated group), was equivalent to approximately 14 mM (60–80 min) and decreased down to ~6 mM (140–160 min). These results, although lower than those obtained using *in vivo* microdialysis by Jamal and collaborators (corresponding to 23 mM; Jamal et al., 2003), are in agreement with data recorded by Yoshimoto and

colleagues, who estimated ECF ethanol at 18 mM under similar conditions (Yoshimoto and Komura, 1993).
In another microdialysis study, Yim and coworkers found a maximum concentration of ethanol in the *nucleus accumbens* corresponding about to 6 mM after i.p. injection of 1 g kg^{-1} of ethanol (Yim et al., 1998). Using proton magnetic resonance spectroscopy, Adalsteinsson and collaborators obtained similar results administering the same dose of ethanol i.g.; however, the maximum averaged ethanol concentration (~30 mM) was reached in the CNS after its i.p. administration (Adalsteinsson et al., 2006).

These differences in attempts at absolute determination of *in vivo* ethanol concentrations may be related both to different experimental setups and analytical methods used for ethanol quantification, and are not surprising in view of the assumptions made in these estimations (Chefer et al., 2006). However, the detailed real-time concentration dynamics achievable with implanted biosensors, such as those shown in Figure 34, are of greater import than absolute levels at this stage of *in-vivo* monitoring methodology development (Rocchitta et al., 2012; Secchi et al., 2013).

As previously discussed (Sections 1.2.1 and 4.7), ranitidine is a competitive histamine H_2 receptor antagonist widely used in peptic ulcer disease treatment (Di Padova et al., 1992). This drug is also considered to affect ethanol metabolism (Brett, 2005) by inhibiting cytochrome P450 (CYP2E1), alcohol dehydrogenase (El-Bakary et al., 2010) and aldehyde dehydrogenase enzymes (Yokoyama et al., 2001). Because of this multitarget pharmacological profile, ranitidine is able to increase the bioavailability of ethanol by modifying its pharmacokinetics (see Sections 1.2-1.2.1 and Arora et al., 2000).
Evidence has shown that BALs increase in drinkers following ranitidine administration (Arora et al., 2000; Di Padova et al., 1992).

As Walt and coworkers showed that ranitidine does cross the blood–brain barrier in small quantities, estimated as 1–20 ng mL^{-1} (Walt et al., 1981), we studied the effects of the drug on the implantable biosensor *in vitro* (Figure 33 in Section 4.7) before its administration *in vivo* (Rocchitta et al., 2012).
Our results showed that ranitidine is not an electroactive molecule, and did not interfere with the ethanol signal (Section 4.7). Moreover, biosensor activity was not affected by this multitarget drug, demonstrating that alcohol oxidase is not inhibited by ranitidine, further justifying its selection as biological element versus alcohol dehydrogenase (Section 1.5.3.2).

The administration of ethanol to ranitidine-pretreated animals (n = 3) resulted in an increase of extracellular ethanol levels estimated at ~16 mM (60–80 min; Figure 34) 30 minutes after ethanol administration, quite higher than peak values obtained in the saline-control group, although not statistically significant. The subsequent decrease in biosensor signal, however, was significantly smaller in the ranitidine-pretreated group, estimated as 14 mM versus ~6 mM of saline-control group (140–160 min; $p < 0.05$; Figure 34 in Section 4.7), consistent with the inhibition of ethanol metabolism.

5.7 Biosensing advantages compared with other ethanol detection approaches

The results of the present study ascertained that the developed ethanol biosensor, design 8-200, is a reliable device for the short-term monitoring of exogenous ethanol in CNS extracellular fluids. The implantable biosensor, integrated into a low-cost telemetry system, represents a new generation of analytical tools for studying ethanol pharmacokinetics and the effect of drugs on ethanol levels in real time (Secchi et al., 2013; Rocchitta et al., 2012).

Moreover, this tool possesses a range of features that makes it more advantageous compared with other methods previously used to measure ethanol concentration in the brain, such as spectroscopic techniques and microdialysis (Table 10).

As stated above (Section 5.2) and more extended in Section 1.5.1 and corresponding sub-headings, clinical and preclinical studies of ethanol kinetics have been carried out by means of spectroscopic techniques, exploiting their main advantage, *i.e.*, the absolute non-invasiveness of the procedures to monitor changes in ethanol tissues concentrations in animal models as well as in humans. These methods used spectroscopic techniques such as magnetic resonance spectroscopy (MRS) and magnetic resonance imaging (MRI) or positron emission tomography (PET), which are principally used to monitor ethanol metabolites (McRobbie et al., 2007; Adalsteinsson et al., 2006; Ross and Bluml, 2001; Sammi et al., 2000; Hetherington et al., 1999).

Despite their non-invasive approach which makes spectroscopic techniques reliable for *in vivo* experiments in humans, ethanol cannot be detected in concentrations lower than millimolar levels, and only for a short time (a few minutes). Moreover, labeled chemicals could be toxic for long-term exposure, and the technique is applicable for only non-dynamic experiments in which, even when no tethering is required, both animals and humans have to stay motionless during the experimental sessions (Rocchitta and Serra, 2013).

In vivo microdialysis (Section 1.5.2, Figure 5) has been applied in preclinical studies to investigate the relationship between ethanol-related behaviors and neurochemical variations (Gonzales et al., 1998). Furthermore, local perfusion of ethanol in specific brain region has been used to investigate the potential involvement of local mechanisms, and also to assess the effects of some therapies for alcoholism (Nurmi et al., 1994).

In spite of microdialysis being a well-known and widespread technique due to its several advantages, such as the possibility of monitoring ethanol pharmokinetics and the concentration dynamics of several neurochemicals at the same time, providing a more complete picture of the metabolic changes induced by alcohol intake (*e.g.*, DA or 5-HT, see Sections 1.3 and sub-headings), this technique possess some limiting factors. For example, it is invasive, because a probe has to be implanted in the brain, limiting its use to preclinical studies (Table 10).

Also, the temporal resolution of microdialysis is poor, and there is a need to have a parallel analytical and usually chromatographic system. Moreover, microdialysis requires connecting tubes to carry out the experiments, which complicate the manipulations of the animals by the operator (Bazzu et al., 2012). This affects the stress of the animals and may induce the release of neurotransmitters that are collected in the samples, finally influencing (overestimating) the measurement of neurochemicals released by ethanol intake.

As shown in Table 10, ethanol biosensors developed in this study have several advantages. The main characteristics of these devices are represented by the potentially very low invasiveness (*e.g.*, 25-µm diameter PPD-based biosensors have been reported; see Rothwell et al., 2009), compared with microdialysis probes, and, most of all, the capability of monitoring variations of analytes on sub-second time scales.

As described in Section 3.2 and schematically shown in Figure 7, the length of active surface of the biosensors designed here was 1 mm, while its diameter measures only 125 µm.

As a consequence of their small dimension, these miniaturized amperometric biosensors are less invasive than microdialysis probes, which have a larger cross-sectional impact on the tissue (Secchi et al., 2013; Rocchitta et al., 2012; Bazzu et al., 2012; Bazzu et al., 2011).

Characteristics of the technique	Technique		
	Microdialysis	Biosensing	Spectroscopic techniques
Preclinical use	+	+	+
Clinical use	-	-	+
Brain invasiveness	++	+	-
Concentration range	µM/mM	µM/mM	mM
Temporal resolution	minutes	seconds	minutes
Spatial resolution	mm	µm/mm	mm
Monitoring period	hours	hours/days	minutes
Monitoring during self-administration	+	+	-
Movement allowed	+	+	-
Untethered detection	-	+ (telemetry)	+

Table 10: Comparison of characteristics of the different techniques available for monitoring of ethanol in the brain

Moreover, by virtue of the electrochemical technique on which the measurement of substances is based, biosensors have proved to be a particularly sensitive tool, capable of detecting concentrations of ethanol in the order of the micromolar range on a very short time-scale. As discussed in Section 4.4, in fact, the response time of ethanol biosensors, corresponding to the time needed for the signal to reach 90% of its maximum response value ($t_{90\%}$) starting from its baseline current following the addition of ethanol aliquots in the electrochemical cell, was quite fast for design 8-200, corresponding to 1.6 ± 0.7 s.

As a rapid detection of ethanol brain level variations is a critical factor to better establish and understand the basis of its mechanism of action and its neurobiological effects on the CNS, biosensors demonstrated a huge improvement with respect to microdialysis and spectroscopic techniques, that require several minutes.

Also, being these tools associated with a telemetric system during the experiments, animals were allowed to be totally free to move, conditions which are not fulfilled by spectroscopic approaches and just partially by microdialysis, where a tethered detection is required.

Unfortunately, although minimally invasive, biosensors have not proven to be suitable for clinical studies, but could be considered the first more reliable approach to monitor the real-time variations of brain ethanol concentrations in animal models (Secchi et al., 2013., Rocchitta et al., 2012).

5.8 New PPD deposition strategies

As stated in Section 3.3, a further investigation of polymer deposition strategies was conducted in a different experimental environment, carried out in the *Biosensors & Electrochemistry Laboratory* of the *School of Chemistry & Chemical Biology* at University College Dublin.

The main purpose of this study, performed after the above-discussed ethanol biosensor characterization and the *in vivo* experiments, was to examine the behavior and the efficiency of the PPD polymer when the *ortho*-phenylenediamine monomer (weak base electrolyte) was dissolved in media other than PBS, which had been used up to this point in our laboratory in Sassari (Section 3.2), in order to improve the shielding efficiency to AA and other electroactive species, as well as to reduce the effects of aging on biosensor functionality (Sections 4.1.2 and 4.2.2 and Figure 25).

The effectiveness of novel polymer layers was assessed by comparing both electropolymerization and AA-calibration parameter values (such as Q(poly), $t½$(poly), I_{max}(AA), t_{max}(AA) and I_L(AA)), and the apparent permeability and selectivity parameters P(HP)%, P(AA)% and S% (see eqs 3–5 in Section 3.3 for a detailed explanation of these parameters). These last three parameters were considered the main discriminative values to evaluate the analytical performance of the different polymers studied.

As a matter of fact, permeability and selectivity parameters define the capacity of the various non-conducting polymers to allow H_2O_2 (the biosensor signal transduction molecule) through while inhibiting the flux of the electroactive interference molecule AA to the electrode surface (see Tables 8-9 in Section 4.8 and Lowry and O'Neill, 1994; Centonze et al., 1994).

Background electrolyte solutions differing from the commonly used deoxygenated PBS were tested, dissolving oPD monomer in MilliQ water and HCl (10 and100 mM in water). Furthermore, once the best medium was found, different oPD concentrations (50 and 100 mM) were investigated.

Values obtained for the new polymers were compared with those from the classic medium commonly used for the polymer coating electrosynthesis, *i.e.*, by dissolving 300 mM oPD in PBS buffer (pH 7.58, conductivity equal to 12.9 mS cm^{-1} see Table 7).

Sensors coated with this classic method showed the best results in terms of I_{max}(AA), equal to 1.1 ± 0.1 nA (n=12), but reached after quite a long time course, t_{max}(AA) value (66 ± 9 min). Nevertheless, this polymer guaranteed a good I_L(AA) value, corresponding to 0.58 ± 0.09, as shown in Table 8.

The reference PBS conditions of deposition resulted in an apparent permeability to hydrogen peroxide, P(HP)%, corresponding to 72 ± 11% (n=12) and in an excellent AA-rejection (P(AA)%) value of 0.15 ± 0.03% (Table 9).
The S% value, indicating polymer selectivity, and defined by eq 5 (Section 3.3), represents the percentage interference by AA in H_2O_2 detection for equimolar concentrations, was estimated 0.17 ± 0.03%.

Among all the new polymers tested, an improvement in hydrogen peroxide permeability was achieved by polymerizing the platinum wires with a 100 mM HCl+300 mM oPD solution (93 ± 5%; n=12, Table 9 in Section 4.8). This indicates that the difference in the slopes (nA mM^{-1}) obtained for the hydrogen peroxide calibration performed before and after the polymer deposition was really marginal.
Unluckily, this improvement was not combined with better AA-rejection values related with PBS conditions. In fact, P(AA)% value was 0.82 ± 0.02 %, and S% corresponded to 0.36 ± 0.02 % (n=12, Table 9). Moreover, the polymer made by deposition in 100 mM HCl+300 mM oPD resulted in the worst I_{max}(AA) value and longest t_{max}(AA) values.

A higher P(HP)% value relative to the PBS reference condition was also reached by polymerizing the sensors using a 10 mM HCl+300 mM solution, corresponding to 81 ± 4% (n=16). In this case, however, these new electropolymerization conditions also

led to the best AA shielding efficacy, showing an excellent P(AA)% value of 0.09 ± 0.02% (n=16), almost halving the one obtained from the common PBS condition. The higher P(HP)% value together with the best AA rejection also resulted in the best polymer selectivity (S%): the percentage interference by AA in H_2O_2 detection for equimolar concentrations for biosensor applications would be ideally zero. By polymerizing the sensors using a 10 mM HCl+300 mM solution, S% was as low as 0.07 ± 0.02% (n=16, see Table 9 in Section 4.8).
So, even if this polymer showed the highest I_{max}(AA) value (4.0 ± 0.5 nA, n=16) compared with PBS, the peak was reached in a shorter time (t_{max}(AA) = 34 ± 2 min, n=16), soon decreasing and stabilizing its 0.5 mM AA limiting current at lower values (data not shown).

The same concentration of oPD monomer was also dissolved in MilliQ Water. The electropolymerization of the sensors performed in this medium yielded an I_{max}(AA) value of 6.0 ± 0.3 nA (n=16) in a time t_{max}(AA) of 65 ± 8 min, while the AA limiting current (I_L(AA)) value was 0.69 ± 0.22 nA (n=16), as shown in Table 8.
This polymer showed the worst hydrogen peroxide permeability (P(HP)% value of 46 ± 7%, n=16), and a high P(AA)% (0.55 ± 0.8%), resulting in the worst selectivity among all the polymer investigated (S% value of 0.74 ± 0.8%, see Table 9 of Section 4.8).

Once determined that the best performing polymer to this point was obtained by 300 mM solution in the 10 mM HCl aqueous medium, our study investigated what may be the effect of dissolving a lower concentration of oPD on polymer permselectivity.

Thus, two new polymers were obtained, electrodepositing the polymer with 10 mM HCl+100 mM oPD and 10 mM HCl+50 mM oPD solutions. These polymers gave essentially the same results in terms of I_{max}(AA) value compared with 300 mM oPD, but showed a drastic worsening of t_{max}(AA) values, and AA limiting currents, found to be higher of a factor of six (Table 8).

Moreover, they showed a lower P(HP)% value and poorer (higher) values of P(AA)% and S%.

So, by virtue of the good hydrogen peroxide permeability (81 ± 4%) and the excellent AA rejection properties (P(AA)%, 0.09 ± 0.02%), the polymer obtained by polymerizing at +0.7 V vs the pseudo Ag reference electrode (± 20 mV vs SCE) in the 300 mM oPD monomer dissolved 10 mM HCl solution resulted in the best selectivity value (S%, 0.07 ± 0.02%, n=16). Surprisingly, wide variations in PPD electrosynthesis conditions only marginally affected the ability of this polymer to transport H_2O_2 to the metal surface, while demonstrating an efficient AA interference rejection. For example, even a three orders of magnitude difference in the half-life of the electropolymerization self-sealing process observed between the pure water and PBS systems (Table 8), only gave rise to a factor of four difference in their resulting permselectivity (S%) values. Thus, the correspondent value of S% obtained by dissolving the monomer in PBS buffer was 0.17 ± 0.03% (n=12). This result revealed that the novel polymer improved the permselectivity by a factor of 2.4.

The above-cited new PPD electropolymerization conditions were tested in experiments done after the *in vivo* work. As a consequence, the stability of the new well-performing 10 mM HCl PPD polymer would have to be determined before its benefits could be exploited for future neurochemical monitoring studies.

5.9 Future biosensor outlooks

If benefits of the new well-performing 10 mM HCl PPD polymer, discussed in Section 5.8, will be confirmed in terms of AA shielding efficency for a time longer than the current limit of 7 days (see Sections 4.1.2 and 4.2.2 and Figure 25), it would be possible to extend the reliability of biosensor *in vivo* use, and enlarge the field of application of this tool also to ethanol self-administration experiments (Loos et al., 2013; June and Gilpin, 2010), where protocols could require a long-term monitoring of ethanol ECF concentration (Secchi et al., 2013; Rocchitta et al., 2012).

Moreover, the contemporary implantation of other sensors could be achievable in specific brain areas, to detect those neurotransmitters particularly involved in ethanol psychotropic and reinforcing effects, such as glutamate (see Section 1.3.2 and McMahon et al., 2007) and dopamine turnover (see Sections 1.3.7-1.4 and O'Neill, 2005).

6 - Summary

In the present thesis, the development, characterization and optimization of an amperometric biosensor for real-time monitoring of ethanol is described.

The detection of ethanol concentration dynamics in the brain kindles a particular interest, due to the fact that alcohol is the most widely-used psychoactive drug whose unregulated use can lead to toxic actions on peripheral organs (chiefly the liver) and CNS, as well as to the development of a severe progressive disease, namely alcoholism.
Alcohol addiction produces physiological changes in the brain in which neurotransmitter systems are disrupted and deeply altered, generating adaptive processes resulting in a compensatory balance. The changes involve the main CNS neurotransmitter systems, such as GABA, glutamate, serotonin, opioids and other neuronal systems (also affected by acute ethanol exposure) that concur to develop neuroadaptive phenomena, such as sensitization, tolerance and psychophysical dependence, in which the mesocorticolimbic dopaminergic system plays the pivotal role.

Several scientific papers cited, discuss ethanol pharmacokinetics and concentrations in the brain of both humans and animals. In fact, a wide range of studies aimed at understanding the complicated basis of ethanol mechanism of action and interactions, using different approaches such as microdialysis and spectroscopic techniques, have been reported. Nevertheless, the above-cited techniques showed weakness and limiting factors that affected their reliability for ethanol detection, mainly related to temporal limitation. Because ethanol concentration in the brain can vary dynamically, as well as those of the neurotransmitters it affects, its optimal study would require a real-time approach.

Thus, the aim of the present study was to develop and characterize an implantable amperometric biosensor capable of real-time recording of ethanol concentration changes in brain ECF of animals.

This miniaturized tool (diameter of 125 µm) exploits the biological element AOx, an oxidoreductase enzyme, to selectively oxidize the ethanol, by producing hydrogen peroxide as by-product, which is further oxidized at the surface of a Pt wire transducer by applying a constant potential between the biosensor (working electrode) and the reference electrode, giving an electrical response (current) directly related to the analyte (ethanol) concentration.

Ten different designs were initially manufactured, all based on the same approach to reject electroactive interference molecules, *i.e.*, the electrodeposition of a nanometer thick PPD polymer. Moreover, AOx was loaded in all these initial designs by dipping the biosensors in a 200 U/mL enzymatic solution.
Then, the effect of PEI, Glyc or the combination of both these enzyme stabilizers on AOx performance was investigated, as well as the deposition of two different kinds of "trapping nets", specifically PU and BSA-GA.

Biosensors were characterized *in vitro* in an electrochemical cell in terms of apparent Michaelis–Menten kinetic parameters (I_{MAX} and K_M), sensitivity in the LRS, LOD and LOQ parameters, as well as in their efficiency to shield electroactive interference species, especially AA.
These parameters were used to compare biosensors performance from the day of their manufacture over a time of 28 days (aging biosensor study), in order to quantify their stability and ascertain the most reliable design for *in vivo* use.

Biosensor characterization determined that design 8 was the best performing and stable biosensor among all those developed, reliable for *in vivo* ethanol monitoring up to 7 days. Having established the benefits of this design, its multilayered configuration was not varied, nor was the deposition sequence, while it was used as a prototype configuration for a further optimization.

Thus, our study re-focused on investigating what the effects may be of depositing a different concentration of the enzyme AOx on biosensors performance, compared to the 200 U/mL solution used until this stage of the project and demonstrated to be successful in design 8, renamed as design 8-200. Hence, the only variable considered to further optimize the biosensor was to change the AOx solution concentration.

Four new biosensor designs were obtained, using 100, 400, 600 and 800 U/mL AOx solution concentrations, and characterized for the same parameters of ethanol sensitivity and efficiency of AA shielding, both at day 1 and over 28 days. Data obtained were then compared with those from design 8-200, carried out in the same experimental conditions.

Biosensors loaded with 400 U/mL of AOx, named design 8-400, improved the performance of the original design 8-200, doubling its I_{MAX} and LRS values up to the seventh day after their manufacture.

After that, the oxygen dependence of the biosensors was studied, due to the fact that *in vitro* working conditions of oxygen tension (260 µM) are quite different from those biosensors would have to face in ECF of the brain, where oxygen concentration was estimated as ~50 µM, and it is fundamental to predict which could be the *in vivo* behavior of biosensors exploiting an oxidase enzyme as biological element. Specifically, it is necessary that the implanted biosensor $K_M(O_2)$ needs to be lower than one half of the oxygen concentration dissolved in the brain ECF (*i.e.*, < 25-18 µM).
Unluckily, design 8-400, the best performing design developed until this stage, displayed an excessive oxygen dependence which could undermine its *in vivo* performance. On the other hand, the original design 8-200 fulfilled the $K_M(O_2)$ requirement, and was therefore considered the most reliable design to monitor ethanol concentration in the brain for up to 7 days.

The biosensor response time, and pH- and temperature-dependence studies successfully completed the *in vitro* characterization of design 8-200.

Then, these biosensors were implanted by means of stereotaxic surgery in the *nucleus accumbens* of male Sprague-Dawley rats. The coupling with a previously-developed telemetric device allowed the performing of the first real-time monitoring of ethanol in the brain of freely moving rats, administered i.g. at the dose of 1 g kg^{-1} to two groups of rodents, either alone or in combination with ranitidine, an inhibitor of enzymes metabolizing alcohol.
The implanted biosensor was demonstrated to be a reliable device for the short-time monitoring of exogenous ethanol in brain ECF, and represents a new generation of analytical tools for studying ethanol toxicokinetics and the effect of drugs on brain ethanol levels.

Moreover, several strategies were tested in order to find the best PPD polymer to shield the interference due to electroactive molecules present in brain ECF, mainly represented by AA, as to extend the temporal limit of a reliable LIVE monitoring.

In this way it would be possible to enlarge the field of application of this tool also to ethanol self-administration experiments, were protocols could require the continuous monitoring of ethanol ECF concentration for a time longer than 7 days.
Moreover, the co-implantation of other sensors in specific brain areas could be very interesting to detect neurotransmitters, chiefly dopamine, particularly involved in ethanol psychotropic and reinforcing effects of ethanol, and that play a critical role in the development of alcohol addiction.

7 - Bibliography

Adalsteinsson E et al., 2006. In vivo quantification of ethanol kinetics in rat brain. Neuropsychopharmacology. 31 (12), 2683-2691.

Adams EC.1988. Method of preparing a test strip for alcohol testing. Patent # 4 786 569, USA.

Agarwal DP, 2001. Genetic polymorphisms of alcohol metabolizing enzymes. Pathol Biol 49:703-9.

Ahmet Koyun, Esma Ahlatcıoğlu and Yeliz Koca İpek (2012). Biosensors and Their Principles, A Roadmap of Biomedical Engineers and Milestones, Prof. Sadik Kara (Ed.), ISBN: 978-953-51-0609-8, InTech, DOI: 10.5772/48824. Available from: http://www.intechopen.com/books/a-roadmap-of-biomedical-engineers-and-milestones/biosensors-and-their-principles

Ahmet Koyun, Esma Ahlatcıoğlu and Yeliz Koca İpek, Biosensors and Their Principles. DOI: 10.5772/48824

Alcohol's actions on neuronal nicotinic acetylcholine receptors.

Allen J Bard, Larry R Faulkner. 2000. Electrochemical Methods: Fundamentals and Applications (2 ed.). Wiley. ISBN 0-471-04372-9.

Alpat S, Telefoncu A. 2010. Development of an alcohol dehydrogenase biosensor for ethanol determination with toluidine blue O covalently attached to a cellulose acetate modified electrode. Sensors (Basel).;10(1):748-64. doi: 10.3390/s100100748. Epub 2010 Jan 21.

Arora S et al., 2000. Alcohol levels are increased in social drinkers receiving ranitidine. Am J Gastroenterol. Jan;95(1):208-13.

Ashton CH. 2001. Pharmacology and effects of cannabis: A brief review. British Journal of Psychiatry, 178, 101–106.

Avena NM, Hoebel BG. 2003. A diet promoting sugar dependency causes behavioral cross-sensitization to a low dose of amphetamine. Neuroscience;122(1):17-20.

Azevedo AM et al., 2005. Ethanol biosensors based on alcohol Oxidase. Biosens Bioelectron. Aug 15;21(2):235-47. Epub 2004 Dec 7. Review.

Barsan MM, Brett CM. 2008. An alcohol oxidase biosensor using PNR redox mediator at carbon film electrodes. Talanta.

Barsan MM; Brett CM. 2008. An alcohol oxidase biosensor using PNR redox mediator at carbon film electrodes. *Talanta*., *74*, 1505–1510.

Bazzu G et al., 2009. Real-time monitoring of brain tissue oxygen using a miniaturized biotelemetric device implanted in freely-moving rats. Anal. Chem., 81, 2235–2241.

Bazzu G et al., 2010. alpha-Synuclein- and MPTP-generated rodent models of Parkinson's disease and the study of extracellular striatal dopamine dynamics: a microdialysis approach. CNS Neurol Disord Drug Targets. 2010 Aug;9(4):482-90. Review.

Bazzu G et al., 2011 Dual asymmetric-flow microdialysis for in vivo monitoring of brain neurochemicals. Talanta. Sep 30;85(4):1933-40.doi:10.1016/ j.talanta .07.018. Epub 2011 Jul 18

Bazzu G et al., 2012. Brain microdialysis in freely moving animals. Methods Mol Biol.;846:365-81. doi: 10.1007/978-1-61779-536-7_31.

Begleiter and Kissin, 1995. The genetics of alcoholism. New York, Oxford University, Press.

Berger M et al., 2009. The expanded biology of serotonin. Annu Rev Med. 2009;60:355-66. doi: 10.1146/annurev.med.60.042307.110802.

Blomqvist O et al., 1992.Ethanol-induced locomotor activity: involvement of central nicotinic acetylcholine receptors? Brain Res Bull. Aug;29(2):173-8.

Blomstrand R, Theorell H. 197 . Inhibitory effect on ethanol oxidation in man after administration of 4-methylpyrazole. Life Sci II. Jun 8;9(11):631-40.

Boileau I et al., 2003. Alcohol promotes dopamine release in the human nucleus accumbens. Synapse. Sep 15;49(4):226-31.

Bolger FB et al, 2005. Lowry, J.P. Brain Tissue Oxygen: In vivo monitoring with carbon paste electrodes. Sensors. 5, 473–487.

Bolivar JM et al., 2009. Coating of soluble and immobilized enzymes with ionic polymers: full stabilization of the quaternary structure of multimeric enzymes. Biomacromolecules. Apr 13;10(4):742-7. doi: 10.1021/bm801162e.

Borg S et el., 1981. Central norepinephrine metabolism during alcohol intoxication in addicts and healthy volunteers. Science. Sep 4;213(4512):1135-7.

Boutelle MG et al., 1989 Rapid changes in striatal ascorbate in response to tail-pinch monitored by constant potential voltammetry. Neuroscience.;30(1):11-7.

Brett S. 2005 Science review: The use of proton pump inhibitors for gastric acid suppression in critical illness. Crit Care. Feb;9(1):45-50. Epub 2004 Oct 8. Review.

Brodie MS et al., 1999. Ethanol directly excites dopaminergic ventral tegmental area reward neurons. Alcohol Clin Exp Res. Nov;23(11):1848-52.

Brunner M, Langer O. 2006. Microdialysis versus other techniques for the clinical assessment of in vivo tissue drug distribution. The AAPS Journal. 8 (2) Article 30.

Burrows D et al, 1993. eds. Illicit psychostimulant use in Australia. Canberra: Commonwealth of Australia.

Calia G et al., 2009. Biotelemetric Monitoring of Brain Neurochemistry in Conscious Rats Using Microsensors and Biosensors. Sensors, 9, 2511-2523.

Carrizzo A et al., 2013. Antioxidant effects of resveratrol in cardiovascular, cerebral and metabolic diseases. Food Chem Toxicol.

Carta M et al., 2003. Alcohol potently inhibits the kainite receptor-dependent excitatory drive of hippocampal interneurons. Proc. Natl. Acad. Sci. U.S.A., , 100:6813-6818. PUBMED

Centonze D et al., 1994. An in situ electrosynthesized amperometric biosensor based on lactate oxidase immobilized in a poly-o-phenylenediamine film: determination of lactate in serum by flow injection analysis. Biosens Bioelectron;9(7):471-9.

Chaplin MF Bucke C. 1990. Enzyme Technology Cambridge University Press, Chapter 3. ISBN: 9780521348843

Charness ME et al, 1989. Ethanol and the nervous system. N Engl J Med.

Chefer VI et al., 2006. Quantitative no-net-flux microdialysis permits detection of increases and decreases in dopamine uptake in mouse nucleus accumbens. J Neurosci Methods. Sep 15;155(2):187-93. Epub 2006 Feb 8.

Clark LC et al., 1985. Chronically implanted polarographic electrodes. J Appl Physiol. 1958, 13, 85-91.Crow KE, Ethanol metabolism by the liver. Rev Drug Metab Drug Interact.

Crabb DW et al., 1993. Alcohol sensitivity, alcohol metabolism, risk of alcoholism, and the role of alcohol and aldehyde dehydrogenase genotypes. J Lab Clin Med. 1993 Sep;122(3):234-40.

Cregg, JM et al., 1989. Functional characterization of the two alcohol oxidase genes from the yeast Pichia pastoris. Mol Cell Biol. 1989 March; 9(3): 1316–1323. PMCID: PMC362724

Dai F et al., 2006. Effect of drug-induced ascorbic acid release in the striatum and the nucleus accumbens in hippocampus-lesioned rats. Brain Res.;1125(1):163-170.

Davis JT and De Fiebre CM. 2006. Alcohol Research & Health 29(3):179PMID 17373406

De Witte P. 2004. Imbalance between neuroexcitatory and neuroinhibitory amino acids causes craving for ethanol. Addict Behav. Sep;29(7):1325-39.

Degani NC et al., 1979. Ethanol-induced spontaneous norepinephrine release from the rat vas deferens. J Pharmacol Exp Ther. Jul;210(1):22-6

Delgado JM et al., 1972. Dialytrode for long term intracerebral perfusion in awake monkeys. Arch Int Pharmacodyn Ther.198(1):9-21

Di Chiara G, Imperato A. 1986. Preferential stimulation of dopamine release in the nucleus accumbens by opiates, alcohol, and barbiturates: studies with transcerebral dialysis in freely moving rats.Ann N Y Acad Sci.;473:367-81.

DiFranza JR, Guerrera MP. 1990. Alcoholism and smoking. J Stud Alcohol. Mar;51(2):130-5.

Dimitrakopoulou-Strauss A et al., 1999. Pharmacokinetic imaging of 11C ethanol with PET in eight patients with hepatocellular carcinomas who were scheduled for treatment with precutaneous ethanol injection. Radiology; 211:681–686.

DiPadova C et al., 1992. Effects of ranitidine on blood alcohol levels after ethanol ingestion. Comparison with other H2-receptor antagonists. JAMA. Jan 1;267(1):83-6.

Dixon BM et al., 2002. Characterization in vitro and in vivo of the oxygen dependence of an enzyme/polymer biosensor for monitoring brain glucose. J. Neurosci. Meth. 119, 135–142.

Duff A, O'Neill RD. 1994. Effect of probe size on the concentration of brain extracellular uric acid monitored with carbon paste electrodes. J. Neurochem. 62, 1496–1502.

Dufour M et al., 1995. Alcohol in the elderly. Annu Rev Med;46. 123–32.

Eckey R et al., 1990. Genetically-induced variability of alcohol metabolism and its effect on drinking behavior and predisposition to alcoholism. Z Rechtsmed.

Edenberg HJ et al., 1999. Polymorphism of the human alcohol dehydrogenase 4 (ADH4) promoter affects gene expression Pharmacogenetics. 1999 Feb;9(1):25-30.

El-Bakary AA et al., 2010 Ranitidine as an alcohol dehydrogenase inhibitor in acute methanol toxicity in rats. Hum Exp Toxicol., 29 (2), 93-101.

El-Bakary AA et al., 2010. Ranitidine as an alcohol dehydrogenase inhibitor in acute methanol toxicity in rats. Hum Exp Toxicol. 2010 Feb;29(2):93-101.

Fein G, Meyerhoff DJ. 2000. Ethanol in human brain by magnetic resonance spectroscopy: correlation with blood and breath levels, relaxation, and magnetization transfer. Alcoholism: Clinical and Experimental Research 24:1227–1235.

Fickert P and Zatloukal K, 2000. Pathogenesis of alcoholic liver disease. In, Handbook of Alcoholism. (Zernig, G., Saria, A., Kurz, M., and O'Malley, S., eds.) CRC Press, Boca Raton, FL., pp. 317-323.

Fumero B et al., 1994. Fixed versus removable microdialysis probes for in vivo neurochemical analysis: implications for behavioral studies. J. Neurochem. 63, 1407–1415.

Gao W et al., 2013. A novel electrochemiluminescence ethanol biosensor based on tris(2,2'-bipyridine) ruthenium (II) and alcohol dehydrogenase immobilized in graphene/bovine serum albumin composite film. Biosens Bioelectron. Mar 15;41:776-82. doi: 10.1016/j.bios.2012.10.005

Gessa GL et al., 1985. Low doses of ethanol activate dopaminergic neurons in the ventral tegmental area. Brain Res. Nov 25;348(1):201-3.

Gilpin NW, Koob GF. 2008. Neurobiology of Alcohol Dependence: Focus on Motivational Mechanisms. Alcohol Res Health.31(3):185-195.

Gonzales RA et al., 1998. Quantitative microdialysis of ethanol in rat striatum. Alcoholism: Clinical and Experimental Research. 22 (4), 858–867.

Gonzales RA et al., 2004. The role of mesolimbic dopamine in the development and maintenance of ethanol reinforcement. Pharmacol Ther. Aug;103(2):121-46. Review.

Gonzales, RA, Jaworski, JN. 1997. Alcohol and glutamate. Alcohol Health Res World 21: 120-7.

Goswami P et al., 2013. An overview on alcohol oxidases and their potential applications. Appl Microbiol Biotechnol. May;97(10):4259-75. doi: 10.1007/s00253-013-4842-9. Epub 2013 Mar 26.

Gronow M. 1999, Biosensors: a marriage of biochemistry and microelectronics. D.G. Springham (Ed.), Biotechnology: The Science and the Business, Harwood Academic Publishers, Amsterdam (1999)

Grünewald RA et al., 1983. The origin of circadian and amphetamine-induced changes in the extracellular concentration of brain ascorbate. Neurochem Int. ;5(6):773-8.

Grunnet et al., 1973. Rate-limiting factors in ethanol oxidation by isolated rat-liver parenchymal cells. Effect of ethanol concentration, fructose, pyruvate and pyrazole. Eur J Biochem.

Haber SN. 2002. The place of dopamine neurons within the organization of the forebrain. G. Di Chiara (Ed.), Dopamine in the CNS I, Springer-Verlag, Berlin (), pp. 43–62

Hämmerle M et al., 2011. Analysis of volatile alcohols in apple juices by an electrochemical biosensor measuring in the headspace above the liquid. Sens. Actuators B, 158 pp. 313–318

Hanstock CC et al., 1990. Measurement of ethanol in the human brain using NMR spectroscopy. J Stud Alcohol;51(2):104–7.

Hardman JG; Limbird LE, 2005. Goodman and Gilman's the Pharmacological Basis of Therapeutics, 11th ed.; Mcgraw-Hill: New York,.

Harris RA et al., 1995. Mutant mice lacking the g isoform of protein kinase C show decreased behavioral actions of ethanol and altered function of g-aminobutyrate type A receptors. Proc. Natl. Acad. Sci. U.S.A., , 92:3658-3662. PUBMED

Harris RA, Schroeder F. 1982. Effects of barbiturates and ethanol on the physical properties of brain membranes. J Pharmacol Exp Ther. 1982 Nov;223(2):424-31.

Hasin DS et al., 2007. Prevalence, correlates, disability, and comorbidity of DSM-IV alcohol abuse and dependence in the United States: results from the National Epidemiologic Survey on Alcohol and Related Conditions. Arch Gen Psychiatry 64, 830-842.

Hetherington HP et al., 1999. Spectroscopic imaging of the uptake kinetics of human brain ethanol. Magn Reson Med. Dec;42(6):1019-26.

Hoffman PL et al., 1989. Selective inhibition by ethanol of glutamate-stimulated cyclics GMP production in primary cultures of cerebellar granule cells. Neuropharmacology, 28 pp. 1239–1243

Holford NH., 1987. Clinical pharmacokinetics of ethanol. Clin Pharmacokinet.

Hou Y et al., 2005. Effects of clozapine, olanzapine and haloperidol on ethanol-induced ascorbic acid release in mouse striatum. Prog Neuropsychopharmacol Biol Psychiatry.;29(1):83-89.

Hou Y et al., 2007. Similar effects of clozapine and olanzapine on ethanol-induced ascorbic acid release in the prefrontal cortex of freely moving mice. Pharmazie.;62(2):158-160

http://www.chem.qmul.ac.uk/iubmb/enzyme/EC1/intro.html

Hyman SE et al., 2006. Neural mechanisms of addiction: the role of reward-related learning and memory. Annu Rev Neurosci.;29:565-98. Review.

Inoue K et al., 1984. Accumulation of acetaldehyde in alcohol-sensitive Japanese: relation to ethanol and acetaldehyde oxidizing capacity. Alcohol Clin Exp Res. May-Jun;8(3):319-22.

Israel Y, Kalant H. 1963 . Effect of ethanol on the transport of sodium in frog skin. Nature. Nov 2;200:476-8.

Jamal M et al., 2003. Microdialysis for the determination of acetaldehyde and ethanol concentrations in the striatum of freely moving rats. J Chromatogr B Analyt Technol Biomed Life Sci., 798 (1), 155-158.

Janecka A et al., 2004. Opioid receptors and their ligands. Curr Top Med Chem;4(1):1-17.

Julien RM. 1993. A primer for drug action: a concise, nontechnical guide to the actions, uses and side-effects of psychoactive drugs (6th ed). New York: W H Freeman and Company.

June and Gilpin, 2010. Operant self-administration models for testing the neuropharmacological basis of ethanol consumption in rats. Curr Protoc Neurosci. 2010 Apr;Chapter 9:Unit 9.12.1-26. doi: 10.1002/0471142301.ns0912s51.

Kamens HM, Phillips TJ. 2008.A role for neuronal nicotinic acetylcholine receptors in ethanol-induced stimulation, but not cocaine- or methamphetamine-induced stimulation. Psychopharmacology (Berl). Feb;196(3):377-87.

Karahanian E et al, 2011. Ethanol as a prodrug: brain metabolism of ethanol mediates its reinforcing effects. Alcohol Clin Exp Res.

Khan A, Ab Ghani, 2012. Multienzyme microbiosensor based on electropolymerized o-phenylenediamine for simultaneous in vitro determination of acetylcholine and choline. S. Biosens. Bioelectron. 31, 433-438.

Kiianmaa, K. 1990 Neuronal mechanisms of ethanol sensitivity. Alcohol Alcohol 25: 257-62.

Killoran SJ and O'Neill RD., 2008 Characterization of permselective coatings electrosynthesized on Pt-Ir from the three phenylenediamine isomers for biosensor applications. Electrochim. Acta, 53, 7303–7312

Kirwan SM et al., 2007. Modifications of Poly(o-phenylenediamine) Permselective Layer on Pt-Ir for Biosensor Application in Neurochemical MonitoringSensors. 7 (4), 420-437.

Kirwan SM et al.; 2007. Modifications of Poly(o-phenylenediamine) Permselective Layer on Pt-Ir for Biosensor Application in Neurochemical Monitoring. Sensors,420–437.

Kissinger Peter, William R. Heineman. 1996. Laboratory Techniques in Electroanalytical Chemistry, Second Edition, Revised and Expanded (2 ed.). CRC

Koob GF 2003. Alcoholism: Allostasis and beyond. Alcoholism: Clinical and Experimental Research 27(2):232–243,. PMID: 12605072

Koob GF, Bloom FE. 1988. Cellular and molecular mechanisms of drug dependence. Science. Nov 4;242(4879):715-23. Review.

Kowalska M et al, 2011. Prussian Blue acts as a mediator in a reagentless cytokinin biosensor. Anal. Chim. Acta. 701, 218-223.

Larsson A et al., 2002. Role of different nicotinic acetylcholine receptors in mediating behavioral and neurochemical effects of ethanol in mice. Alcohol. Nov;28(3):157-67.

Leblanc AE et al., 1975.Generalization of behaviorally augmented tolerance to ethanol, and its relation to physical dependence. Psychopharmacologia 44(3):241–246, PMID: 1239781

Lee SL et al., 2004. Functionality of allelic variations in human alcohol dehydrogenase gene family: assessment of a functional window for protection against alcoholism. Pharmacogenetics. Nov;14(11):725-32.

LeMarquand D et al., 1994. Serotonin and alcohol intake, abuse, and dependence: findings of animal studies. Biol Psychiatry. Sep 15;36(6):395-421. Review.

Lemoine P et al., 2003. Children of alcoholic parents--observed anomalies: discussion of 127 cases. Ther Drug Monit. Apr;25(2):132-6.

Li TK. 2000. Pharmacogenetics of responses to alcohol and genes that influence alcohol drinking. J Stud Alcohol.

Liaw HW et al., 2006. Development of an amperometric ethanol biosensor based on a multiwalled carbon nanotube-Nafion-alcohol dehydrogenase nanobiocomposite. J Nanosci Nanotechnol. Aug;6(8):2396-402.

Littleton J, Little H. 1994. Current concepts of ethanol dependence. Addiction 89: 1397-412.

Liu J et al., 1999. Involvement of the corticostriatal glutamatergic pathway in ethanol-induced ascorbic acid release in rat striatum. Addict Biol. 1999 Jul;4(3):273-81. doi: 10.1080/13556219971489.

Loos M et al., 2013. Enhanced alcohol self-administration and reinstatement in a highly impulsive, inattentive recombinant inbred mouse strain. Front Behav Neurosci. Oct 30;7:151. doi: 10.3389/fnbeh.2013.00151.

Lovinger DM et al., 1989. Ethanol inhibits NMDA-activated ion current in hippocampal neurons. Science 243(4899):1721– 1724, PMID: 2467382

Lovinger DM. 1999. 5-HT3 receptors and the neural actions of alcohols: an increasingly exciting topic. Neurochem Int 35: 125-30.

Lowry et al., 1998. An amperometric glucose-oxidase/poly(o-phenylenediamine) biosensor for monitoring brain extracellular glucose: in vivo characterisation in the striatum of freely-moving rats. J Neurosci Methods. Jan 31;79(1):65-74.

Lowry JP, O'Neill RD. 1994. Electroanalysis, 6, 369–379

Luo P et al., 2008. Electrochemical detection of blood alcohol concentration using a disposable biosensor based on screen-printed electrode modified with Nafion and gold nanoparticles. Clin Chem Lab Med.;46(11):1641-7. doi: 10.1515/CCLM.2008.308.

Luo P et al., 2008b. Determination of serum alcohol using a disposable biosensor. Forensic Sci Int. Aug 6;179(2-3):192-8. doi: 10.1016/j.forsciint.2008.06.002. Epub 2008 Jul 23.

McCarver DG et al., 1997. Alcohol dehydrogenase-2*3 allele protects against alcohol-related birth defects among African Americans. J Pharmacol Exp Ther. Dec;283(3):1095-101.

McMahon CP et al., 2005. Design variations of a polymer-enzyme composite biosensor for glucose: enhanced analyte sensitivity without increased oxygen dependence. J Electroanal Chem. 2005, 580, 193–202.

McMahon CP et al., 2006. The efficiency of immobilised glutamate oxidase decreases with surface enzyme loading: an electrostatic effect, and reversal by a polycation significantly enhances biosensor sensitivity. Analyst. 2006 Jan;131(1):68-72. Epub 2005 Nov 9.

McMahon CP et al., 2007. Oxygen tolerance of an implantable polymer/enzyme composite glutamate biosensor displaying polycation-enhanced substrate sensitivity. Biosens Bioelectron. 22, 1466–1473.

McMahon CP et al., 2007. Oxygen tolerance of an implantable polymer/enzyme composite glutamate biosensor displaying polycation-enhanced substrate sensitivity. Biosens Bioelectron. 2007 Feb 15;22(7):1466-73. Epub 2006 Aug 2.

McMahon CP, O'Neill RD. 2005. Polymer-enzyme composite biosensor with high glutamate sensitivity and low oxygen dependence. Anal. Chem. 77, 1196–1199.

McRobbie Det al., 2007. MRI from picture to proton. 2nd edn. Cambridge: Cambridge University. Press,:13.

Meier-Tackmann D et al., 1990. Effect of acute ethanol drinking on alcohol metabolism in subjects with different ADH and ALDH genotypes. Alcohol.

Melis M et al., 2005. The dopamine hypothesis of drug addiction: Hypodopaminergic state. International Review of Neurobiology 63:101– 154, PMID: 15797467

Miele M, Fillenz M. 1996. In vivo determination of extracellular brain ascorbate. J Neurosci Methods. Dec;70(1):15-9.

Migheli R et al., 2008. Novel integrated microdialysis-amperometric system for in vitro detection of dopamine secreted from PC12 cells: design, construction, and validation. Anal. Biochem., 380, 323–330.

Mogenson GJ, Huang YH. 1973. The neurobiology of motivated behavior. Prog Neurobiol, 1, pp. 55–83

Mohd Zain Z et al., 2012. Amperometric microbiosensor as an alternative tool for investigation of D-serine in brain. Amino Acids. 2012 Nov;43(5):1887-94. doi: 10.1007/s00726-012-1365-0. Epub Aug 4. Review.

Mokdad et al., 2004. Actual causes of death in the United States, 2000. JAMA 291, 1238-1245.

Moran LA et al., 2005. *Principles of Biochemistry,* 4th ed.; Prentice Hall: New Jersey, USA.

Mostofa J et al., 2003. J Chromatogr B Analyt Technol Biomed Life Sci. 798 (1), 155-158.

Munson PL et al, 1995. Principles of Pharmacology. Basic concepts & clinical application, 1st ed; Chapman & Hall Inc.: New York, USA.

Murr R et al., 1994. A novel, remote-controlled suspension device for brain tissue PO_2 measurements with multiwire surface electrodes. *Pflugers Arch*. **1994**, *426*, 348–350.

Mushahwar IK, Koeppe RE.1972. Incorporation of label from(1- 14 C)ethanol into the glutamate-glutamine pools of rat brain in vivo. Biochem J. Feb;126(3):467-9.

Myron Loewen. 2003. Designing Loop Antennas for the rfPIC12F675, Application Note n° 868 (AN868) Microchip Technology Inc., 1-18. www.microchip.com.

Nair PK et al., 1987. Comparisons of oxygen metabolism and tissue PO_2 in cortex and hippocampus of gerbil brain. *Stroke*. *18*, 616–622.

Narahashi T et al., 1999. Neuronal nicotinic acetylcholine receptors: a new target site of ethanol. Neurochem Int. Aug;35(2):131-41. Review.

Niaura RS et al., 1987. Gender differences in acute psychomotor, cognitive, and pharmacokinetic response to alcohol. Addict Behav. 1987;12(4):345-56.

Nirenberg MJ et al., 1997. The dopamine transporter: comparative ultrastructure of dopaminergic axons in limbic and motor compartments of the nucleus accumbens J Neurosci, 17, pp. 6899–6907

Njagi, J et al, 2010. Amperometric detection of dopamine in vivo with an enzyme based carbon fiber microbiosensor. Anal. Chem. 82, 989-996.

Nolan L et al, 1988. Prescribing for the elderly: part II. J Am Geriatr Soc;36:245-54.

Noth RH and Walter RM Jr, 1984. The effects of alcohol on the endocrine system. Med Clin North Am.

Nurmi M et al, 1994. Brain ethanol in AA, ANA, and Wistar rats monitored with one-minute microdialysis. Alcohol, 11 (4), 315-321.

O'Brien CP, 2005. Goodman and Gilman's the Pharmacological Basis of Therapeutics, 11th ed.; Mcgraw-Hill: New York.

O'Neill et al., 2008. Designing sensitive and selective polymer/enzyme composite biosensors for brain monitoring in vivo. TRAC-Trends in Analytical Chemistry. 27 (1), 78-88.

O'Neill RD et al., 2008. Trends Anal. Chem. 27, 78–88.

Olive MF et al., 2001. Stimulation of endorphin neurotransmission in the nucleus accumbens by ethanol, cocaine, and amphetamine. Journal of Neuroscience 21(23):RC184. PMID: 11717387

O'Neill RD, 2005. Long-term monitoring of brain dopamine metabolism *in vivo* with carbon paste electrodes. *Sensors,* **5**, 317–342.

O'Neill RD, Fillenz M. 1985. Circadian changes in extracellular ascorbate in rat cortex, accumbens, striatum and hippocampus: correlations with motor activity. Neurosci Lett. Oct 10;60(3):331-6.

Oslin D et al, 1998. Alcohol related dementia: proposed clinical criteria. Int. J. Geriatr. Psychiatry, 13:203-212.

Pagnacco G et al., 1997. Oversampling data acquisition to improve resolution of digitized signals. Biomed. Sci. Instrum., 34, 137–142.

Paille FM et al., 1995. Double-blind randomized multicentre trial of acamprosate in maintaining abstinence from alcohol. Alcohol Alcohol. Mar;30(2):239-47.

Panzak G et al. 1998. Isometric muscle strength in alcoholic and nonalcoholic liver-transplantation candidates. Am. J. Drug Alcohol Abuse, 24:449-512.

Paxinos, G.; Watson, C. *Rat Brain in Stereotaxic Coordinates*, 6th ed.; Academic Press: San Diego, CA, **2007**.

Patel NG et al., 2001. Screen-printed biosensors using different alcohol oxidases. Sensor Actuat. B: Chem., 75 (1–2) pp. 101–110

Peris J et al., 2006. Brain ethanol levels in rats after voluntary ethanol consumption using a sweetened gelatin vehicle. Pharmacol Biochem Behav. Nov;85(3) :562-8.

Pfefferbaum A et al, 1998. A controller study of cortical grey matter and ventricular changes in alcoholic men over a 5-year interval. Arch. Gen. Psichiatry, 55:905-912.

Pivac N et al., 2004. Platelet serotonin concentration in alcoholic subjects. Life Sci 76: 521-31.

Qian JM et al., 2004. Polyelectrolyte-stabilized glucose biosensor based on woodceramics as electrode. Clin Biochem. Feb;37(2):155-61.

Quertemont E et al., 2003. Brain ethanol concentrations and ethanol discrimination in rats: effects of dose and time. Psychopharmacology (Berl). Jul;168(3):262-70.

Rassnick S et al., 1993.The effects of 6-hydroxydopamine lesions of the nucleus accumbens and the mesolimbic dopamine system on oral self-administration of ethanol in the rat. Brain Research 623(1):16–24. PMID: 8221085

Risto Roine MD et al., 1990. Aspirin Increases Blood Alcohol Concentrations in Humans After Ingestion of Ethanol JAMA.264(18):2406-2408

Robinson TE, Berridge KC. 1993. The neural basis of drug craving: an incentive-sensitization theory of addiction. Brain Res Brain Res Rev. Sep-Dec;18(3):247-91.

Rocchitta G et al, 2012. Development and characterization of an implantable biosensor for telemetric monitoring of ethanol in the brain of freely moving rats. Anal Chem.

Rocchitta G et al., 2007. Development of a distributed, fully automated, bidirectional telemetry system for amperometric microsensor and biosensor applications. Sens. Actuat. B, 126, 700-709.

Rocchitta G et al., 2013 Simultaneous telemetric monitoring of brain glucose and lactate and motion in freely moving rats. Anal Chem. 2013 Nov 5;85(21):10282-8. doi: 10.1021/ac402071w. Epub Oct 21.

Rocchitta G, Serra PA. 2013. Direct monitoring of ethanol in the brain. OA Alcohol Sep 01;1(2):15.

Rocchitta, G et al., 2007. Sens. Actuators B: Chem, 126, 700-709.

Rooney WD et al., 2000. 4.0 T water proton T1 relaxation times in normal human brain and during acute ethanol intoxication. Alcohol Clin Exp Res. Jun; 24(6):830-6.

Ross B , Bluml S. 2001. Magnetic resonance spectroscopy of the human brain. Anat Rec. Apr;265(2):54-84.

Rothwell SA et al., 2009. Contributions by a novel edge effect to the permselectivity of an electrosynthesized polymer for microbiosensor applications. Anal Chem. May 15;81(10):3911-8. doi: 10.1021/ac900162c.

Rothwell SA et al., 2010. Enzyme immobilization strategies and electropolymerization conditions to control sensitivity and selectivity parameters of a polymer-enzyme composite glucose biosensor. Sensors., 10, 6439-6462.

Roy A, Pandey SC. 2002. The decreased cellular expression of neuropeptide Y protein in rat brain structures during ethanol withdrawal after chronic ethanol exposure. Alcoholism: Clinical and Experimental Research 26(6):796–803,. PMID: 12068247

Ryan MR et al., 1997. Biosensor for neurotransmitter L-glutamic acid designed for efficient use of L-glutamate oxidase and effective rejection of interference. Analyst 112, 1419-1424.

Salaspuro MP et al., 1977. Ethanol-induced hypoglycaemia in man: its suppression by the alcohol dehydrogenase inhibitor 4-methylpyrazole. Eur J Clin Invest. Dec;7(6):487-90.

Sammi MK, et al., 2000. Measurements of human brain ethanol T(2) by spectroscopic imaging at 4 T. Magn Reson Med. Jul;44(1):35-40.

Santhakumar V et al., 2007. Ethanol acts directly on extrasynaptic subtypes of GABAA receptors to increase tonic inhibition. Alcohol 41 (3): 211–21. doi:10.1016/j.alcohol.2007.04.011. PMC 2040048. PMID 17591544.

Saunders JB. 1986. Drugs and alcohol – their interactions and how to avoid them. Current Therapeutics; 27(12):31–53.

Schuckit MA, 1995. Drug and Alcohol Abuse: Clinical Guide to Diagnosis and Treatment, 4th ed. Plenum Press, New York,.

Schultz W. 2007. Multiple dopamine functions at different time courses. Annu Rev Neurosci.;30:259-88.

Secchi O et al, 2013. Further in-vitro characterization of an implantable biosensor for ethanol monitoring in the brain. Sensors (Basel)

Seitz HK et al, 1994. Ethanol metabolism in the gastrointestinal tract and its possible consequences. Alcohol Alcohol Suppl. ;2:157-62. Review.

Sellers EM, Busto U. 1982. Benzodiazepines and ethanol: assessment of the effects and consequences of psychotropic drug interactions. J Clin Psychopharmacol. 1982 Aug;2(4):249-62.

Serra PA et al., 2000. Manganese increases L-DOPA auto-oxidation in the striatum of the freely moving rat: potential implications to L-DOPA long-term therapy of Parkinson's disease. Br J Pharmacol. Jun;130(4):937-45.

Serra PA et al., 2002. The neurotoxin 1-methyl-4-phenyl-1,2,3,6-tetrahydropyridine induces apoptosis in mouse nigrostriatal glia. Relevance to nigral neuronal death and striatal neurochemical changes. J Biol Chem. 2002 Sep 13;277(37):34451-61. Epub 2002 Jun 25.

Serra PA et al., 2007. Design and Construction of a Distributed Sensor NET for Biotelemetric Monitoring of Brain Energetic Metabolism using Microsensors and Biosensors. Sens. Actuators B: Chem, 1, 118-126.

Serra PA et al., 2007. Design and construction of a low cost single-supply embedded telemetry system for amperometric biosensor applications. Sens. Actuat B, 122, 118-126.

Sesack SR, 2002. Synaptology of dopamine neurons. G. Di Chiara (Ed.), Dopamine in the CNS I, Springer-Verlag, Berlin, pp. 63–119

Siegel GJ et al., 1999. Basic Neurochemistry: Molecular, Cellular and Medical Aspects, Sixth Edition. GABA Receptor Physiology and Pharmacology. American Society for Neurochemistry. Lippincott Williams and Wilkins.

Smyth AB et al., 1999. Ethanol biosensor can detect low-oxygen injury in modified atmosphere packages of fresh-cut produce. Posthaverst Biol. Technol., 15 (2) (1999), pp. 127–134

Stead AH, Moffat AC. 1983. Quantification of the interaction between barbiturates and alcohol and interpretation of fatal blood concentrations. Hum Toxicol. Jan;2(1):5-14.

Sullivan JT et al. 1989. Assessment of alcohol withdrawal: the revised clinical institute withdrawal assessment for alcohol scale (CIWA-Ar). Br J Addict. Nov;84(11):1353-7.

Theile JW et al, 2011.GABAergic transmission modulates ethanol excitation of ventral tegmental area dopamine neurons. Neuroscience;172:94-103.

Thévenot DR et al., 2001. Electrochemical biosensors: recommended definitions and classification. Biosens Bioelectron. Jan;16(1-2):121-31.

Thorsell A et al. 2007 . Viral vector-induced amygdala NPY overexpression reverses increased alcohol intake caused by repeated deprivations in Wistar rats. Brain 130:1330–1337, PMID: 17405766

Tossman U, Ungerstedt U. 1986. Microdialysis in the study of extracellular levels of amino acids in the rat brain. Acta Physiol Scand. Sep;128(1):9-14.

Tung BT et al, 2013. Modulation of Endogenous antioxidant activity by resveratrol and exercise in mouse liver is age aependent. A Biol Sci Med Sci.

Ungerstedt U, Hallström A. 1987. In vivo microdialysis--a new approach to the analysis of neurotransmitters in the brain. Life Sci. Aug 17;41(7):861-4.

Valenzuela CF and Harris RA. 1997. Alcohol: Neurobiology. In, Substance Abuse: A Comprehensive Textbook. (Lowinson, J.H., Ruiz, P., Millman, R.B., Langrod, J.B., eds.) Williams & Wilkins, Baltimore, pp. 119-142.

Valenzuela CF, Harris RA. 1997. Alcohol: Neurobiology. in: Lowinson, JH, Ruiz, P, Millman, RB, Langrod, JG. Eds. Substance Abuse: A Comprehensive Textbook. Baltimore: Williams and Wilkins, pp. 119–142.

Vasylieva et al, 2011. Covalent enzyme immobilization by poly(ethylene glycol) diglycidyl ether (PEGDE) for microelectrode biosensor preparation. Biosens. Bioelectron. 26, 3993-4000.

Ventura R et al., 2006. Ethanol consumption and reward depend on norepinephrine in the prefrontal cortex. Neuroreport. Nov 27;17(17):1813-7.

Vestal RE et al. 1977. Aging and ethanol metabolism. Clin Pharmacol Ther;21:343-54.

Voas RB, 2013. Commentary on Callaghan et al. Minimum legal drinking age laws protect high school students from both crashes and alcohol abuse. Addiction.

Voas RB, Fell JC, 2013. Strengthening impaired-driving enforcement in the United States. Traffic Inj Prev.

Volkow ND et al., 2007. Profound decreases in dopamine release in striatum in detoxified alcoholics: Possible orbitofrontal involvement. Journal of Neuroscience 27(46): 12700–12706, 2007. PMID: 18003850

Walt RP et al., 1981. Investigations on the penetration of ranitidine into the cerebrospinal fluid and a comparison of the effects of ranitidine and cimetidine on male sex hormones. Scand J Gastroenterol Suppl. 1981 Jun;69:19-25.

Walters BS et al., 1998. Fiber-optic biosensor for ethanol, based on an internal enzyme concept. Talanta. 1988 Feb;35(2):151-5.

Wartenberg AA, 1998. Management of common medical problems. In, Principles of Addiction Medicine, 2d ed. (Graham, A.W. and Shultz, T.K., eds.) American Society of Addiction Medicine, Chevy Chase, MD, pp. 731-740.

Watson PE et al, 1980. Total body water volumes for adult males and females estimated from simple anthropometric measurements. Am J Clin Nutr;33:27-39.8. Chumlea WC et al. Total body water reference val.

Williams KL, Broadbridge CL. 2009. Potency of naltrexone to reduce ethanol self-administration in rats is greater for subcutaneous versus intraperitoneal injection Original Research Article. Alcohol, Volume 43, Issue 2, , Pages 119-126

Wise RA and Rompre PP. 1989. Brain dopamine and reward. Annu Rev Psychol.;40:191-225. Review.

Wolfensohn, S.; Lloyd, M. Handbook of Laboratory Animal Management and Welfare, 3rd ed.; Blackwell Publishing: Oxford, U.K., 2003.

www.ich.org. 2005. ICH Q2 (R1). Validation of analytical procedures: text and methodology, International Conference on Harmonization of Technical Requirements for Registration of Pharmaceuticals for Human Use. 11-12.

Xiang Y , Shen J. 2011. In vivo detection of intermediate metabolic products of [1-(13) C]ethanol in the brain using (13) C MRS. NMR Biomed. Nov;24(9):1054-62.

Yim HJ et al., 1998.. Comparison of local and systemic ethanol effects on extracellular dopamine concentration in rat nucleus accumbens by microdialysis Alcohol Clin Exp Res. Apr;22(2):367-74.

Yokoyama H et al., 2001. Nicotinamide adenine dinucleotide-dependent retinoic acid formation from retinol in the human gastric mucosa: inhibition by ethanol, acetaldehyde, and H2 blockers. Alcohol Clin Exp Res. 2001 Jun;25(6 Suppl):24S-8S.

Yoshimoto K; Komura S. 1993. Monitoring of ethanol levels in the rat nucleus accumbens by brain microdialysis. Alcohol Alcohol. 28 (2),171-174

Yun Xiang and Jun Shen. 2011. In vivo detection of intermediary metabolic products of [1-13C] ethanol in the brain using 13C magnetic resonance spectroscopy NMR Biomed. November; 24(9): 1054–1062.

Zauner A et al., 1995. Brain oxygen, CO_2, pH, and temperature monitoring: evaluation in the feline brain. *Neurosurgery*. *37*, 1168–1176.

Zhen S et al., 2011 A novel microassay for measuring blood alcohol concentration using a disposable biosensor strip. Forensic Sci Int. Apr 15;207(1-3):177-82. doi: 10.1016/j.forsciint.2010.10.002. Epub 2010 Oct 28.

Zoski CG. 2007. Handbook of Electrochemistry. Elsevier Science. ISBN 0-444-51958-0.